# High Energy Astrophysics

- Blue (star forming) and Red (quenched) Galaxies
- Supermassive Black Holes in Galaxies, Jets & Blazars
- Extragalactic Background Light (EBL)
- Measuring the EBL Using Gamma Ray Astronomy
- Gamma Ray Atmospheric Cherenkov Telescopes
- Highest Energy Cosmic Rays, GZK Cutoff
- Cosmic Ray Composition and Spectrum
- Cosmic Ray Acceleration
- Secondary Cosmic Rays: Pions and Muons
- Pierre Auger Observatory for Energetic Cosmic Rays
- Low Energy Cosmic Rays, Van Allen Belts, Auroras
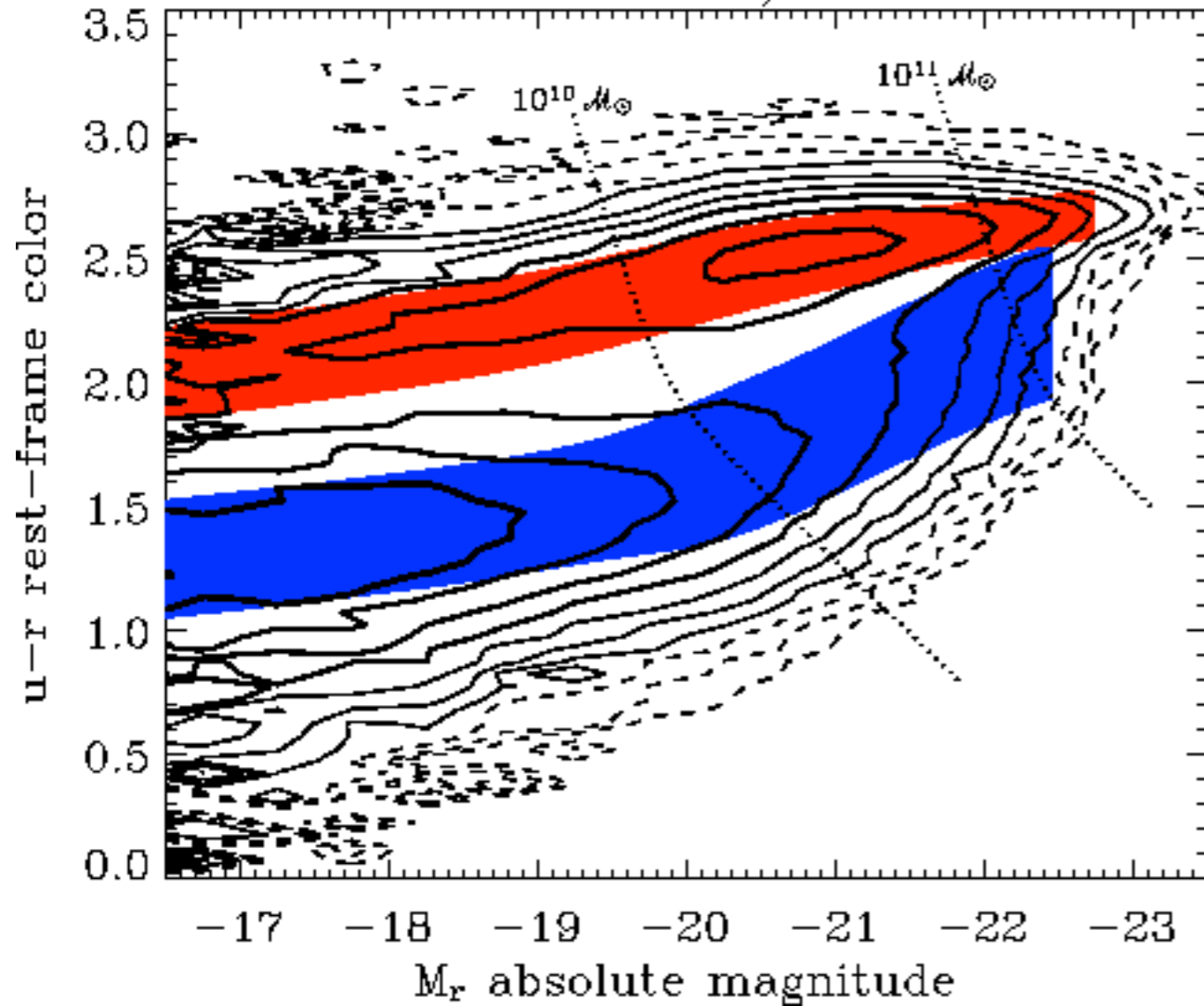
Color bimodality of galaxies on color-magnitude plot from [Baldry et al. (2004)](). The black solid and dashed contours represent the number density of galaxies: logarithmically spaced with four contours per factor of ten. The distribution is bimodal: there are two peaks corresponding to a red sequence (generally early types) and a blue sequence (late types).

Sersic n is the radial distribution: $\exp[-(r/r_0)^{1/n}]$,
 n < 2.5 for disks, n>2.5 for sphroids

blue
disks   red
         spheroids

red
spheroids

blue

red
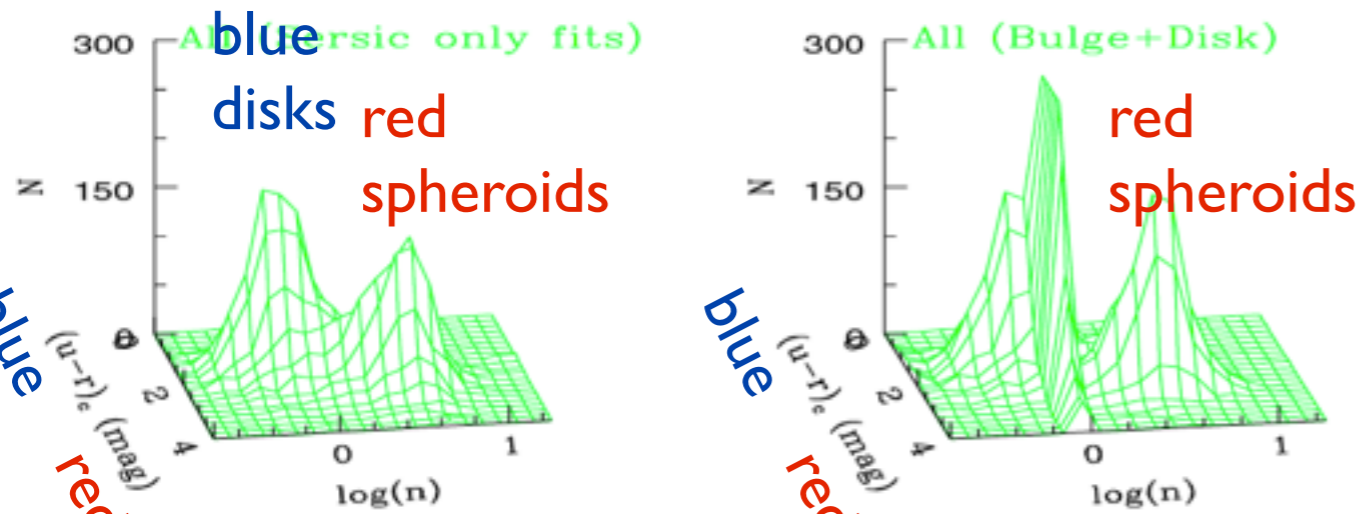
Galaxy bimodality in the color-structure plane
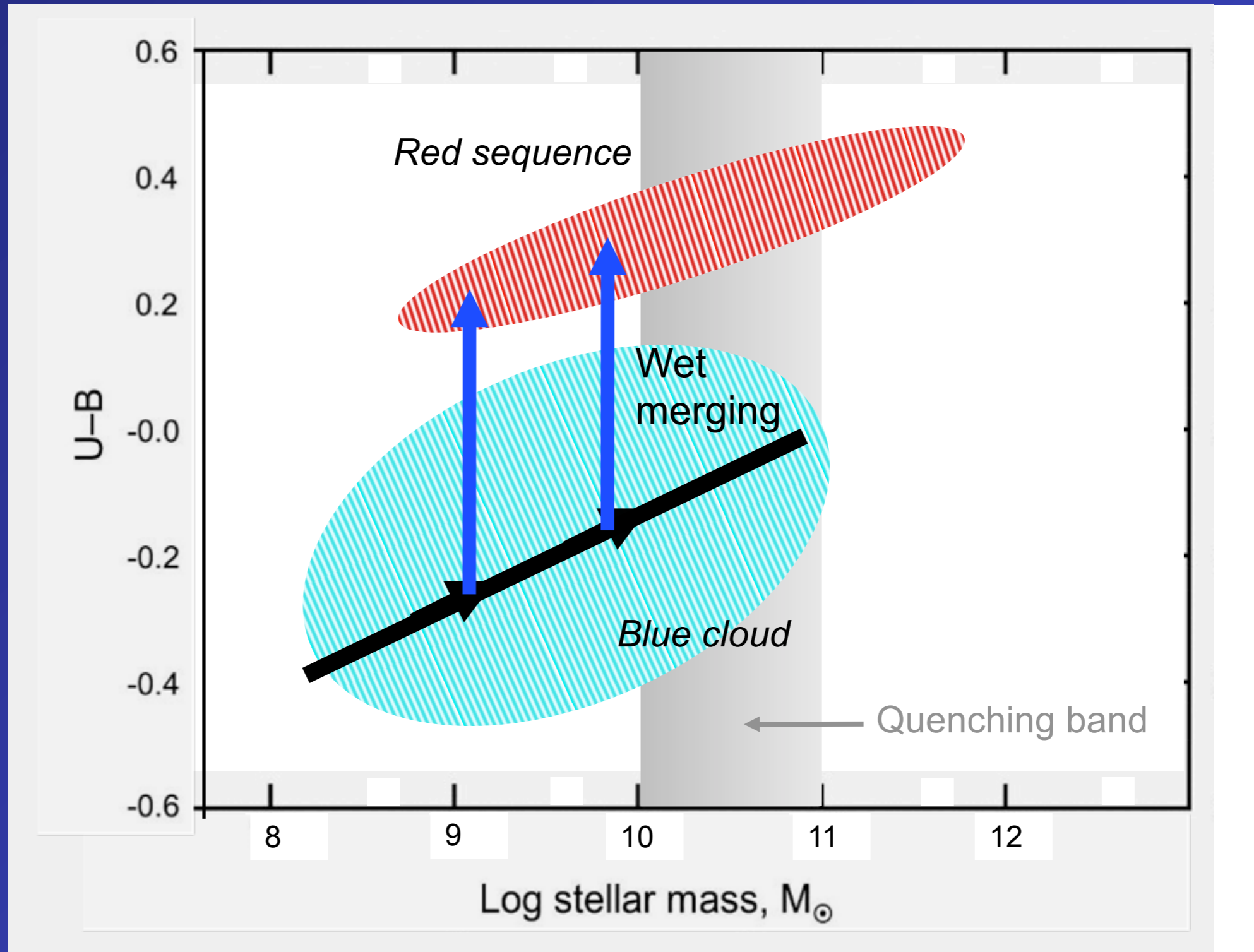(S. Driver et al. 2006)

The Bi-Modal Distribution of Galaxies

Early-Type

Late-Type

Spheroidal Morphology
Old Stellar Populations
No or Little Cold Gas
Red Colors

Disk-Like Morphology
Young Stellar Populations
Abundant Cold Gas
Blue colors

Flow through the color-mass diagram for "central" galaxies
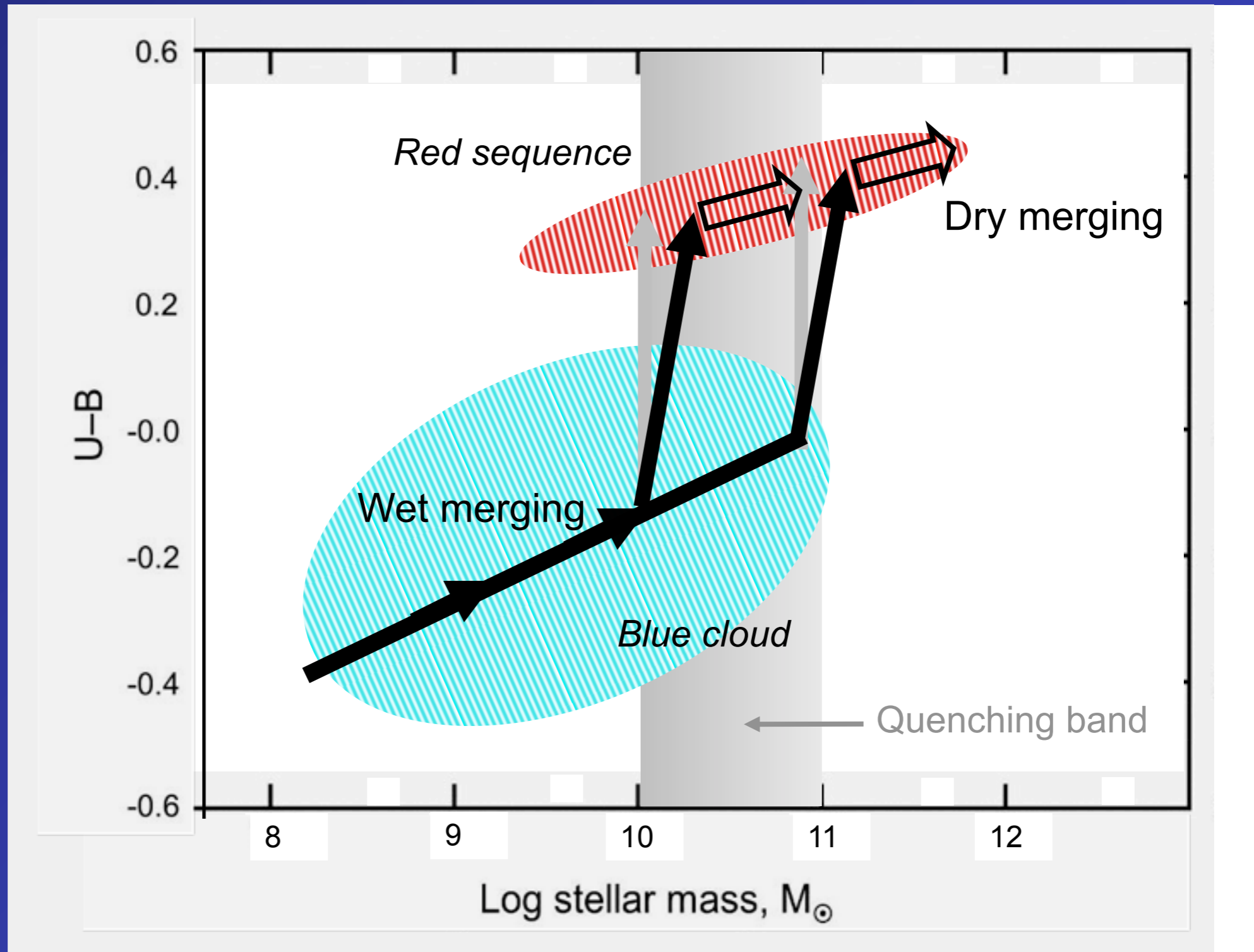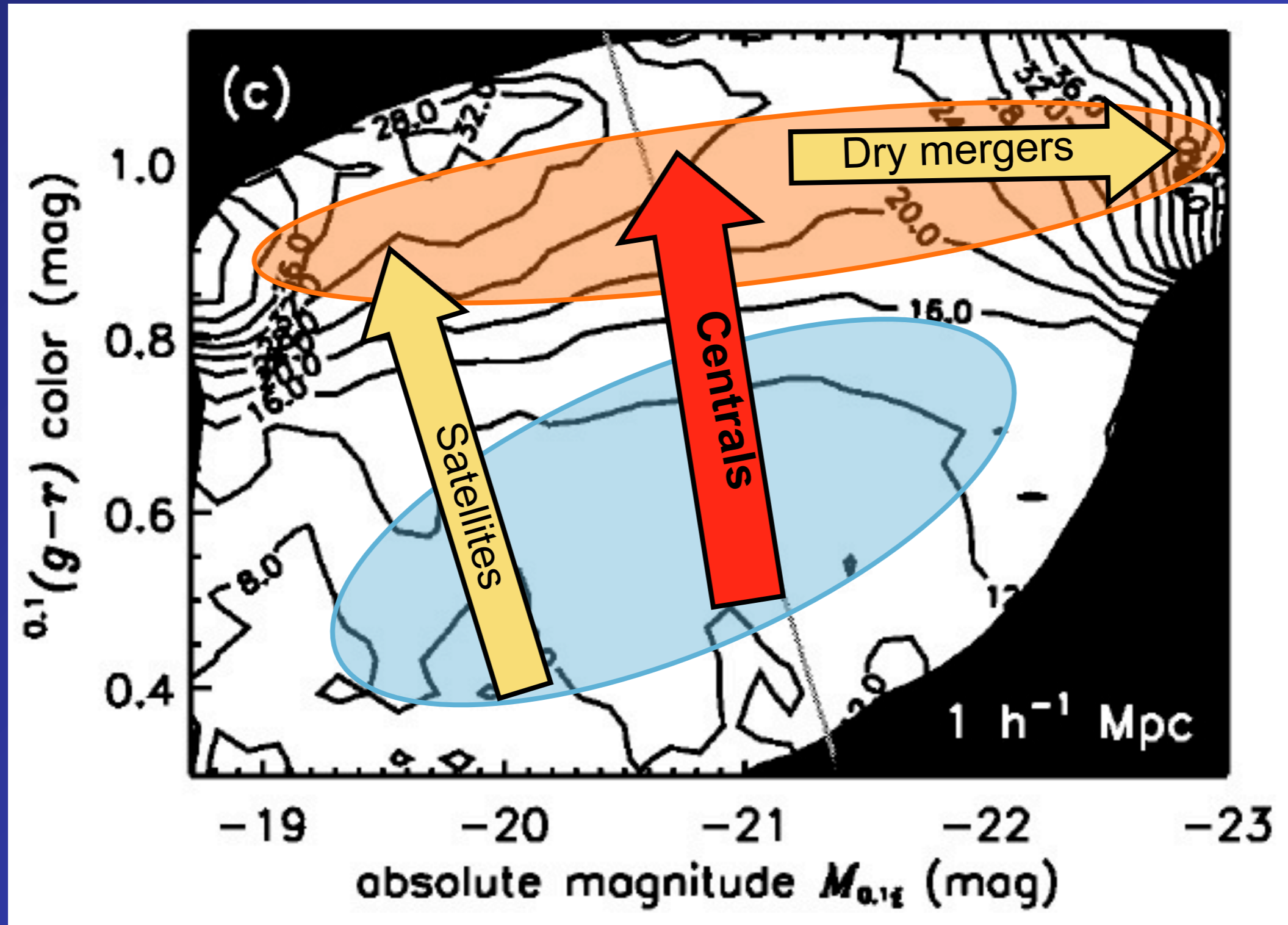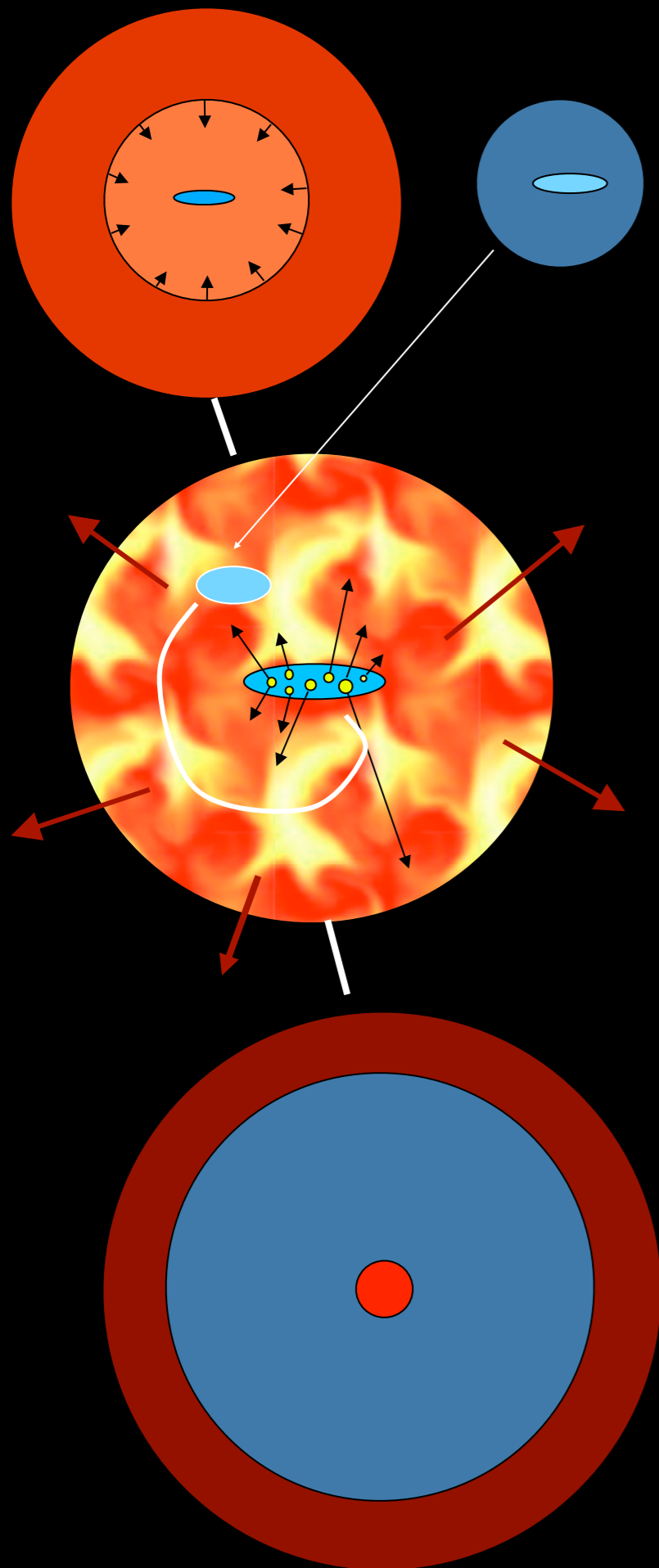
Flow through the color-mass diagram for "satellite" galaxies

Flow through the CM diagram versus environment

Hogg et al. 2003: Sloan Survey

Galaxy Formation in ΛCDM

- gas is collisionally heated when perturbations 'turn around' and collapse to form gravitationally bound structures

- gas in halos cools via atomic line transitions (depends on density, temperature, and metallicity)

- cooled gas collapses to form a rotationally supported disk

- cold gas forms stars, with efficiency a function of gas density (e.g. Schmidt-Kennicutt Law)

- massive stars and SNae reheat (and in small halos expel) cold gas and some metals

- galaxy mergers trigger bursts of star formation; 'major' mergers and disk instabilities transform disks into spheroids and fuel AGN

- AGN feedback cuts off star formation

White & Frenk 1991; Kauffmann+1993; Cole+94; Somerville & Primack 99; Cole+00; Somerville, Primack, & Faber 01; Croton et al. 2006; Somerville +08; Fanidakis+09; Guo+2011; Somerville, Gilmore, Primack, & Domínguez 2012 & Gilmore +2012 (discussed here); Porter, Somerville, Primack 2014ab

Forward Evolution

...nt status of ΛCDM
...le Dark" theory:

...nological parameters
...w well constrained
...servations

Now

BOLSHOI Simulation

Thursday, March 13, 14

Wechsler et al. 2002
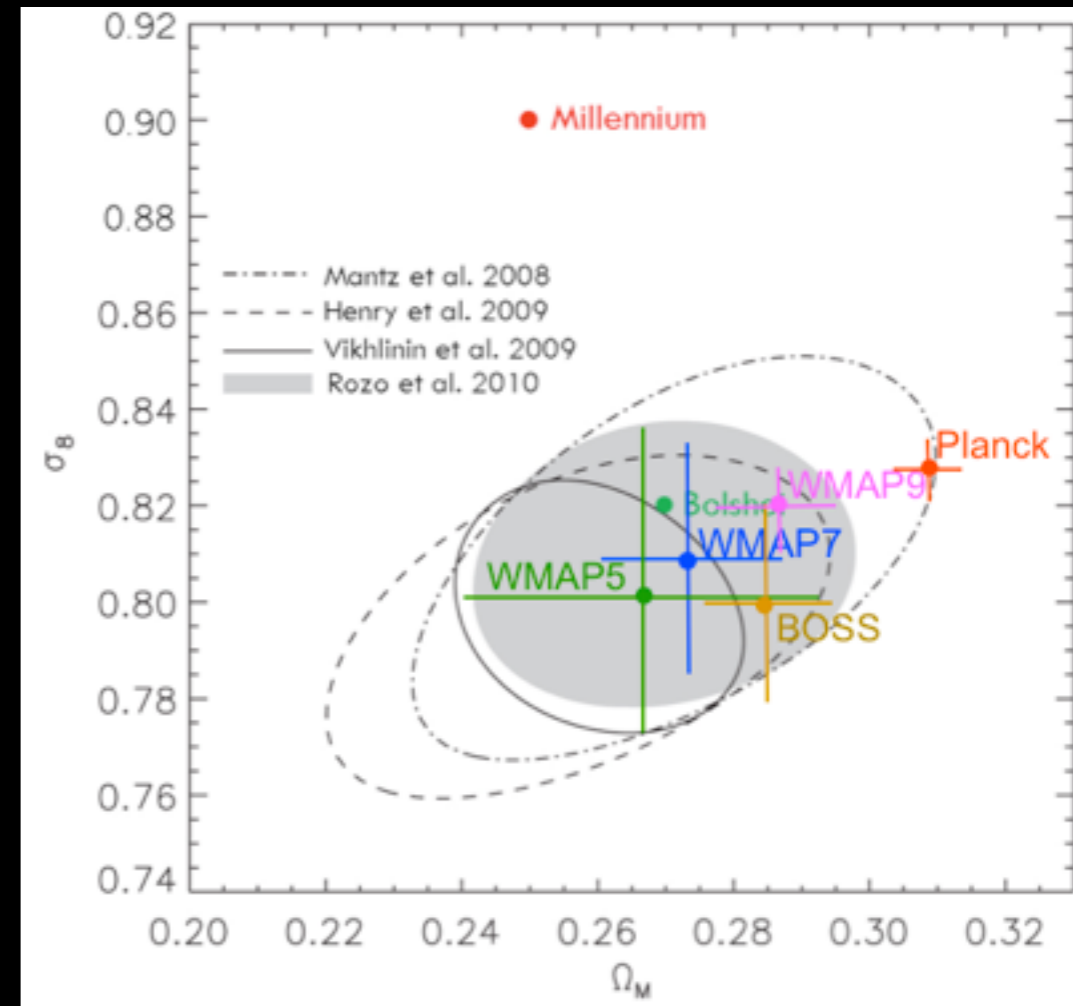
...s accretion history of
...natter halos is
...ented by 'merger
trees' like the one at left

BLACK HOLES AT CENTERS OF GALAXIES

X-ray: Jets

Optical image of Cen A

Cen A is known to be a peculiar galaxy with strong radio emission.

Chandra image of Cen A

But it is also a strong X-ray emitter, and has an X-ray jet.

At a mere 10 million light years, Cen A is the nearest AGN.

The mass of the black hole is about 1/1000 the mass of the central spheroid of stars.
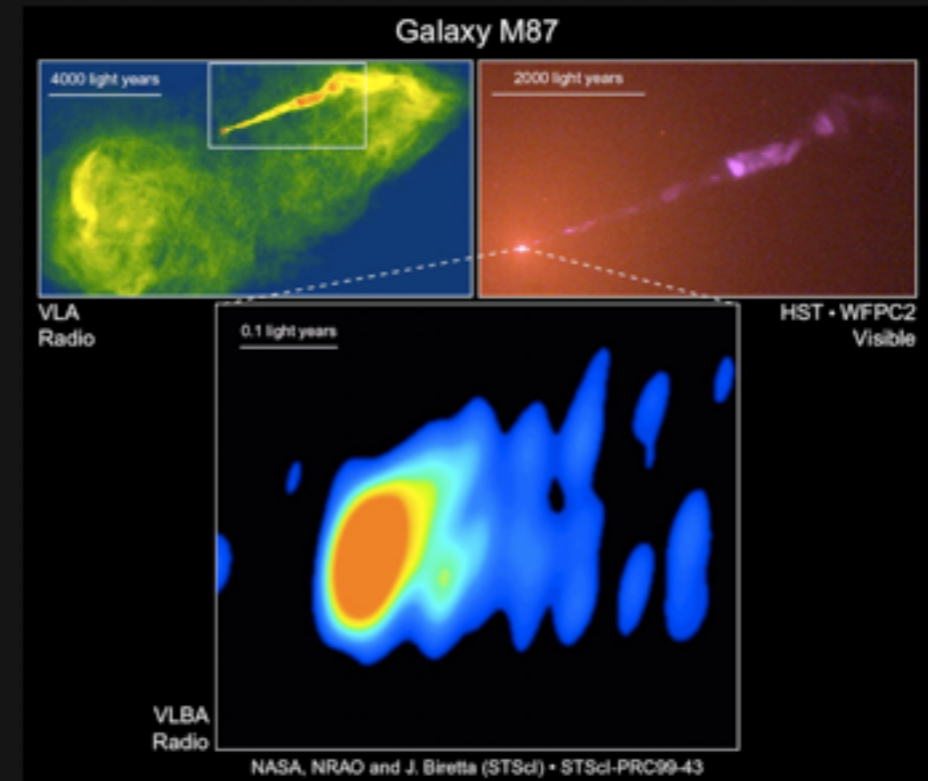
BLACK HOLES AT CENTERS OF GALAXIES

M87 - An Elliptical Galaxy

With a curious feature

Radio shows the origin of the Jet

Galaxy M87

4000 light years

2000 light years

VLA
Radio

0.1 light years

HST · WFPC2
Visible

VLBA
Radio

NASA, NRAO and J. Biretta (STScI) · STScI-PRC99-43
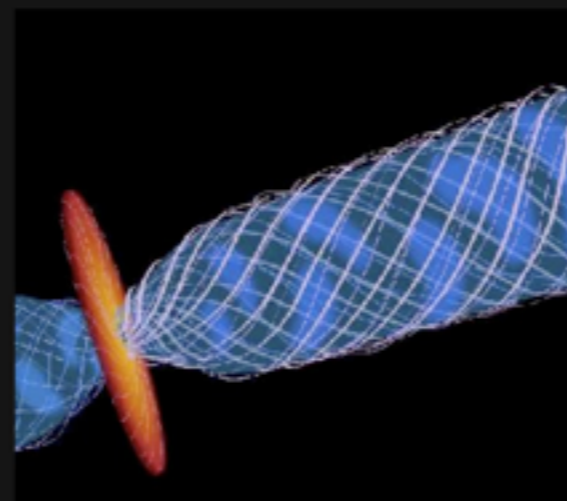
M87 is a giant ellptical galaxy at the center of the Virgo Cluster, about 70 million light years away

Our picture of what's happening

Magnetic field from surrounding disk funnels material into the jet

The black hole at the center of M87 has a mass about 3 billion times that of the sun.

Radio, optical and X-ray images of the jet in M 87

Chandra X-Ray

VLA Radio

HST Optical
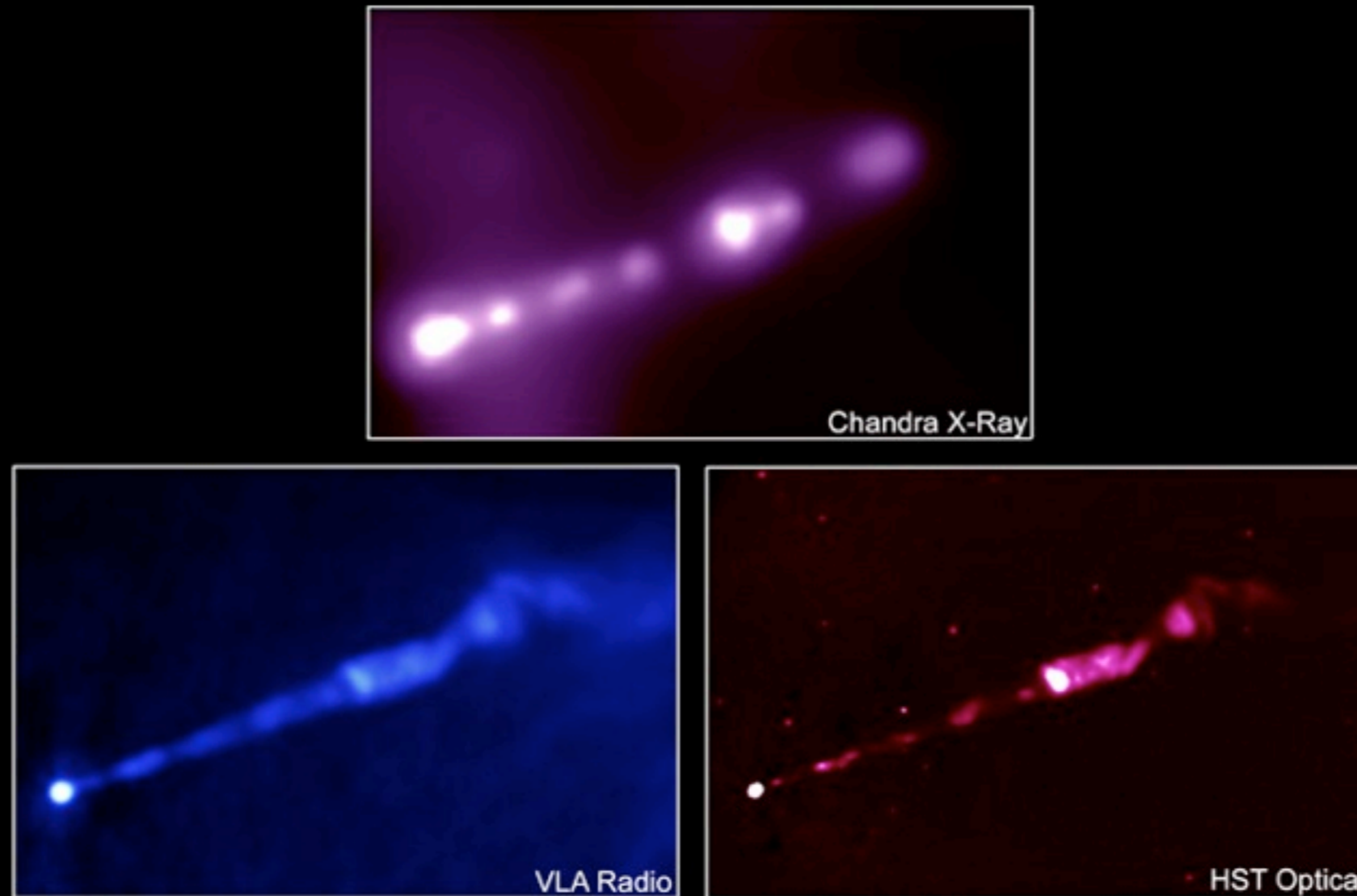
* Jets are common in AGN – and radiate in radio, optical and X-ray wavelengths

* Blazars are the objects where jet is pointing close to the line of sight

* In many (but not all) blazars, the jet emission dominates the observed spectrum

Unified picture of active galaxies

- Presumably all AGN have the same basic ingredients: a black hole accreting via disk-like structure

- In blazars the jet is most likely relativistically boosted and thus so bright that its emission masks the isotropically emitting "central engine"

- But… the nature of the isotropically emitting AGN should hold the clue to the nature of the conversion of the gravitational energy to light

- Again, X-ray and γ-ray emission varies most rapidly – potentially best probe of the "close-in" region

Narrow Line Region
Broad Line Region
Jet
Black Hole
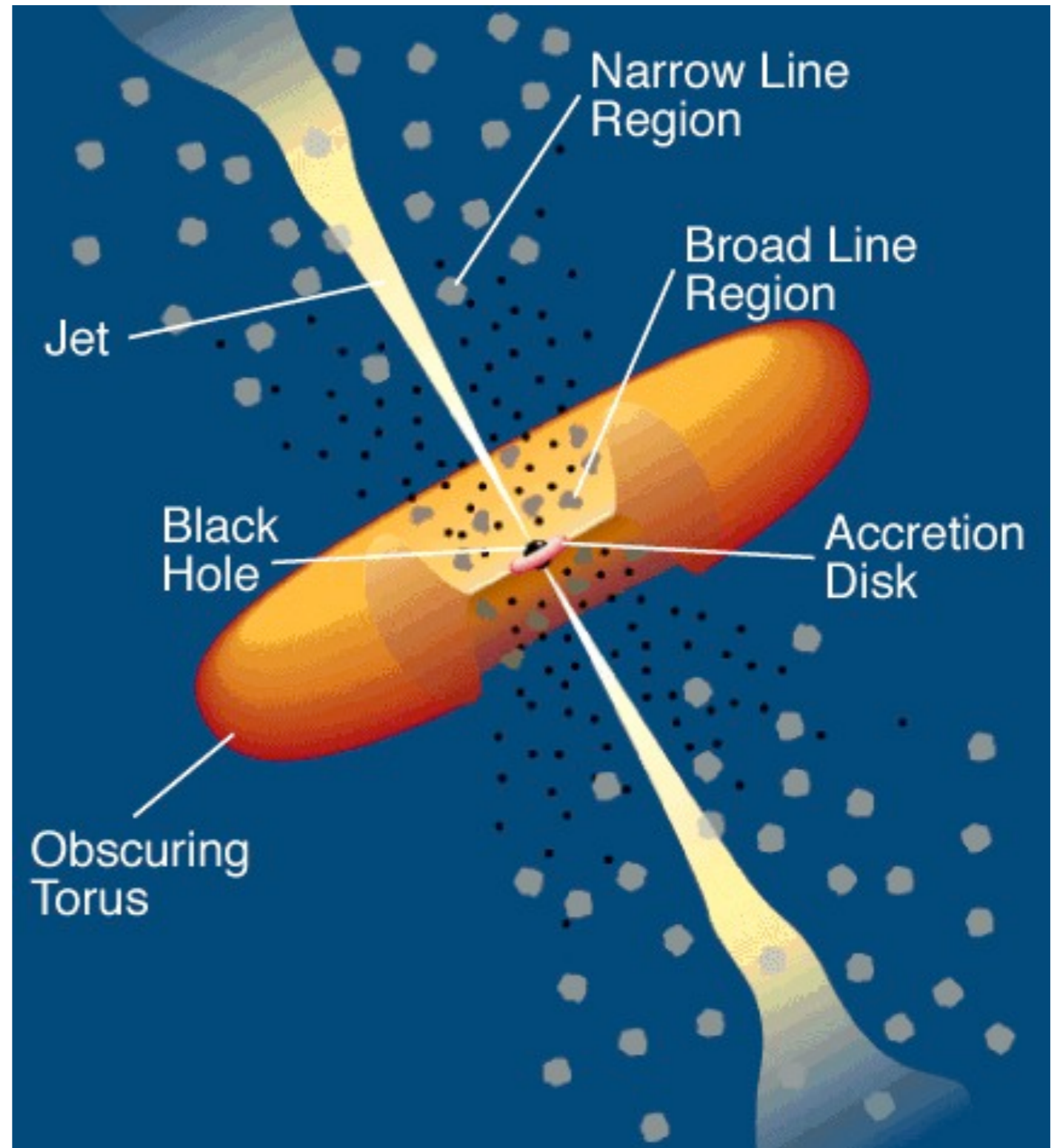Accretion Disk
Obscuring Torus

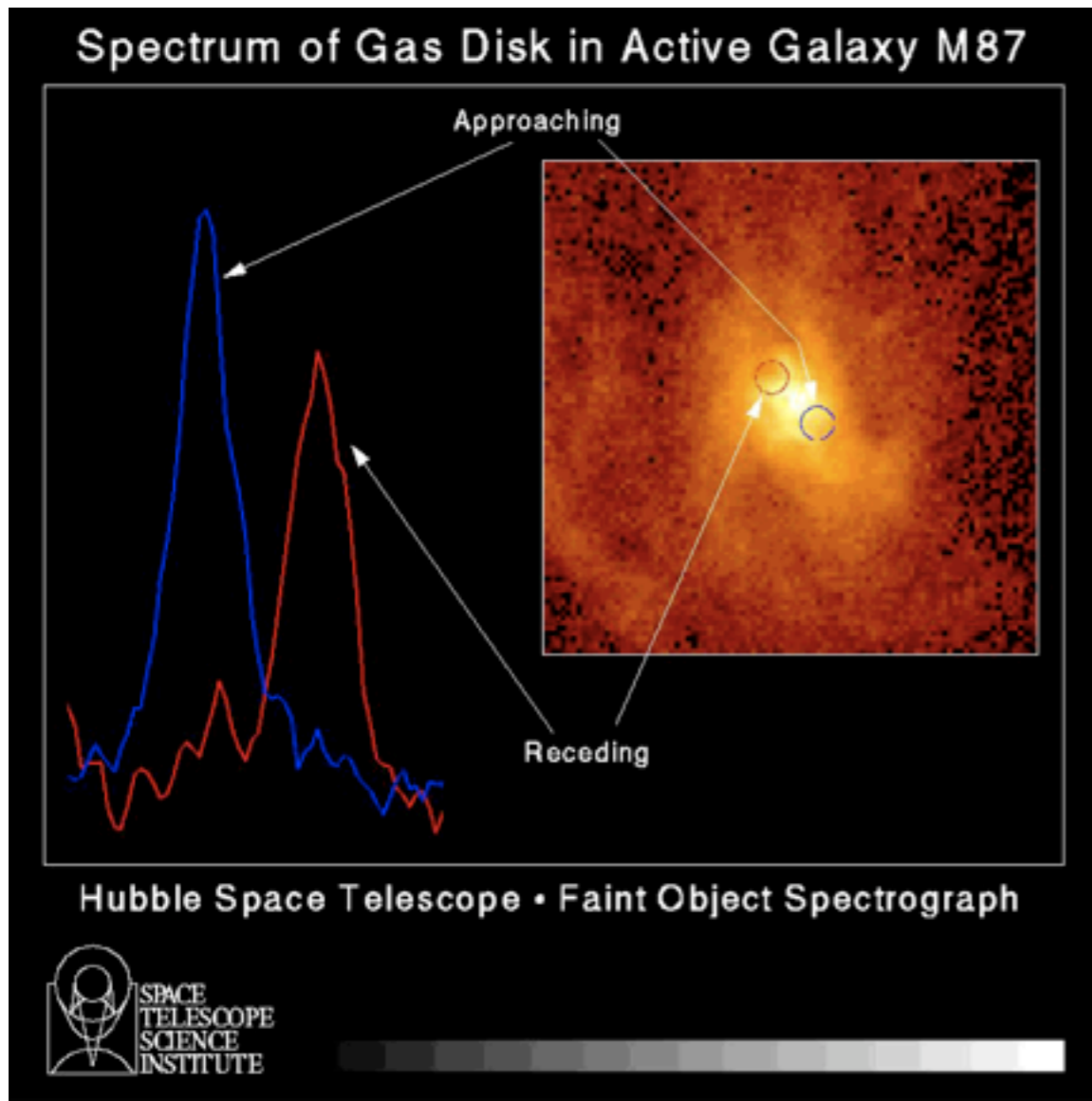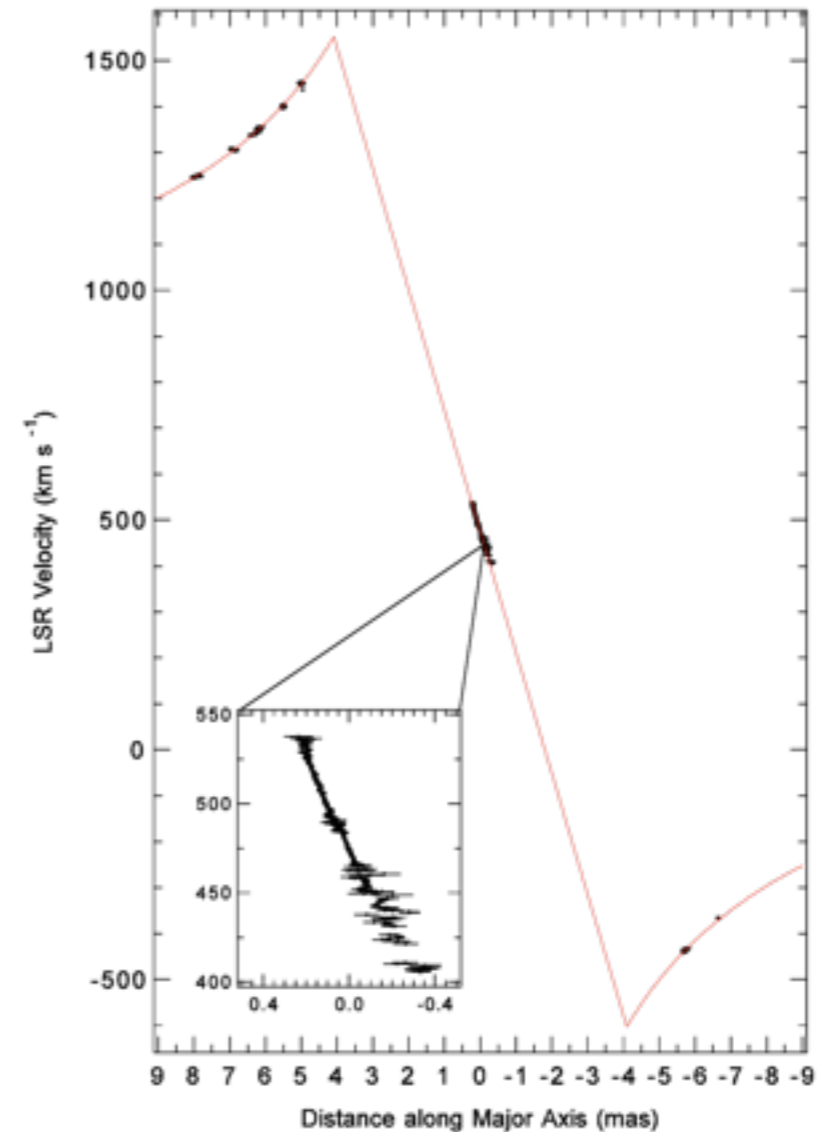Diagram from Padovani and Urry

Weighing the central black hole

Radio galaxy M87 (Virgo-A) studied with the HST

Seyfert galaxy NGC 4258 studied using H_2O megamaser data

- Black holes are a common ingredient of galaxies with massive stellar spheroids
- When fed matter, they shine – or produce jets – or both
- Efficient production of radiation by supermassive black holes can shut off star formation

The Disk-Jet System in Heart of the Active Nucleus of NGC 4258

   Seyfert galaxies possess active nuclei that have strong nonstellar components in their emissions. Well-collimated jets of relativistic particles emerge from the very centers of many active nuclei and extend for kiloparsecs. NGC 4258, about 400 million light years away, is special because it exhibits microwave (maser) emission from water vapor deep in the heart of the nucleus. (The microwave emission is not attenuated by the dust and gas that enshroud galactic nuclei and often make study with optical telescopes very difficult.) The spectrum of the water emission in NGC 4258 betrays bulk motion of gas in the nucleus at velocities of +/-1000 km/s with respect to the velocity of the galaxy. This striking result prompted a coordinated observation with a very-long-baseline array of radio telescopes, which permitted the water emission to be mapped with angular resolutions of < 1 milliarcsecond on the sky.
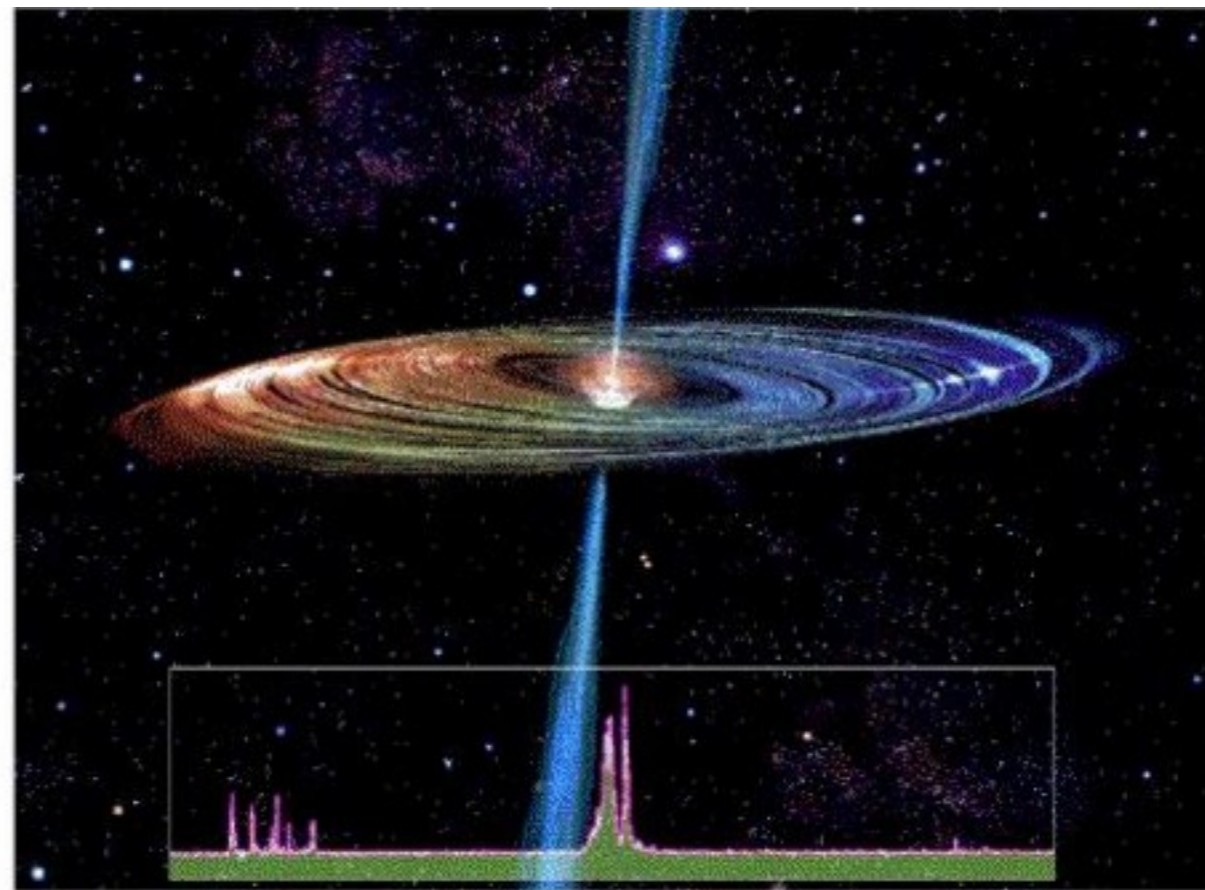
NGC 4258

0.5 ly
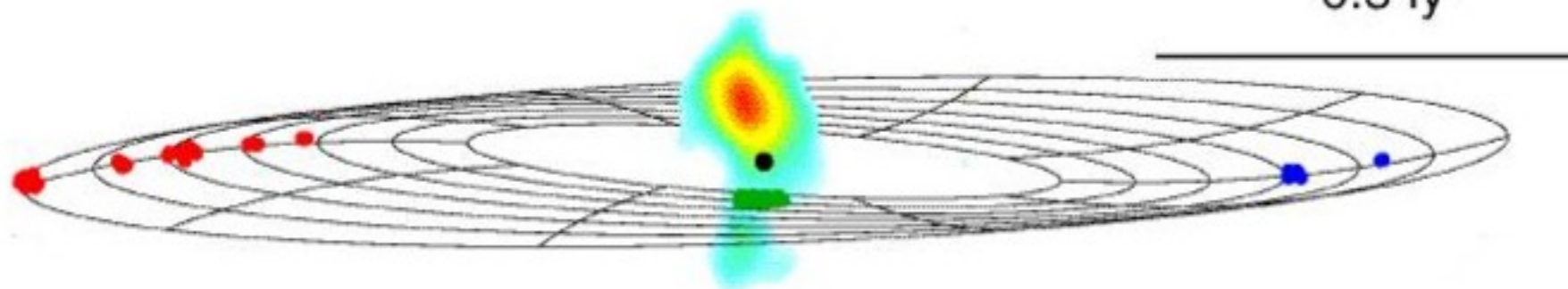
3C 120 galaxy at z=0.033 with M_{BH} = 30 million M_{sun}

Traced below from half a million light years to 15 light years:

3C 120

VLA D
20 cm
150 kpc

VLA C
18 cm
50 kpc

VLA C
6 cm
25 kpc

VLBI
6 cm
5 pc

VLBI
18 cm
40 pc

VLA A
2 cm
500 pc

VLA A
6 cm
3 kpc
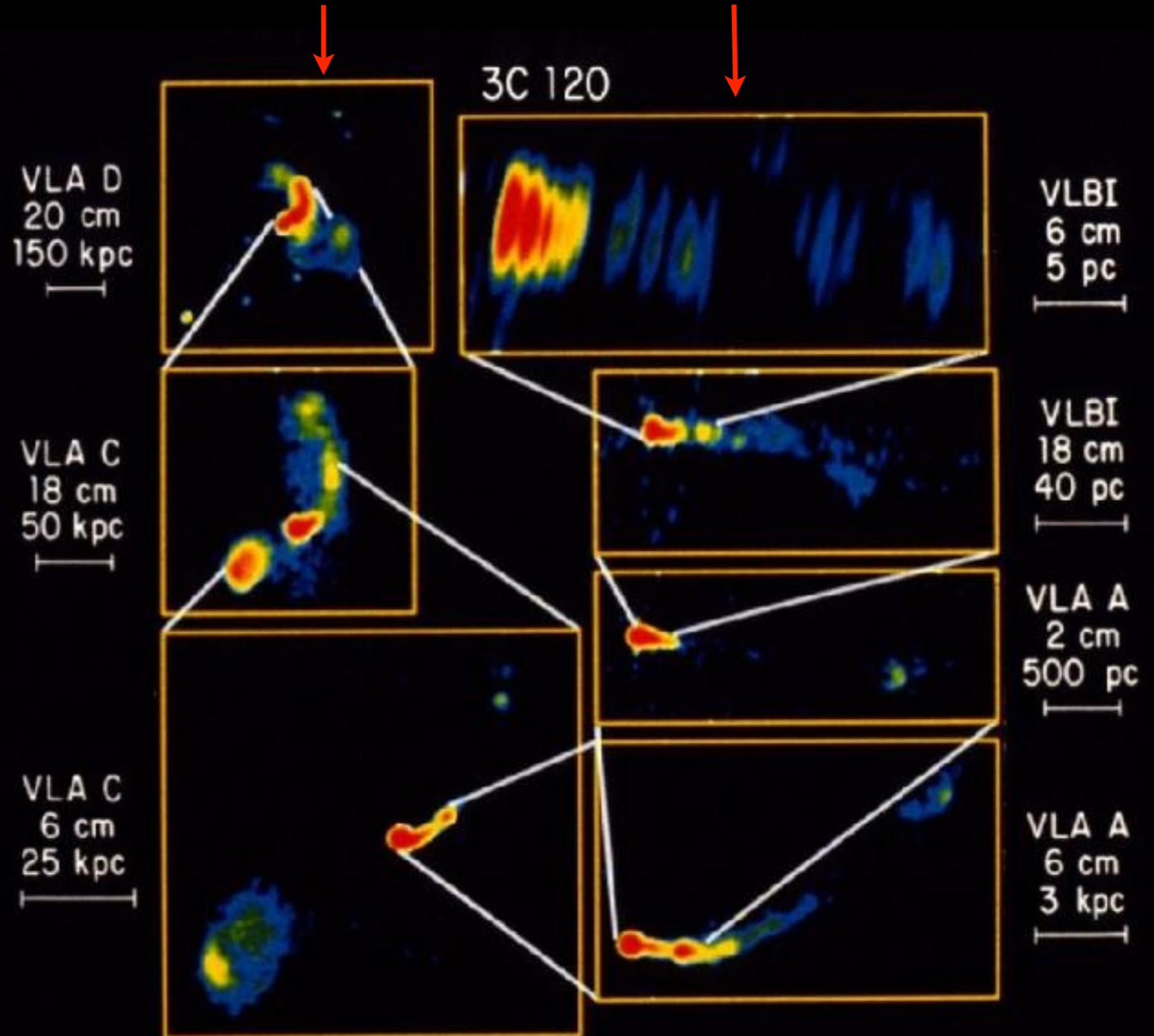
3C 120 APPARENT SUPERLUMINAL MOTION

Blobs in the jet near the black hole in 3C 120 appear to move faster than light.

Such apparent "super-luminal motion" is explained in the next slide.
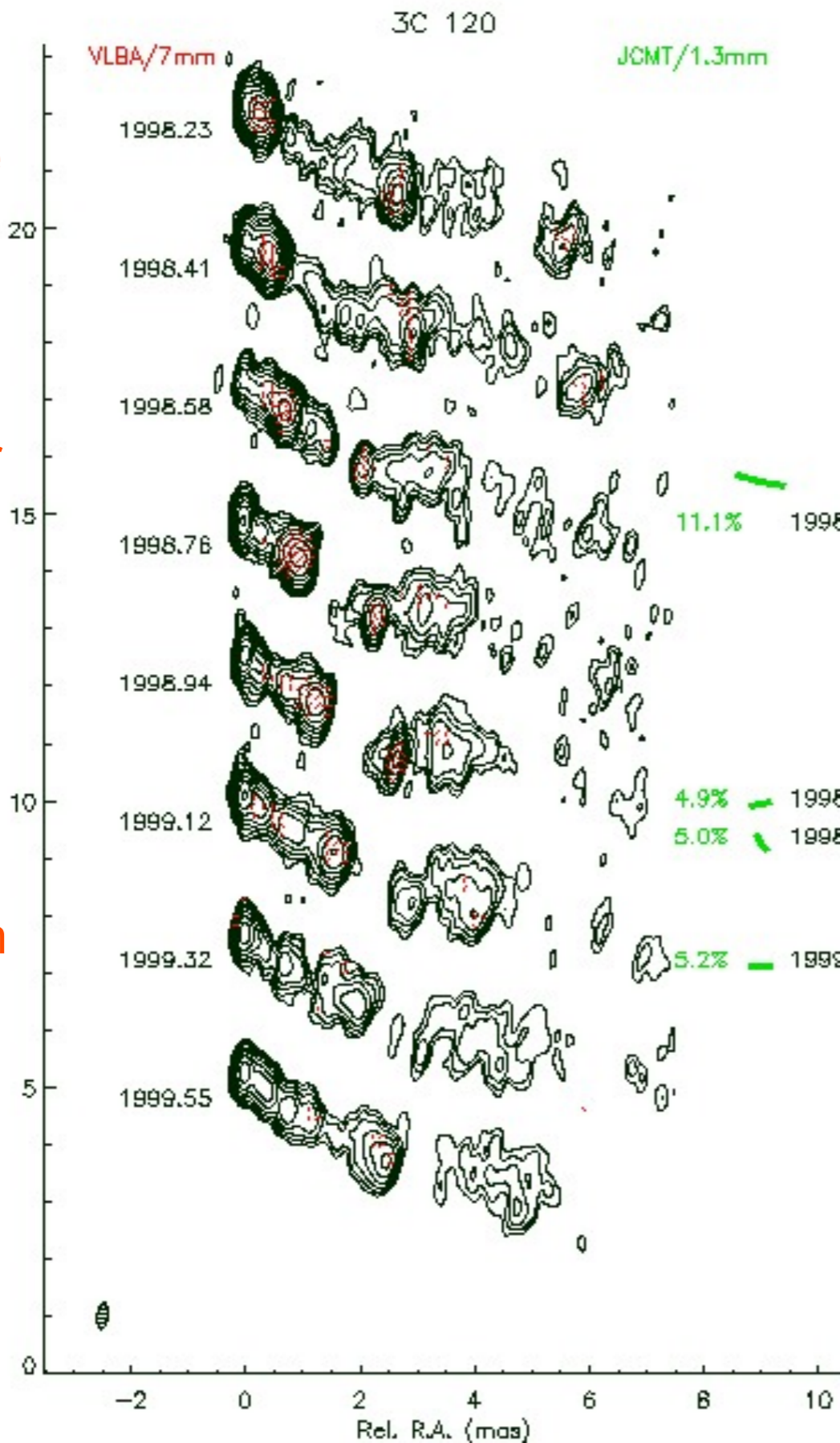
The geometry of superluminal expansion. If the blob in this example moved exactly at the speed of light, it would appear to have a transverse speed of 7 times the speed of light. It would actually take the blob 2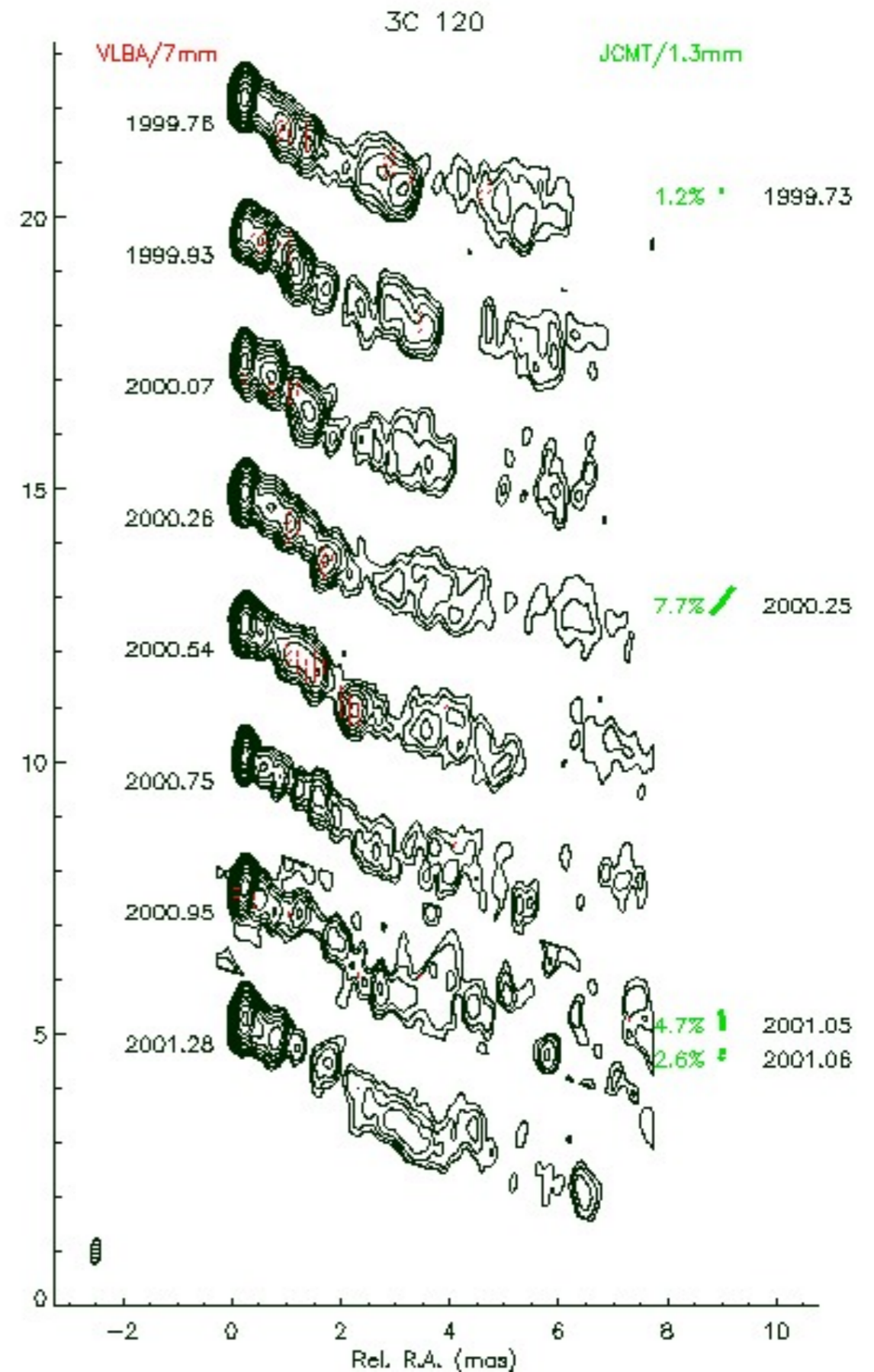5 years to move from point A to point B, but light emitted when the blob starts out at point A would reach us only one year before the light signaling its arrival at point B. It would therefore appear to make the trip in only one year! Nothing can, of course, move at exactly the speed of light. However, this example shows that an object moving at 96 percent ($\frac{24}{25}$) of the speed of light would appear to move 7 light-years transversely in just over 2 years, implying a transverse speed nearly 3.5 times that of light.
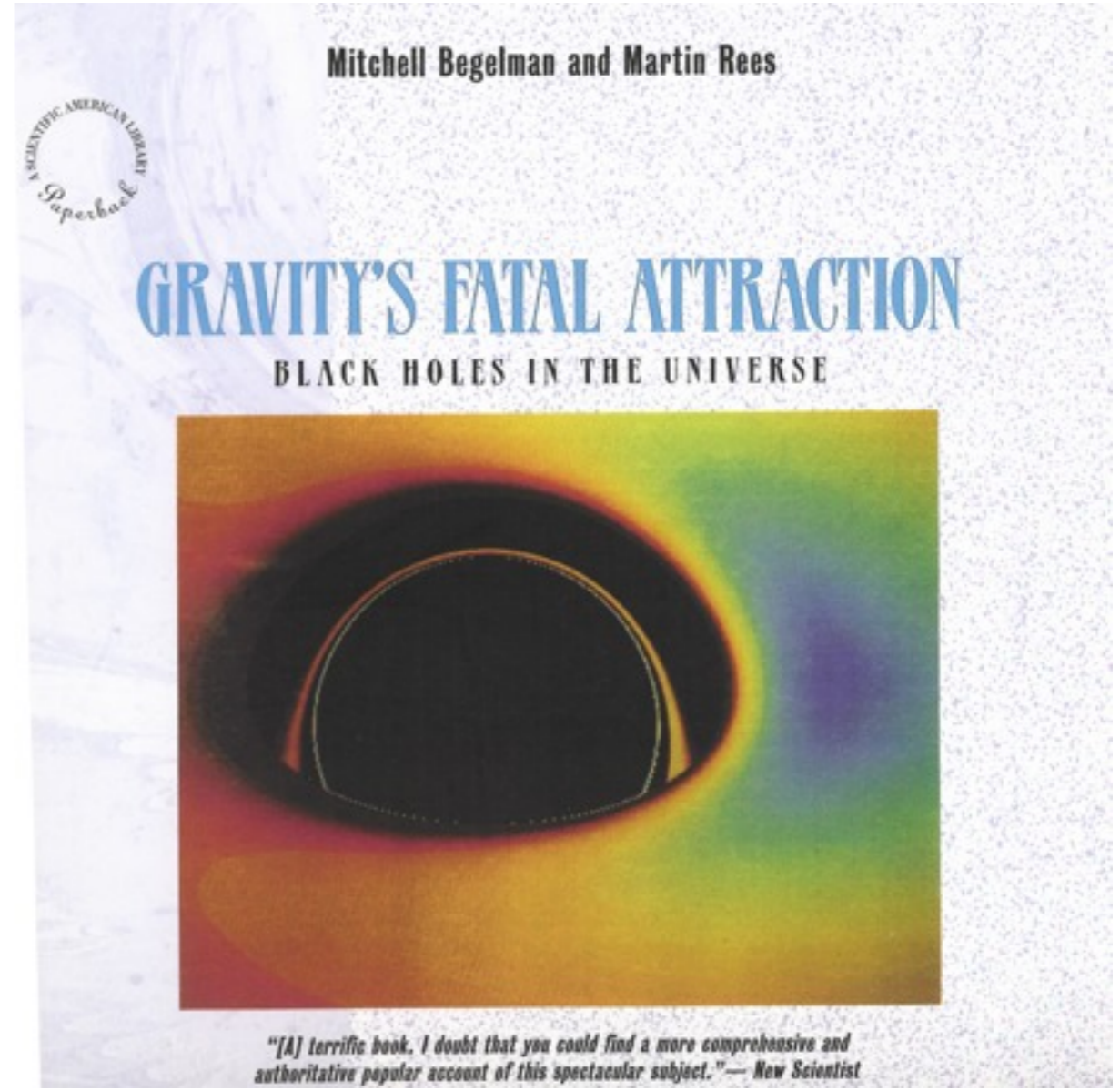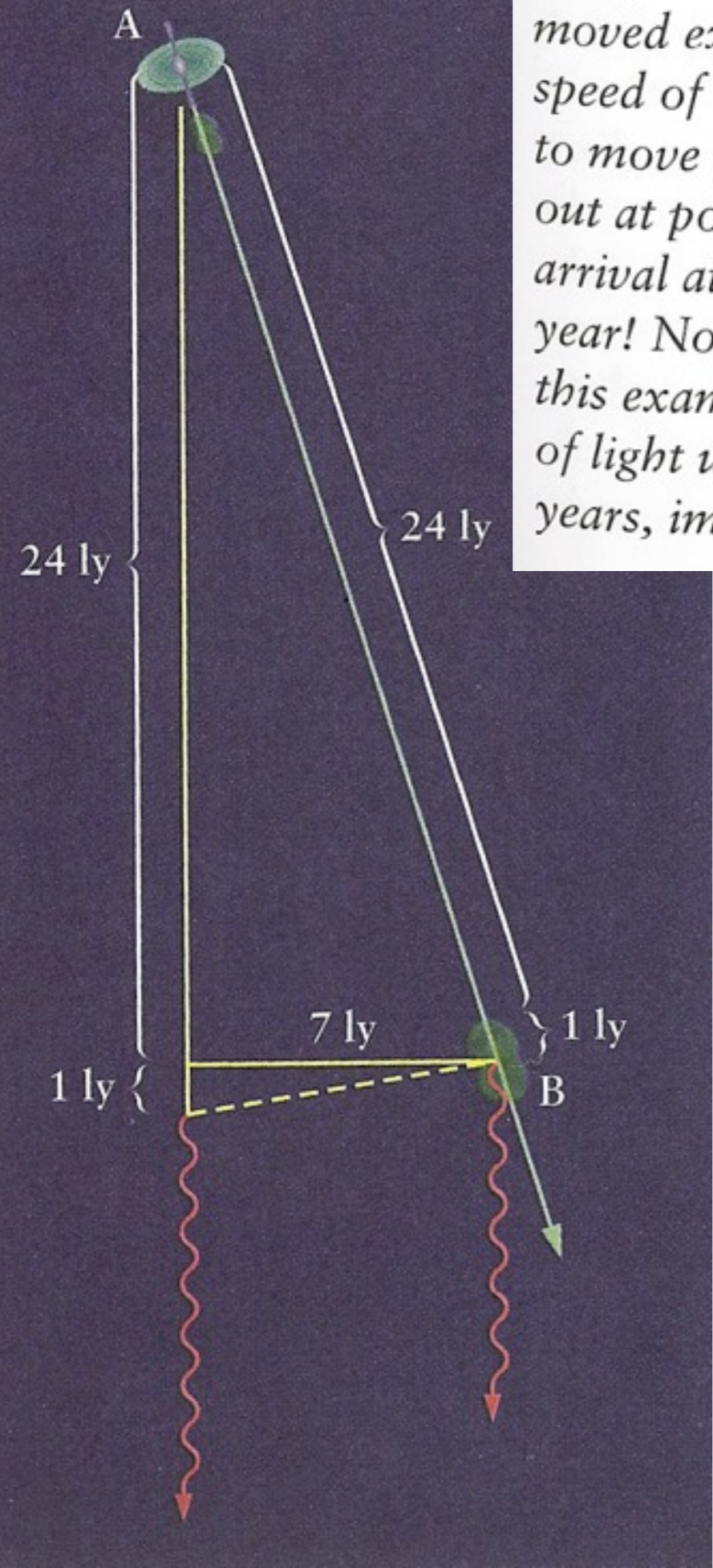
We see TeV Gamma Rays when the AGN jet points toward us
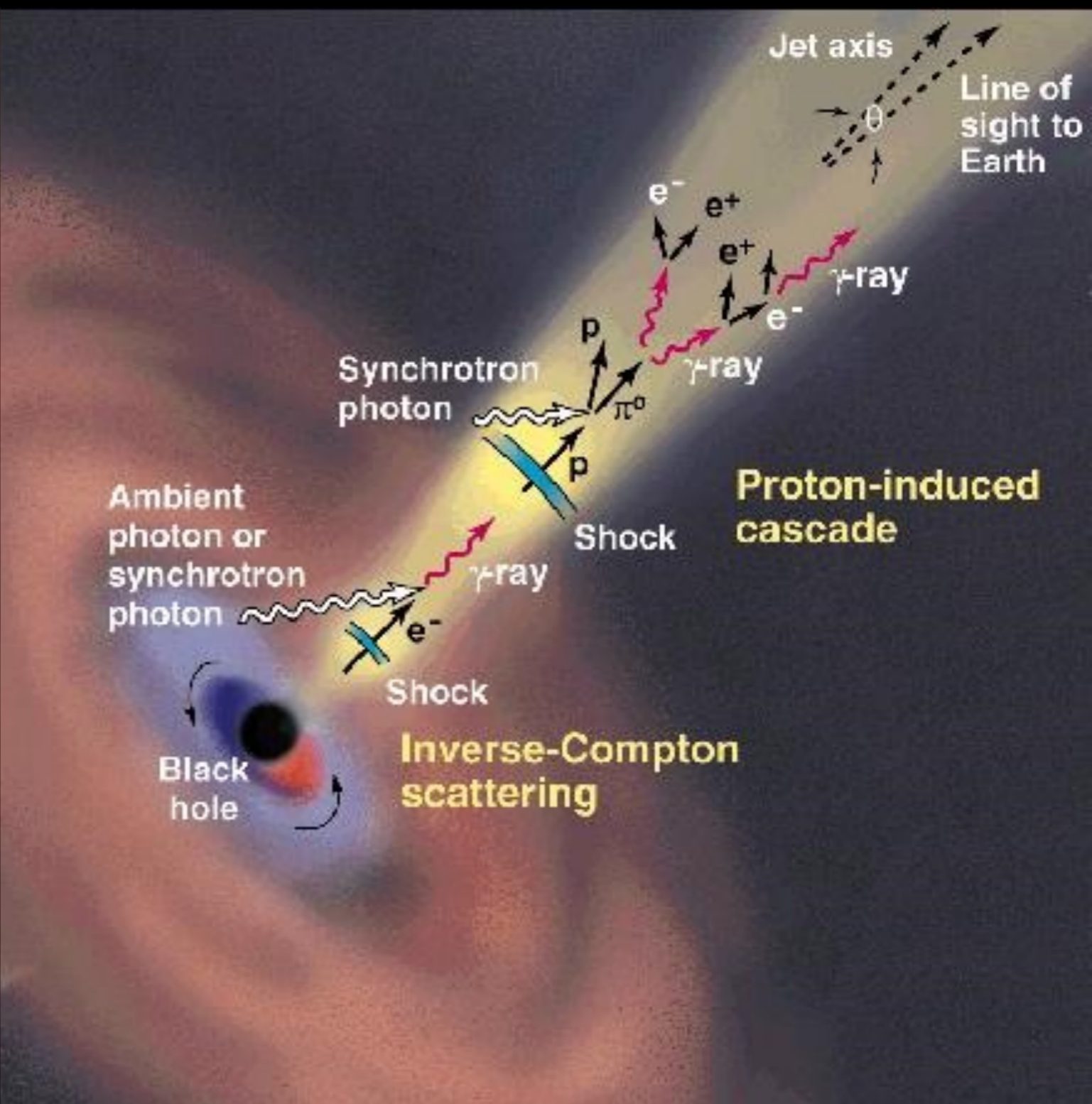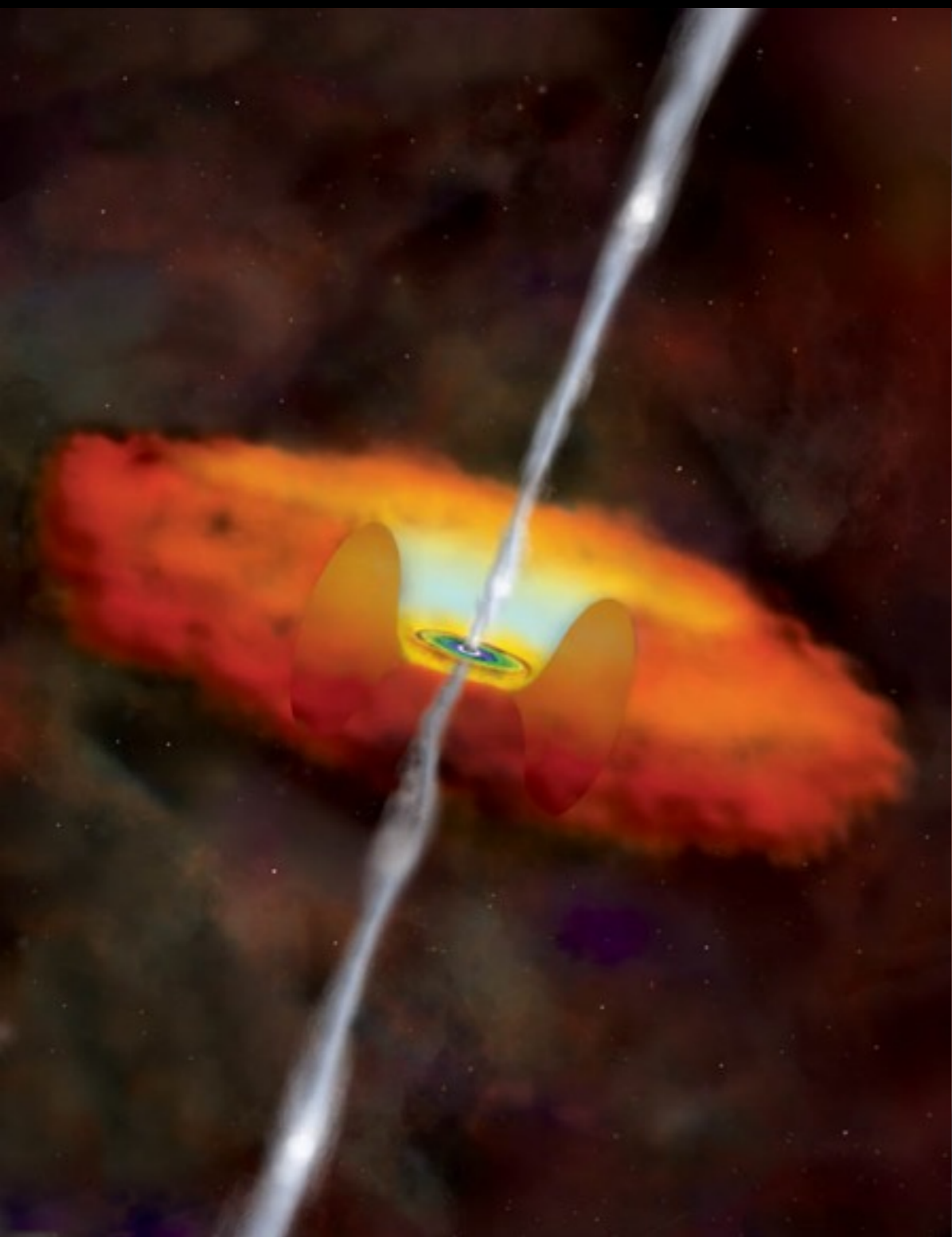
The Atmosphere is Transparent to Light and Radio

Fermi

Kitt Peak (visible)

Ground-based observatory

Blue curve: high-altitude observatory (Mauna Kea)

| Compton (γ-rays) | Chandra (X-rays) | Fuse (UV) | Spitzer (infrared) | JCMT (microwave) | VLA (radio) | Green Bank (radio) | Arecibo (radio) |

Visible window   Infrared windows

Atmosphere is opaque

Atmosphere is opaque

Radio window

Atmosphere is opaque

Transparency (%)

100
50
0

| 10^{-12} | 10^{-11} | 10^{-10} | 10^{-9} | 10^{-8} | 10^{-7} | 10^{-6} | 10^{-5} | 10^{-4} | 10^{-3} | 10^{-2} | 10^{-1} | 1 | 10^{1} | 10^{2} | 10^{3} |

| 0.001 nm | 0.01 nm | 0.1 nm | 1 nm | 10 nm | 100 nm | 1 μm | 10 μm | 100 μm | 1 mm | 1 cm | 10 cm | 1 m | 10 m | 100 m | 1 km |

Wavelength

Cosmic Extragalactic Backgrounds

Herschel far-IR
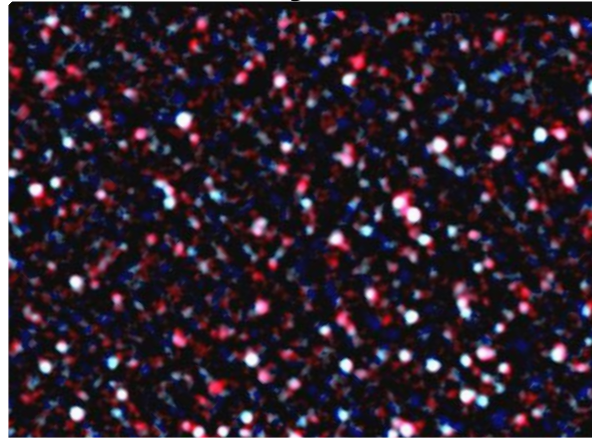
Spitzer mid-IR
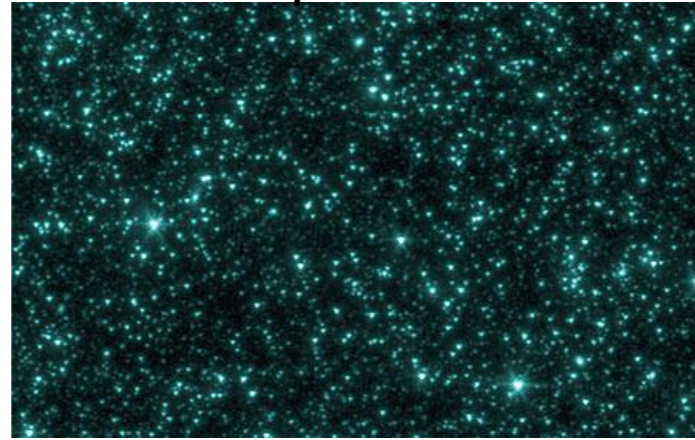
HST-optical/UV

0.850-1.2mm

in the future:
ALMA, CCAT..

CMB
Big Bang

cosmic extragalactic backgrounds

stars + black holes

Extragalactic Background Light (EBL)

black holes

ν S$_ν$
(nW m^{-2} Hz^{-1})

100μm   1μm   1Å

10000

100

1

0.01

0.0001

1.0E+09   1.0E+14   1.0E+19   1.0E+24

Frequency [Hz]
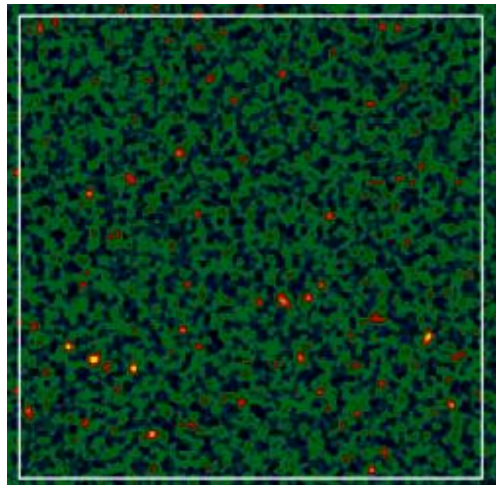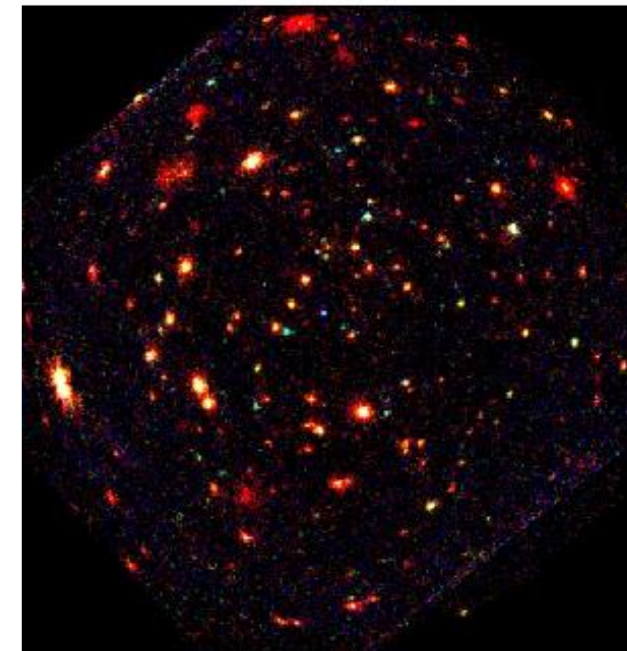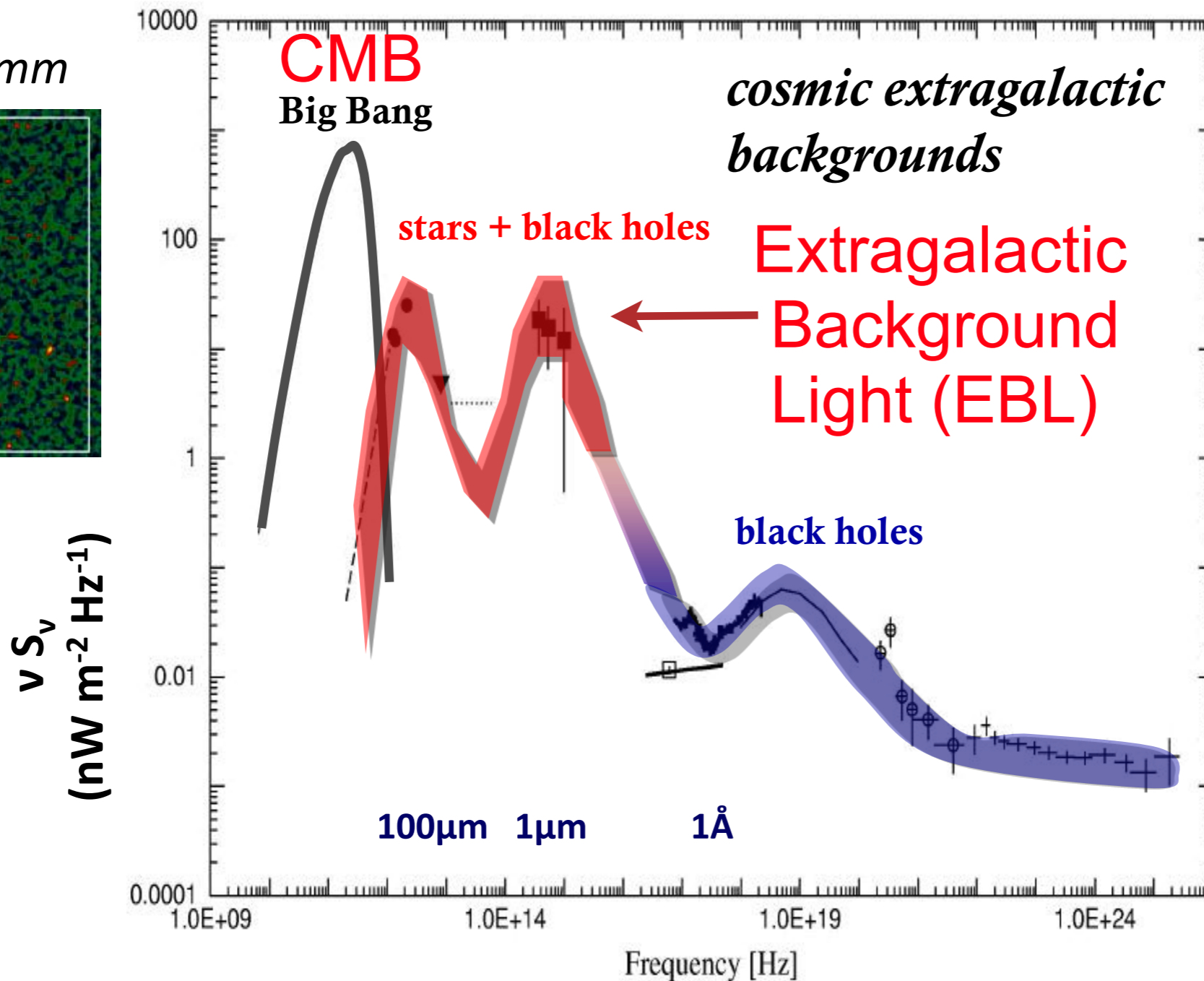
Chandra/XMM –X-ray

Extragalactic Background Light (EBL)

- The usual plot of $\lambda I_\lambda = dI/d(\log \lambda)$ vs. $\log \lambda$ shows directly the

  ENERGY DENSITY $\rho_\lambda = (4\pi/c) \lambda I_\lambda$ in the EBL:

  $$1 \text{ nW/m}^2\text{/sr} = 10^{-6} \text{ erg/s/cm}^2\text{/sr} = 2.6 \times 10^{-4} \text{ eV/cm}^3$$

  Total EBL $\Omega_{EBL}^{obs} = (4\pi/c) I_{EBL}/(\rho_{crit} c^2) = 2.0 \times 10^{-4} I_{EBL} h_{70}^{-2}$

  The estimated $I_{EBL}^{obs} = 60\text{-}100 \text{ nW/m}^2\text{/sr}$ translates to
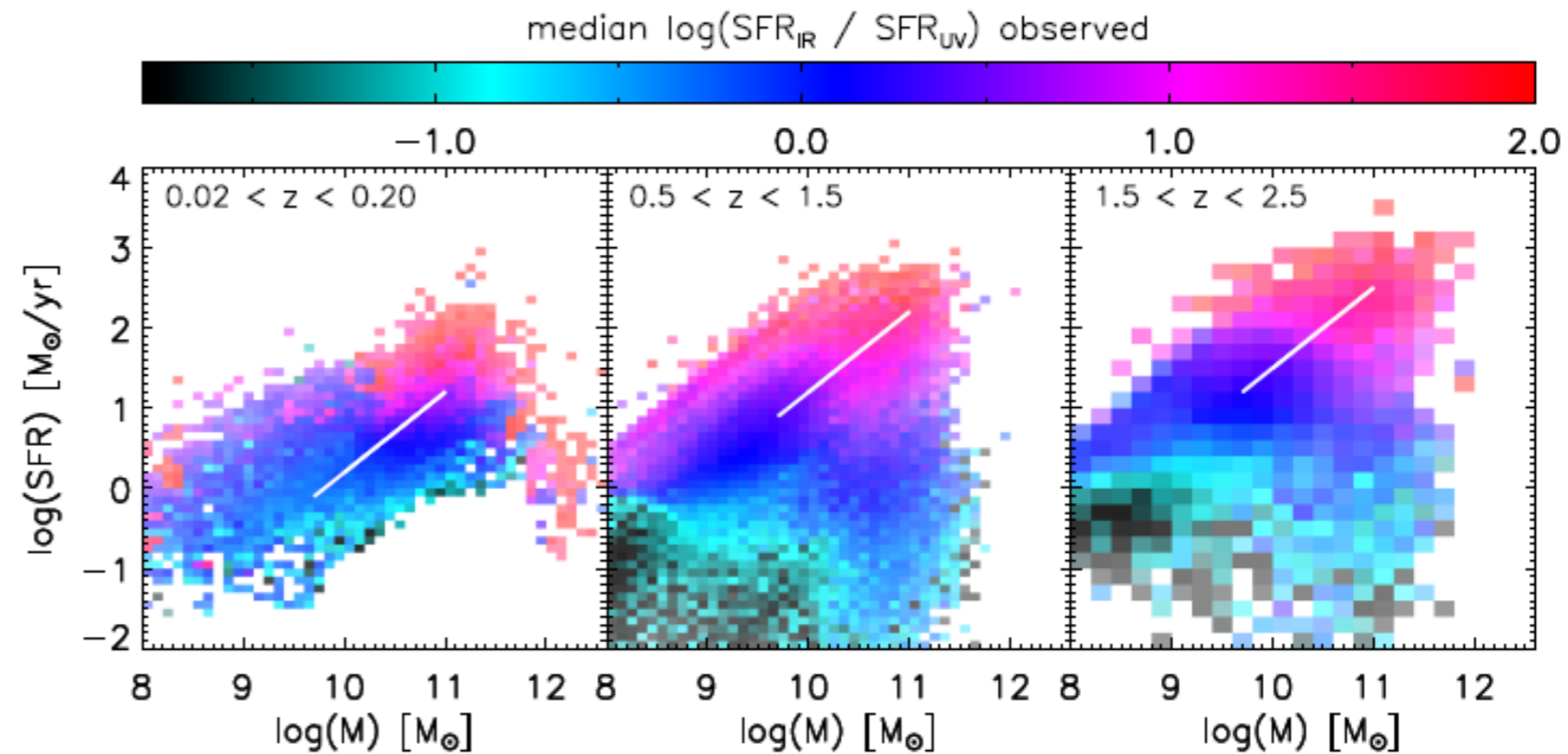
  $$\Omega_{EBL}^{obs} = (3\text{-}5) \times 10^{-6} \quad (\text{about 5\% of } \Omega_{CMB})$$

- Local galaxies typically have $E_{FIR}/E_{opt} \approx 0.3$,

  while the EBL has $E_{FIR}/E_{opt} = 1\text{-}2$. **Hence**

  most high-redshift radiation was emitted

  in the far IR.

EBL

FIR   IR-Opt

100μm   1μm

Luminosity-Dustiness Correlation

LIRG: $L_{FIR} \geq 10^{11} L_{\odot}$ ULIRG: $L_{FIR} \geq 10^{12} L_{\odot}$ HLIRG: $L_{FIR} \geq 10^{13} L_{\odot}$
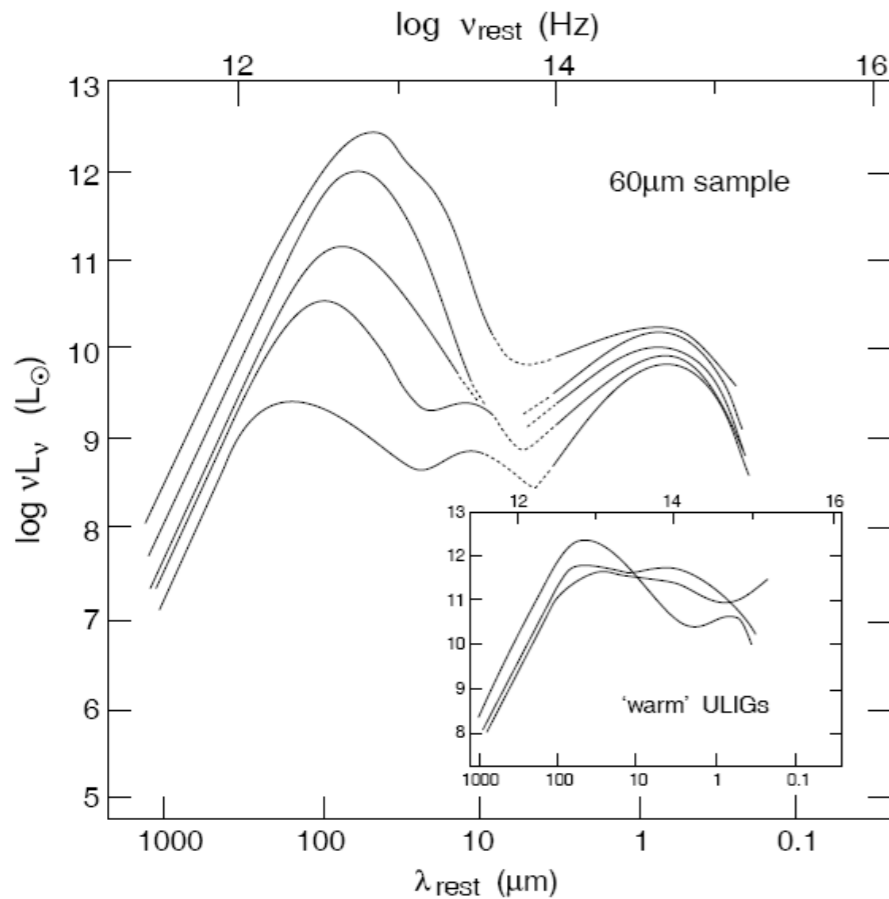
more luminous and massive galaxies are (much) more obscured: for starbursts and (U)LIRGs a de-reddening of the UV-emission does not succeed: the central starburst is behind a 'black screen' and the UV emission comes from a lower obscuration component; even de-reddened Hα fails by about a factor of 10; ULIRGs/starbursts often have 'post-starburst' UV/optical SEDs while the real starburst is completely hidden

Sanders & Mirabel 1996, Meurer et al. 1999,Wuyts et al. 2011

Some Results from our Semi-Analytic Models

z=0-2 Luminosity Density
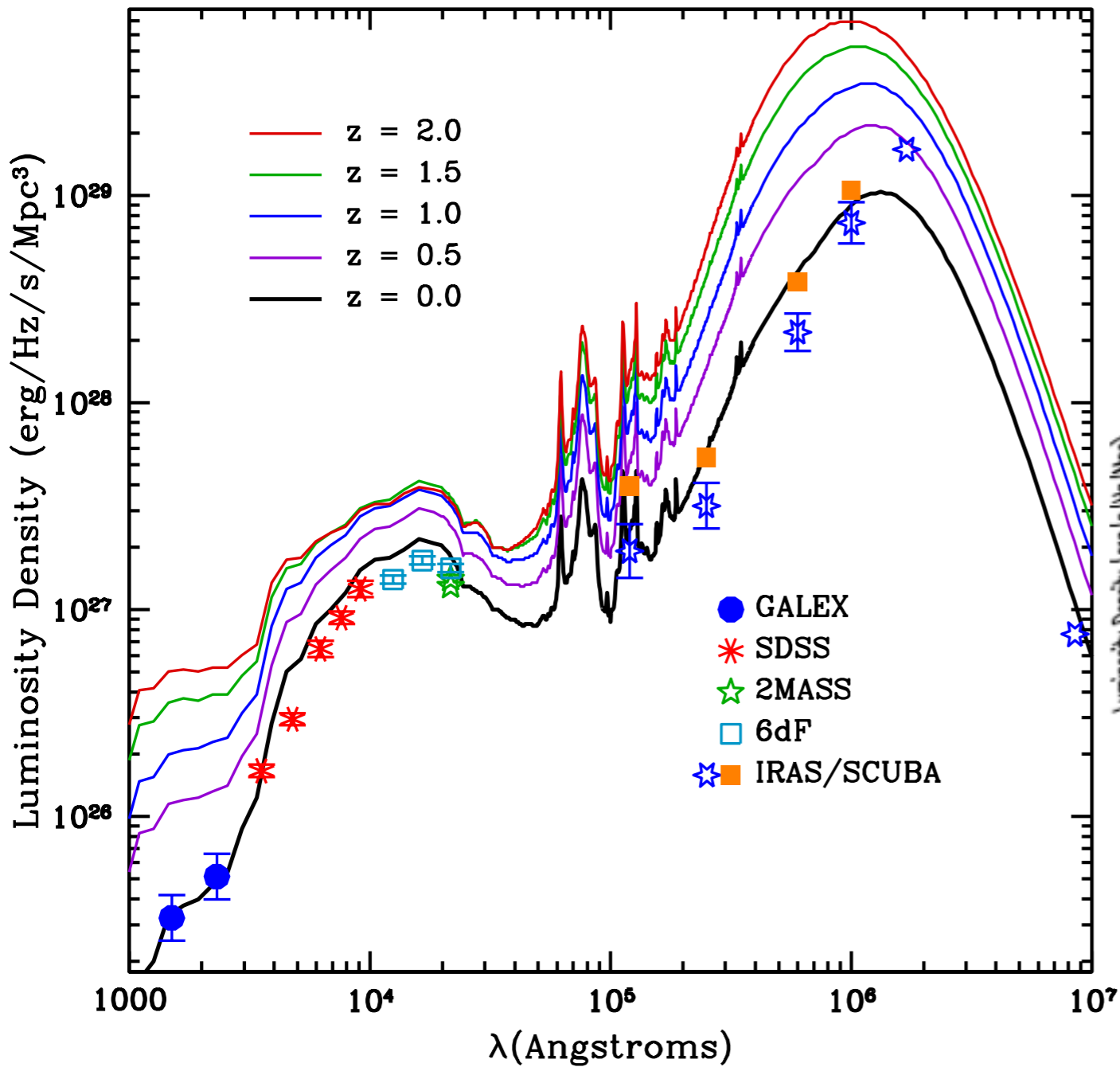
z=0-8 Luminosity Density

Somerville, Gilmore, Primack, & Dominguez (2012)   Gilmore, Somerville, Primack, & Dominguez (2012)
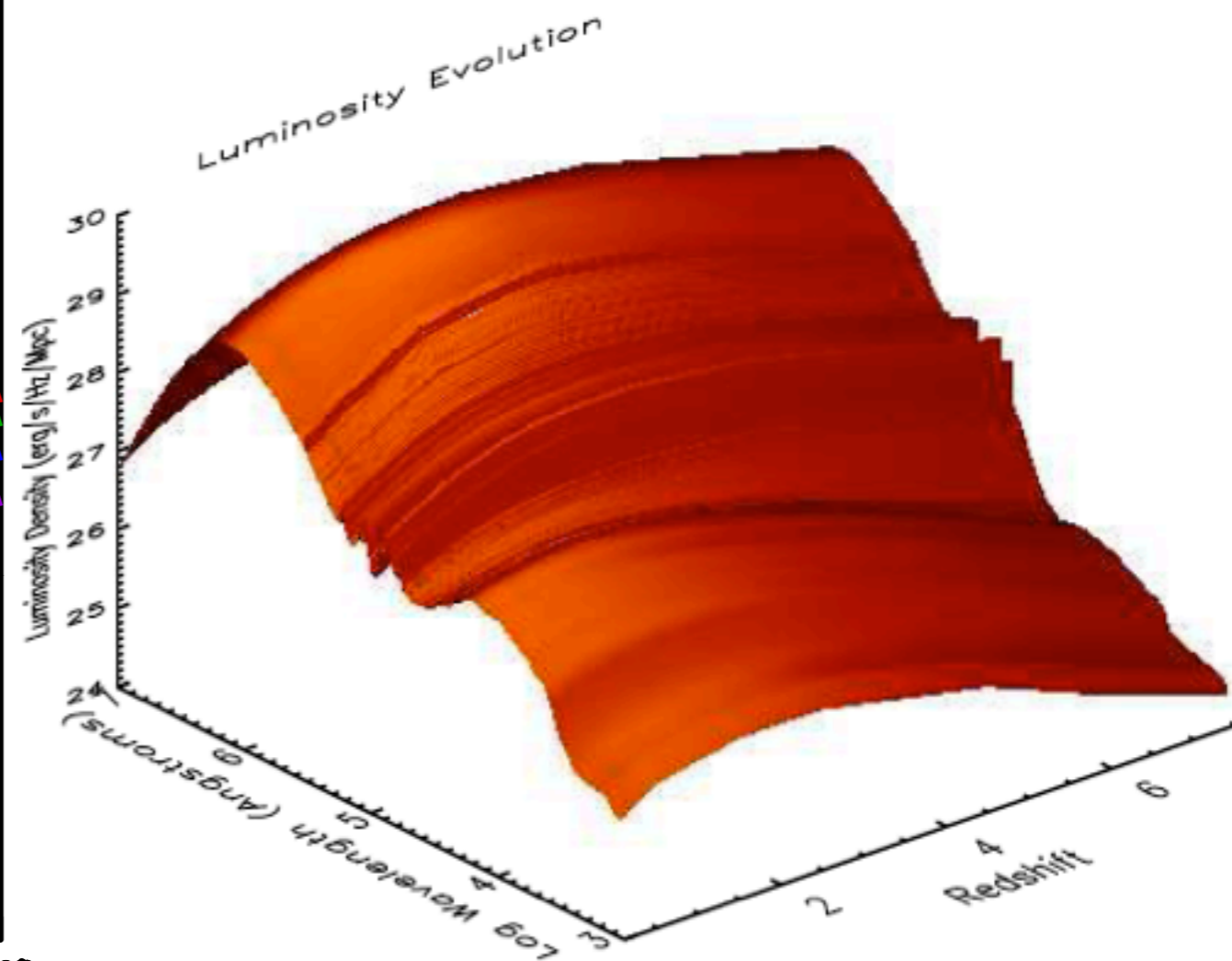
Some Results from our Semi-Analytic Models
z=0 Luminosity Functions

Fiducial
CΛCDM
Calzetti dust
no dust

Somerville,
Gilmore,
Primack, &
Dominguez
(2012)
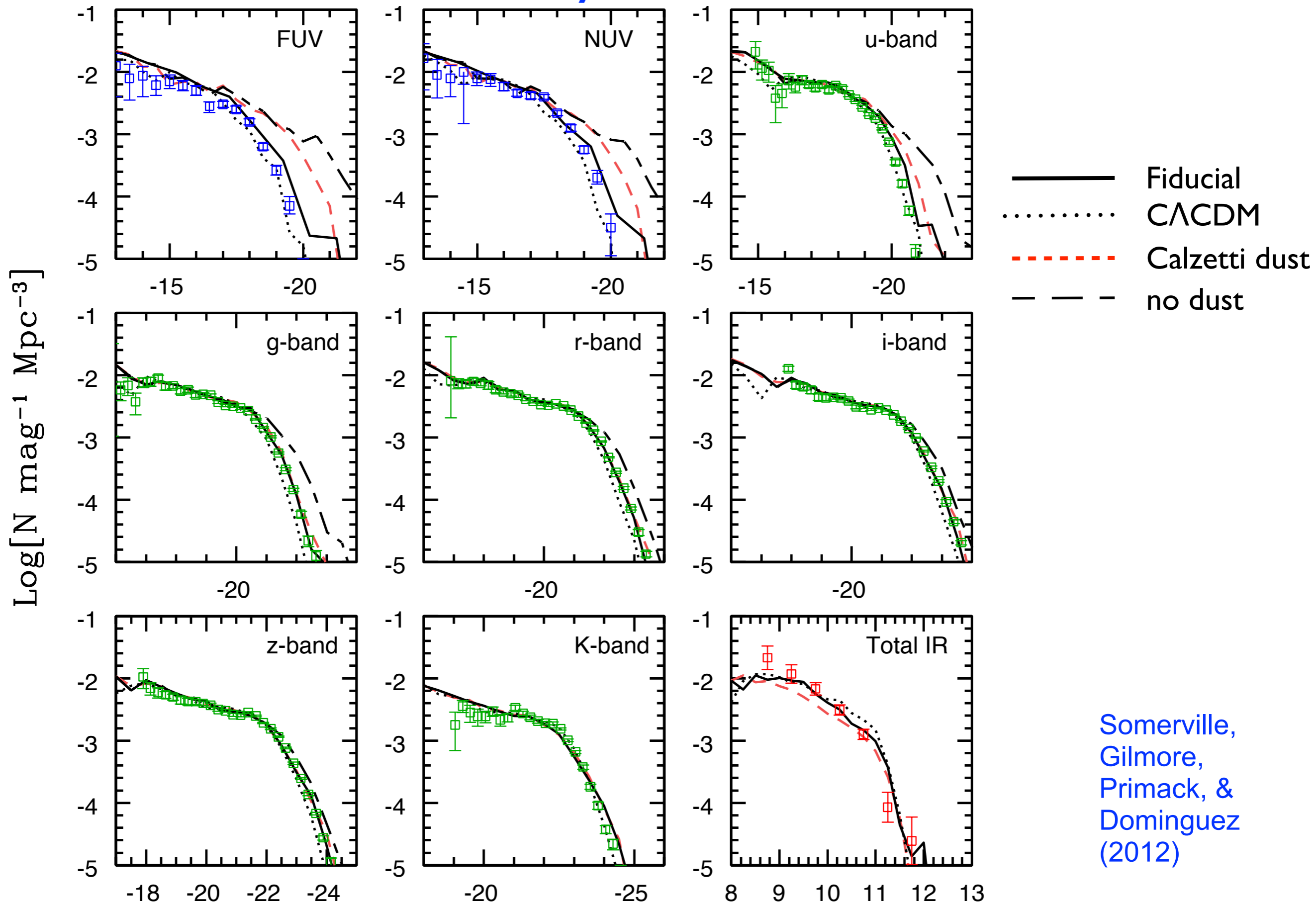
Some Results from our Semi-Analytic Models

Number Counts in UV, b, i, z, K Bands

Number Counts in 3.6, 8, 24, 70, 250, & 850 μm Bands
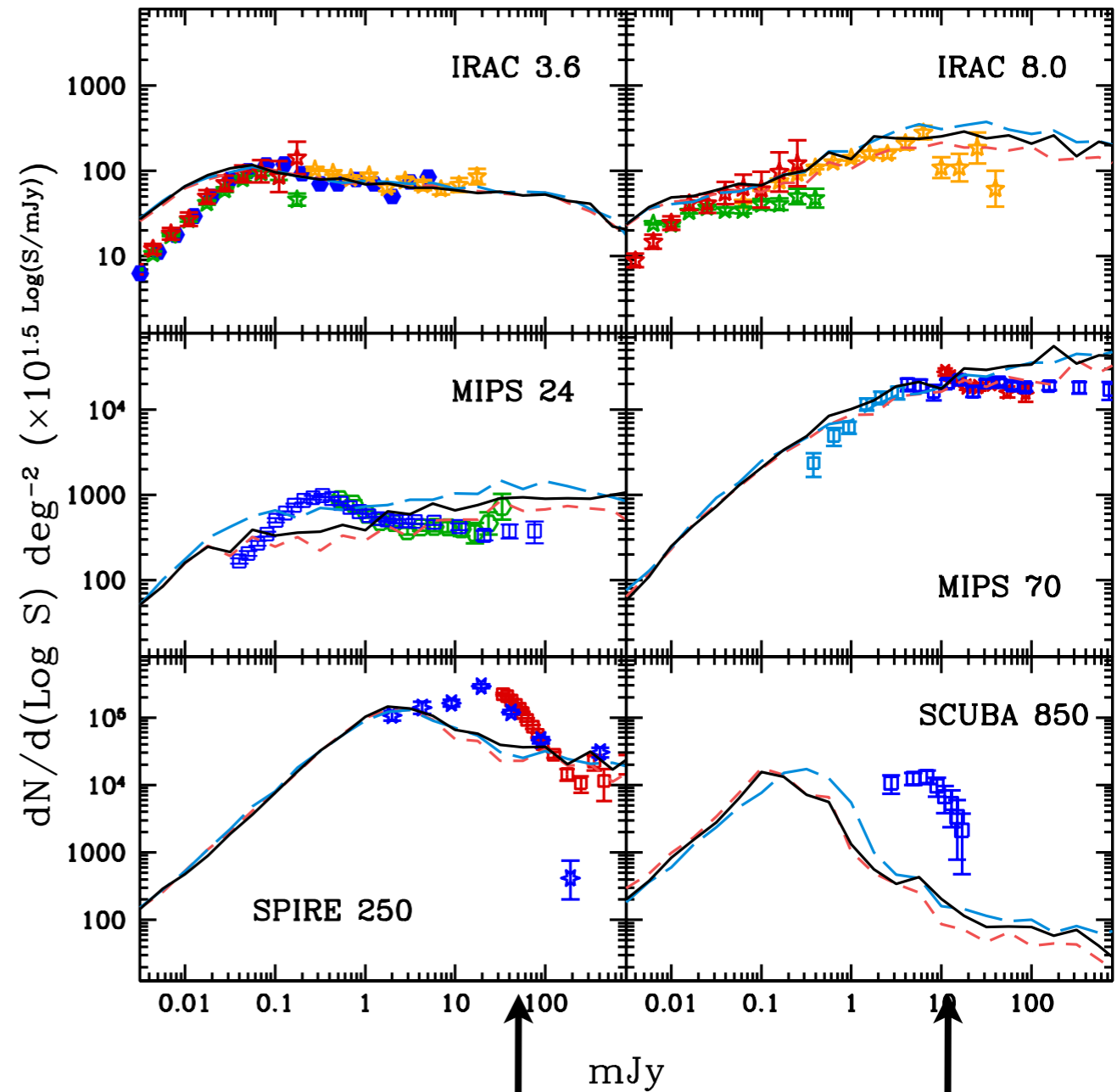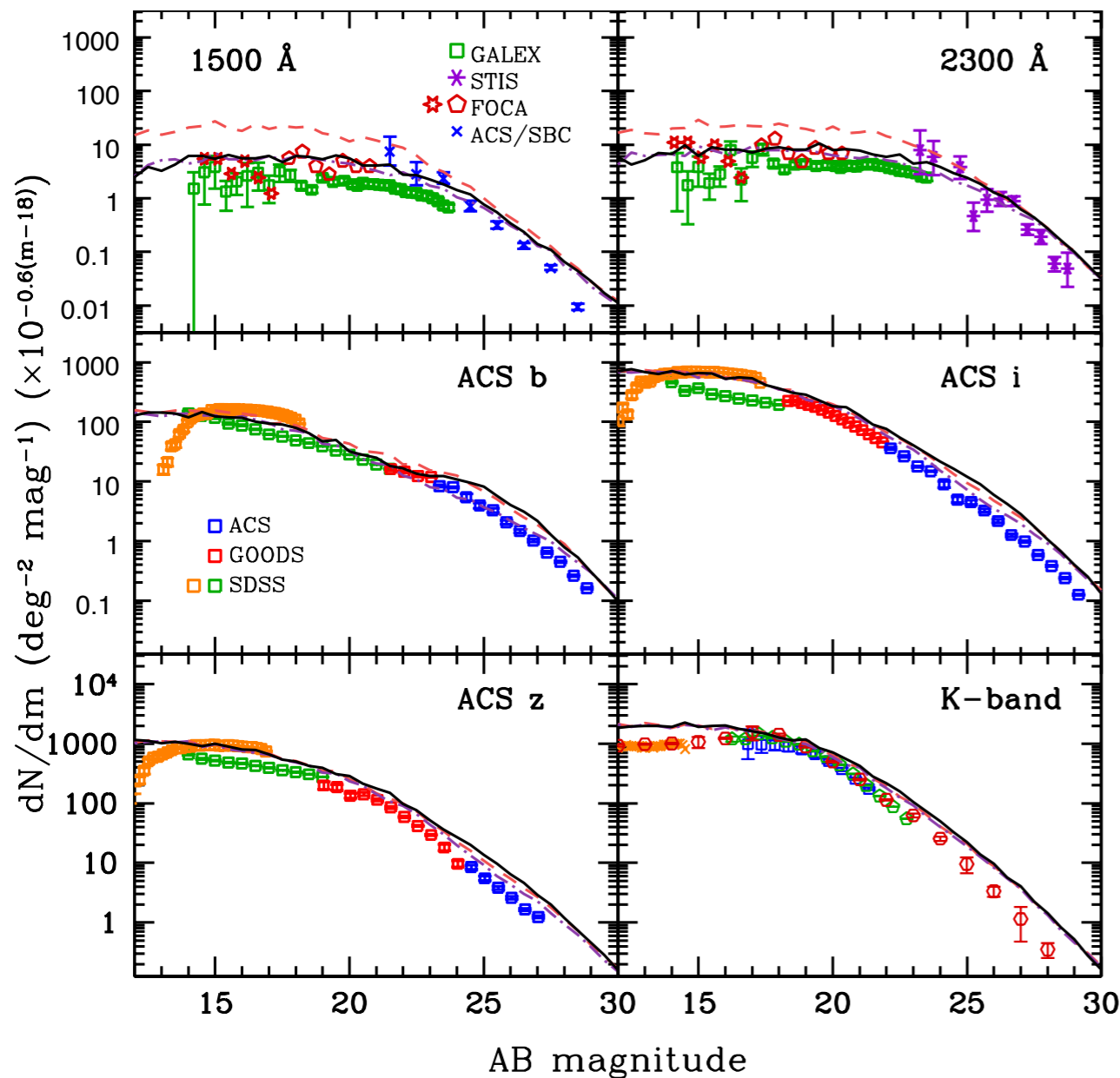
Somerville, Gilmore, Primack, & Dominguez (2012)

Far-IR problems

PILLAR OF STAR BIRTH
Carina Nebula in UV Visible Light

WFC3/UVIS

PILLAR OF STAR BIRTH
Carina Nebula in IR Light

Longer wavelength light penetrates the dust better

Longer wavelength gamma rays also penetrate the EBL better

WFC3/IR

Extragalactic Background Light (EBL)

blazar

$$\gamma_{ev} + \gamma_{TeV}$$
$$= 1 \text{ MeV in CM}$$
$$= e+ \ e- \ \text{pair}$$

FERMI Telescope

VERITAS

Data from (non-) attenuation of gamma rays from blazars and gamma ray bursts (GRBs) give upper limits on the EBL from the UV to the mid-IR that are only a little above the lower limits from observed galaxies. New data on attenuation of gamma rays from blazars now lead to statistically significant measurements of the cosmic gamma ray horizon (CGRH) as a function of source redshift and gamma ray energy that are independent of EBL models. These new measurements are consistent with recent EBL calculations based both on multiwavelength observations of thousands of galaxies and also on semi-analytic models of the evolving galaxy population. Such comparisons account for (almost) all the light, including that from galaxies too faint to see.

$$\gamma_{\mathbf{eV}} + \gamma_{\mathbf{TeV}} \longrightarrow \mathbf{e^+e^-}$$

$$= 1 \text{ MeV in CM}$$

$$\sigma\left(\gamma\gamma \to e^+e^-\right) = \left(\frac{4\pi\alpha^2}{s}\right)\left[\ln\left(\frac{s}{m^2}\right) - 1\right]$$

The energy threshold for this process is $s_{th} = 4m_e^2$, and $\sigma \sim \beta\alpha^2/s$, where $\beta = (1 - 4m_e^2/s)^{\frac{1}{2}}$ is the CM velocity of the produced electron and positron. This process is the main way that high energy gamma rays from blazars are removed on their way to us, by interacting with low-energy photons ("extragalactic background light," EBL) radiated as starlight or as radiation from cool dust, and producing e^+e^- pairs.

Energetic gamma rays (dashed lines) from a distant blazar strike photons of extragalactic background light (wavy lines) in intergalactic space, annihilating both gamma ray and photon. Different energies of EBL photons waylay different energies of gamma rays, so comparing the attenuation of gamma rays at different energies from different spacecraft and ground-based instruments indirectly measures the spectrum of EBL photons.
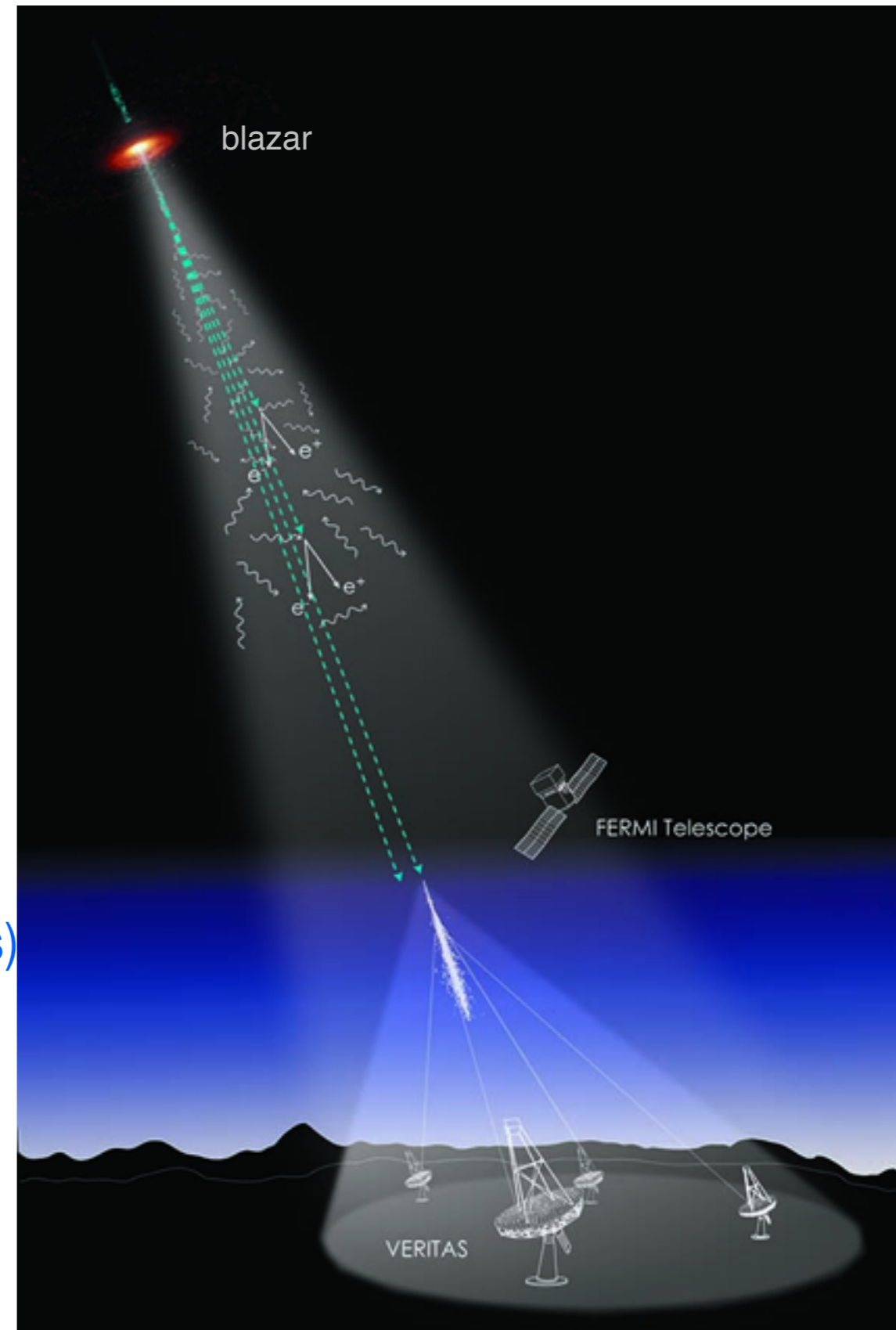
Early Atmospheric Cherenkov Telescopes
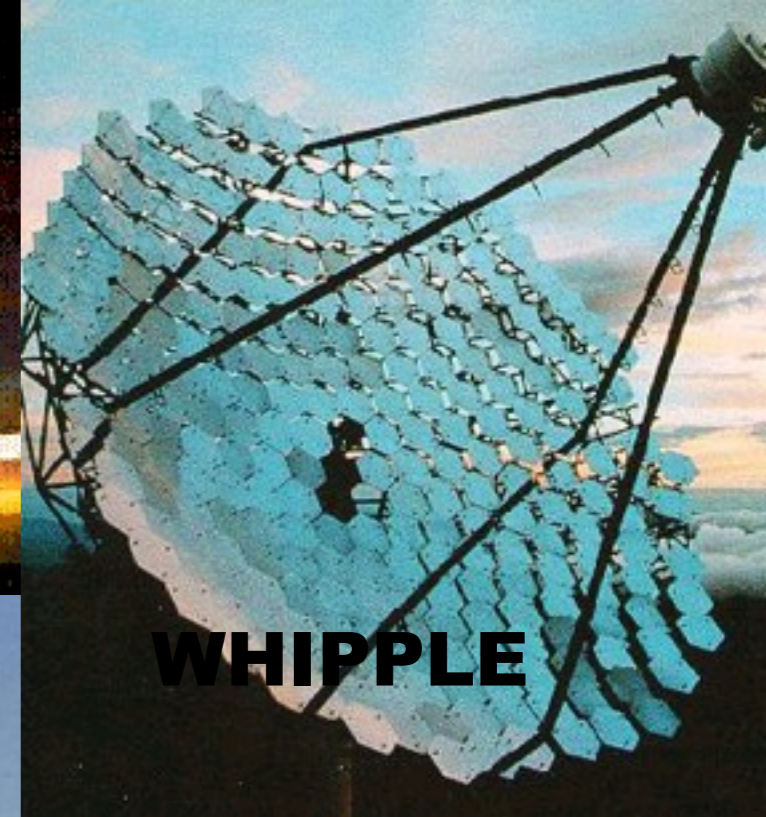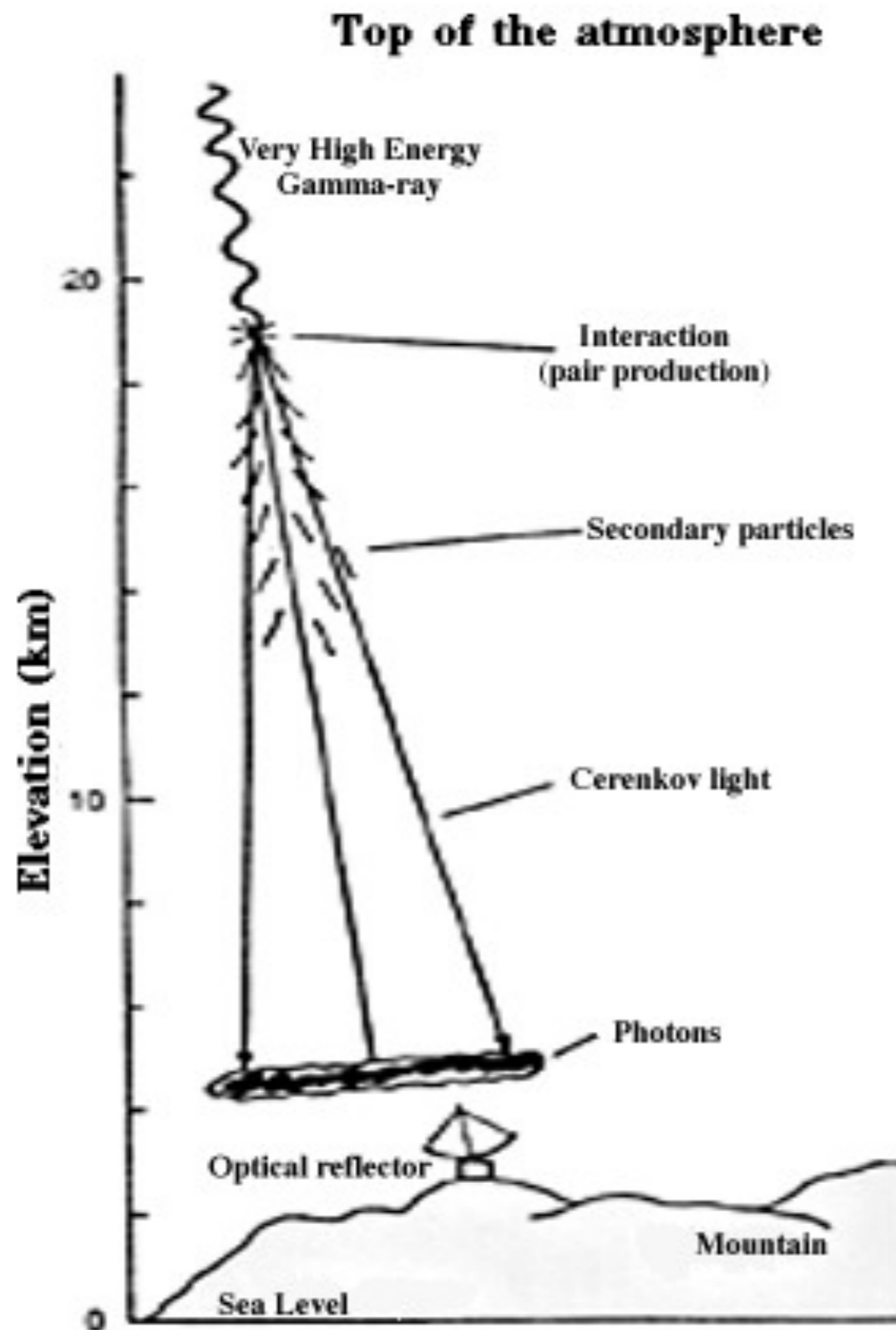
Ground and Space Based Telescopes

Ground-based Gamma Ray Telescopes
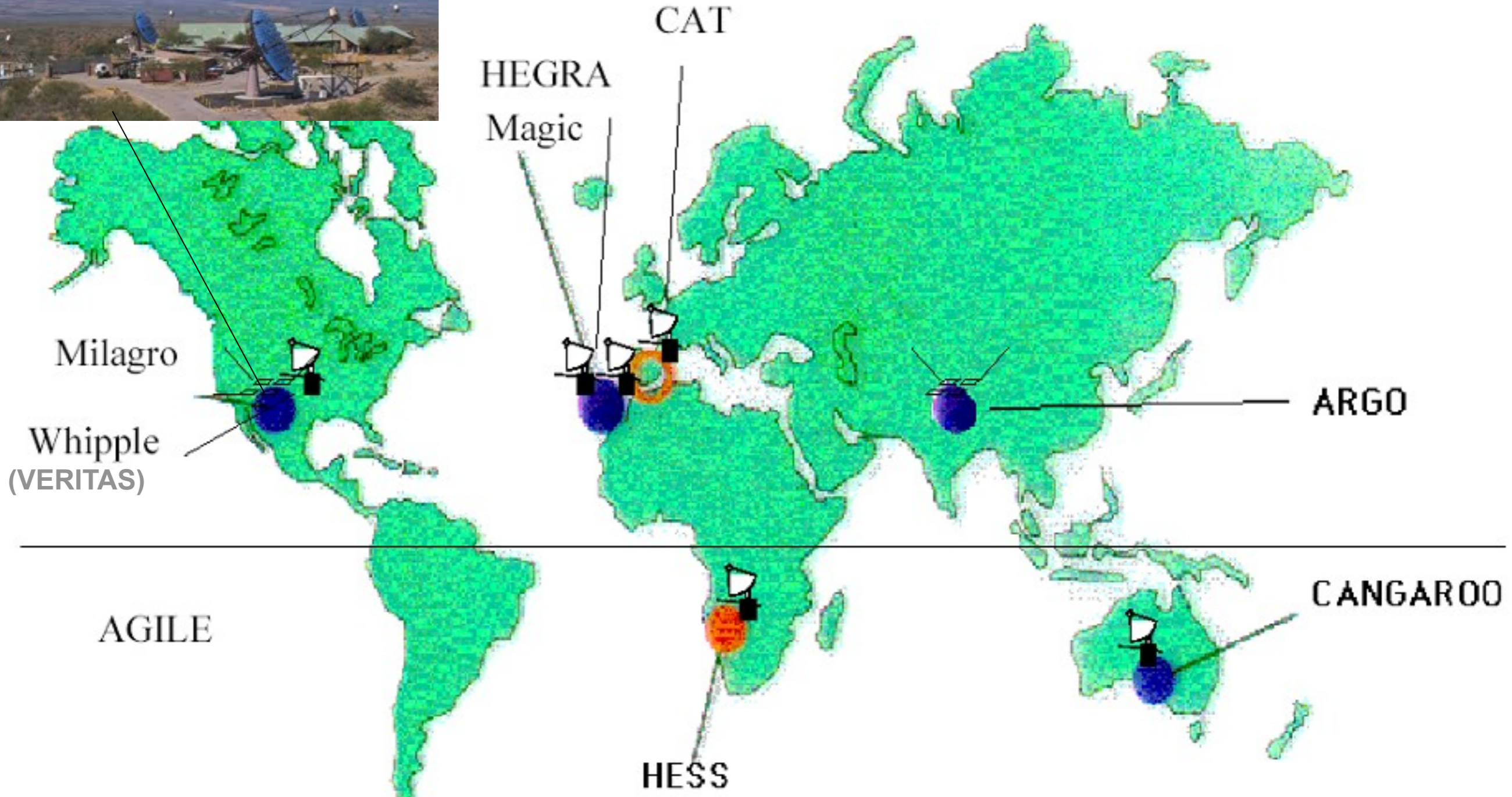
H.E.S.S.: High Energy Stereoscopic System

- Array 4 telescopes,   diam. ~12 m
- Field of view   ~5°
- Spatial resolution (single photon): ~ 6 '
  (with hard cuts) ~ 4 '

- Energy resolution   ~15%
- Location: Namibia, 1800 m asl
  Coord.: 23°16' S, 16°30' E
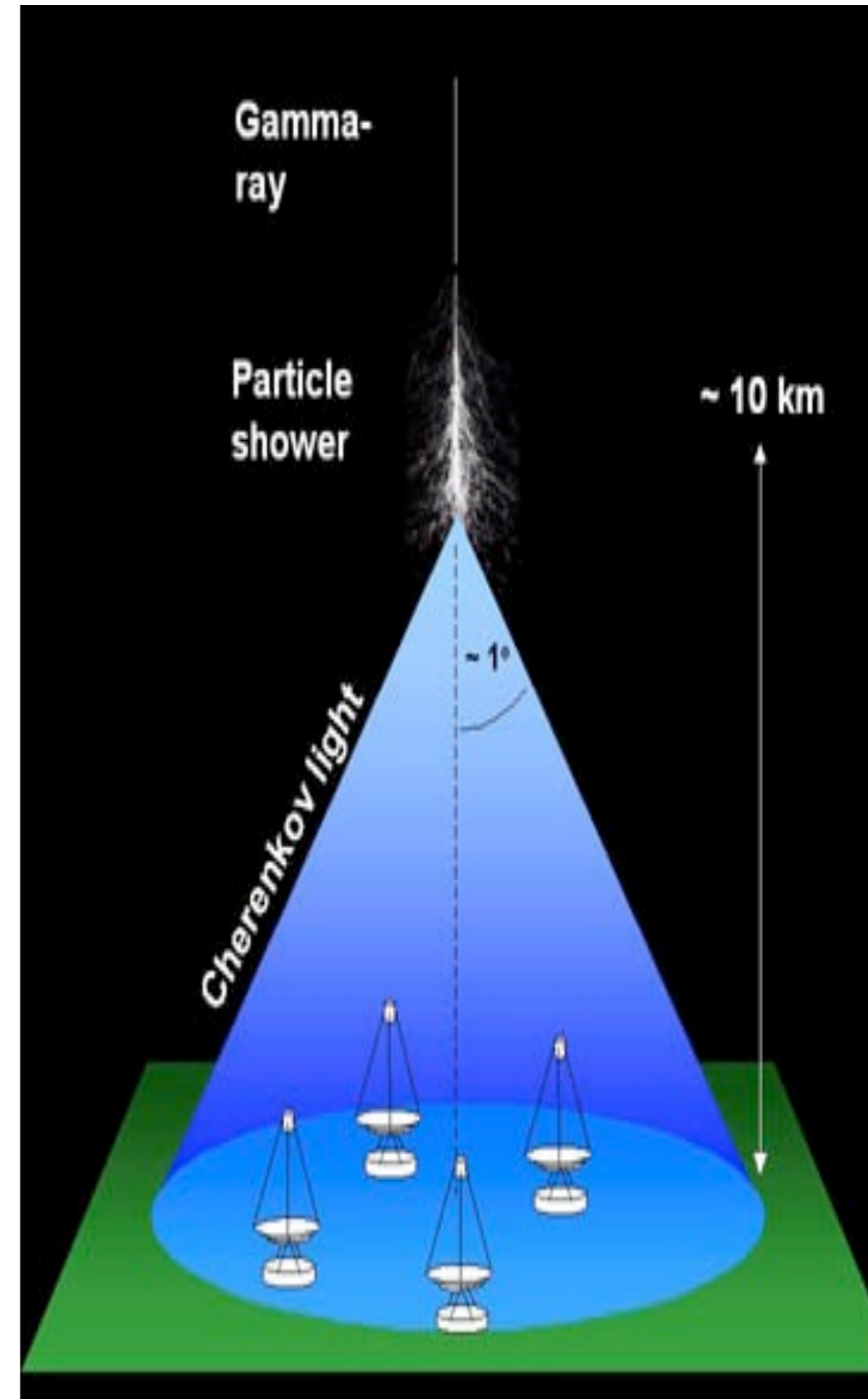
Victor Hess
1912 balloon flight to 6 km: "cosmic ray" intensity increased with altitude

Gamma-ray

Particle shower

~ 10 km

~ 1°

Cherenkov light

H.E.S.S.: High Energy Stereoscopic System

Star

Reconstructed direction
of primary gamma ray

Superposition of
camera images

Cone of
Cerenkov light

~10 km

~240 meters
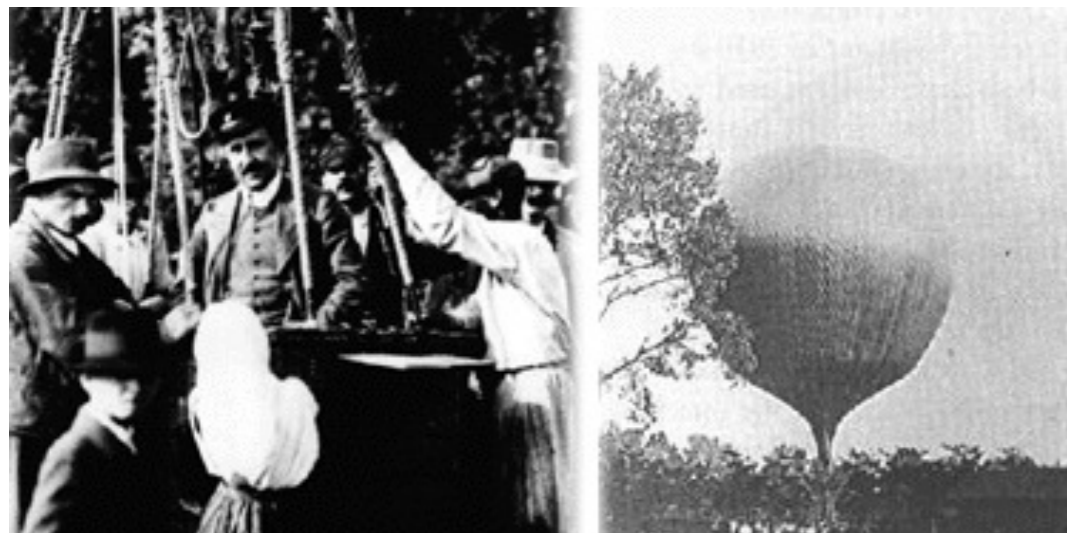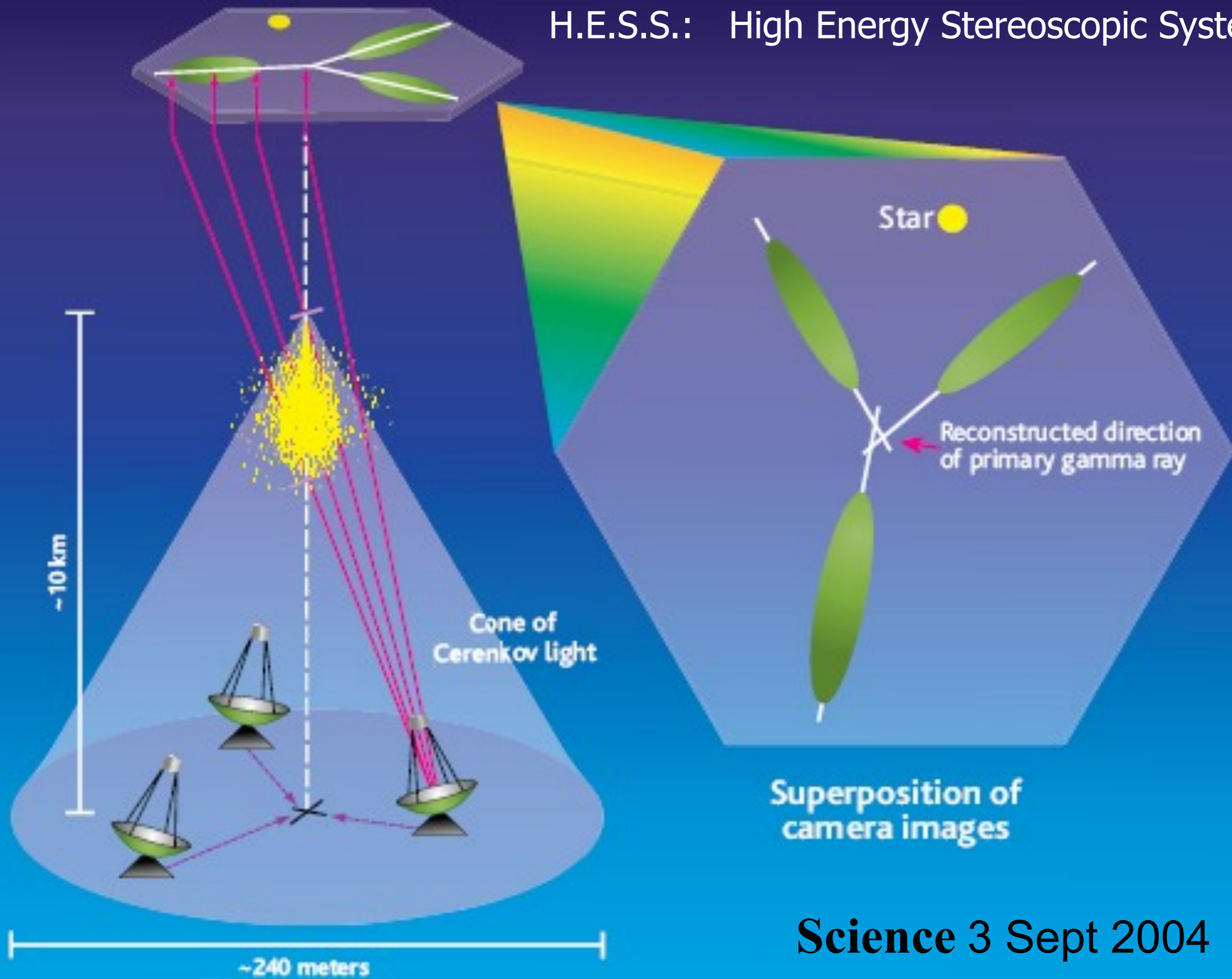
Science 3 Sept 2004

Gamma Ray Attenuation due to γγ → e+e-

Illustration: Mazin & Raue

$$\frac{dN}{dE}\bigg|_{obs} = \frac{dN}{dE}\bigg|_{int} \exp\left[-\tau(E, z)\right]$$
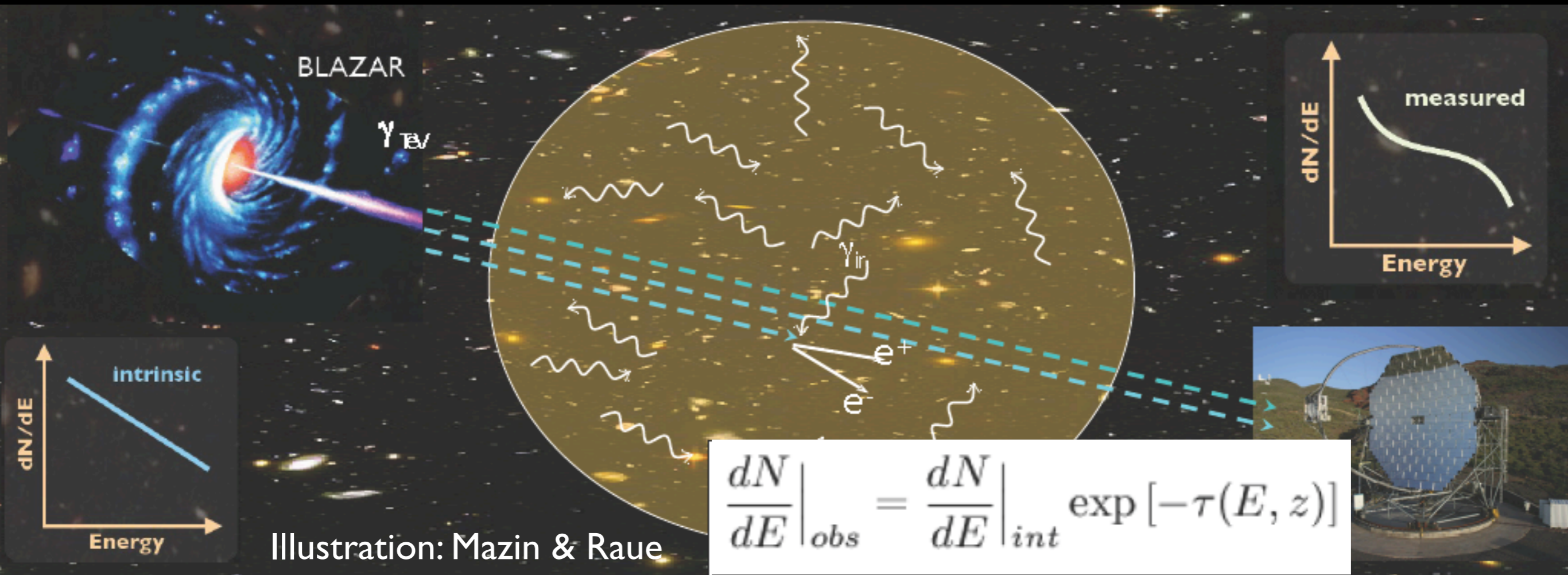
If we know the intrinsic spectrum, we can infer the optical depth $\tau(E,z)$ from the observed spectrum. In practice, we typically *assume* that $dN/dE|_{int}$ is not harder than $E^{-\Gamma}$ with $\Gamma = 1.5$, since local sources have $\Gamma \geq 2$. More conservatively, we can assume that $\Gamma \geq 2/3$.

EBL Observations & Theory

Extragalactic Background Light

Legend:
- Domínguez+ 11
- Franceschini+ 08
- Gilmore+ 12
- Aharonian+ 06
- Mazin & Raue 07 - realistic
- Mazin & Raue 07 - extreme
- Albert+ 08
- Schlegel+ 98
- Hauser+ 98
- Finkbeiner+ 00
- Lagache+ 00
- Gardner+ 00
- Gorjian+ 00
- Cambrésy+ 01
- Madau & Pozzetti 01
- Metcalfe+ 03
- Chary+ 04
- Fazio+ 04; Franceschini+ 08
- Xu+ 05
- Matsumoto+ 05
- Frayer+ 06
- Bernstein+ 07
- Levenson & Wright 08
- Matsuura+ 10
- Hopwood+ 10
- Béthermin+ 10
- Berta+ 10
- Keenan+ 10
- Matsuoka+ 11
- Mattila+ 11

$\Gamma \geq 1.5$
$\Gamma \geq 1.5$
$\Gamma \geq 2/3$
$\Gamma \geq 1.5$

Axis labels: λI_λ [nW m^{-2} sr^{-1}], λ [μm]

Thursday, March 13, 14

Evolution of the EBL

The evolution of the EBL in our WMAP5 Fiducial model. This is plotted on the left panel in standard units. The right panel shows the build-up of the present-day EBL by plotting the same quantities in comoving units. The redshifts from 0 to 2.5 are shown by the different line types in the key in the left panel.

Gilmore, Somerville, Primack, & Domínguez (2012)

Predicted Gamma Ray Attenuation
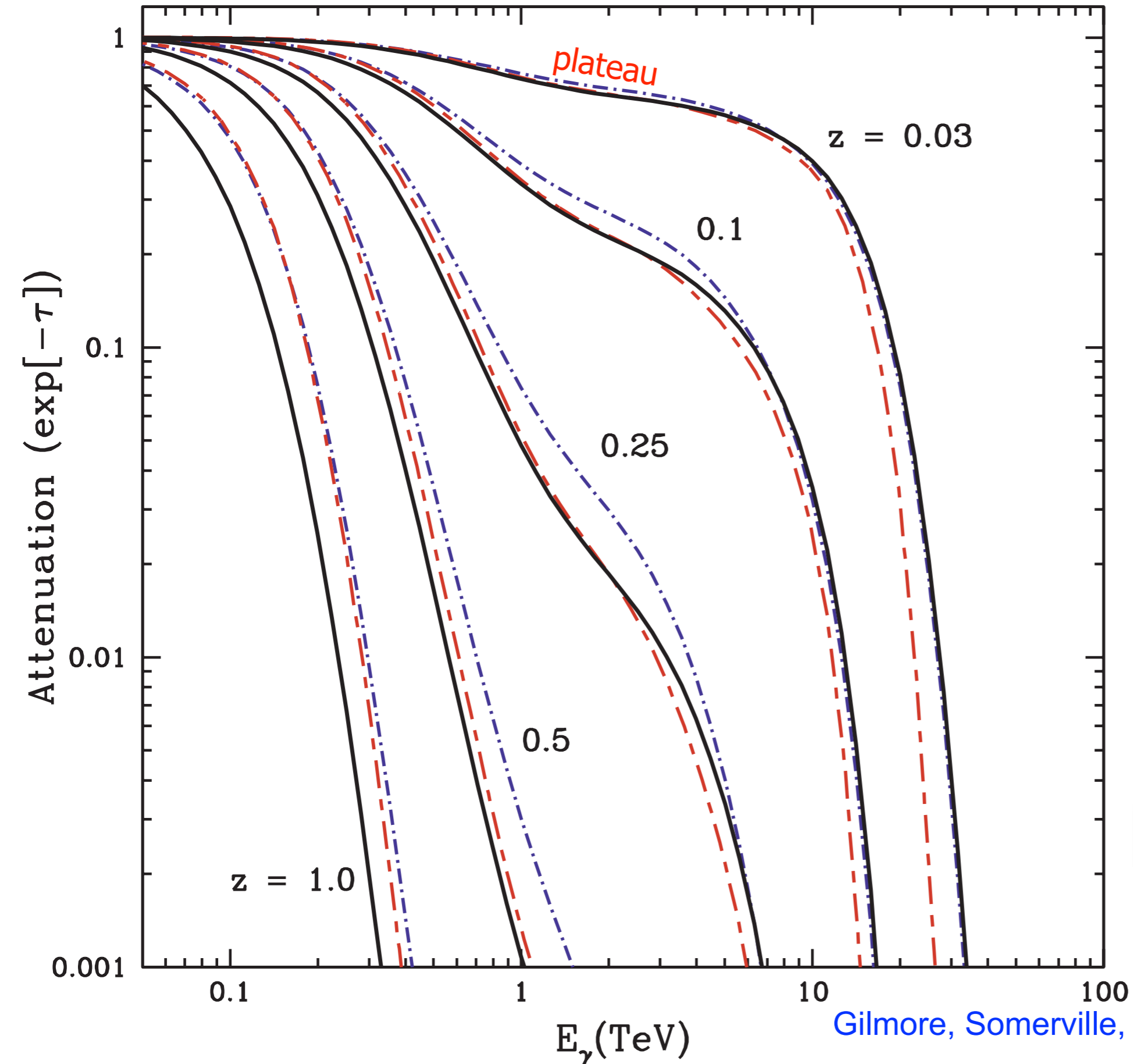
Increasing distance causes absorption features to increase in magnitude and appear at lower energies. The plateau seen between 1 and 10 TeV at low z is a product of the mid-IR valley in the EBL spectrum.
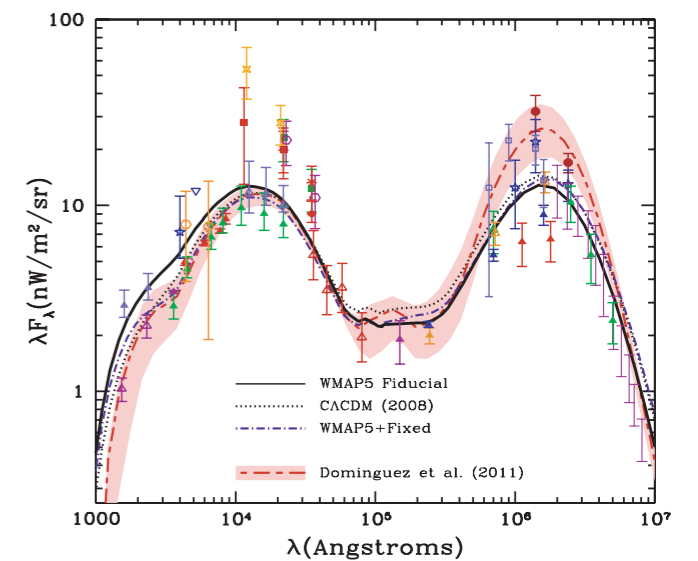
WMAP5 Fiducial
WMAP5 Fixed
Domiínguez+11

Gilmore, Somerville, Primack, & Domínguez (2012)

Predicted Gamma Ray Attenuation

The Cosmic Gamma Ray Horizon is the observed gamma ray energy as a function of redshift where the attenuation is $1/e = 0.368$

z = 0.03

0.1

0.25

0.5

z = 1.0

Attenuation $(\exp[-\tau])$

E_γ(TeV)

WMAP5 Fiducial
WMAP5 Fixed
Domiínguez+11
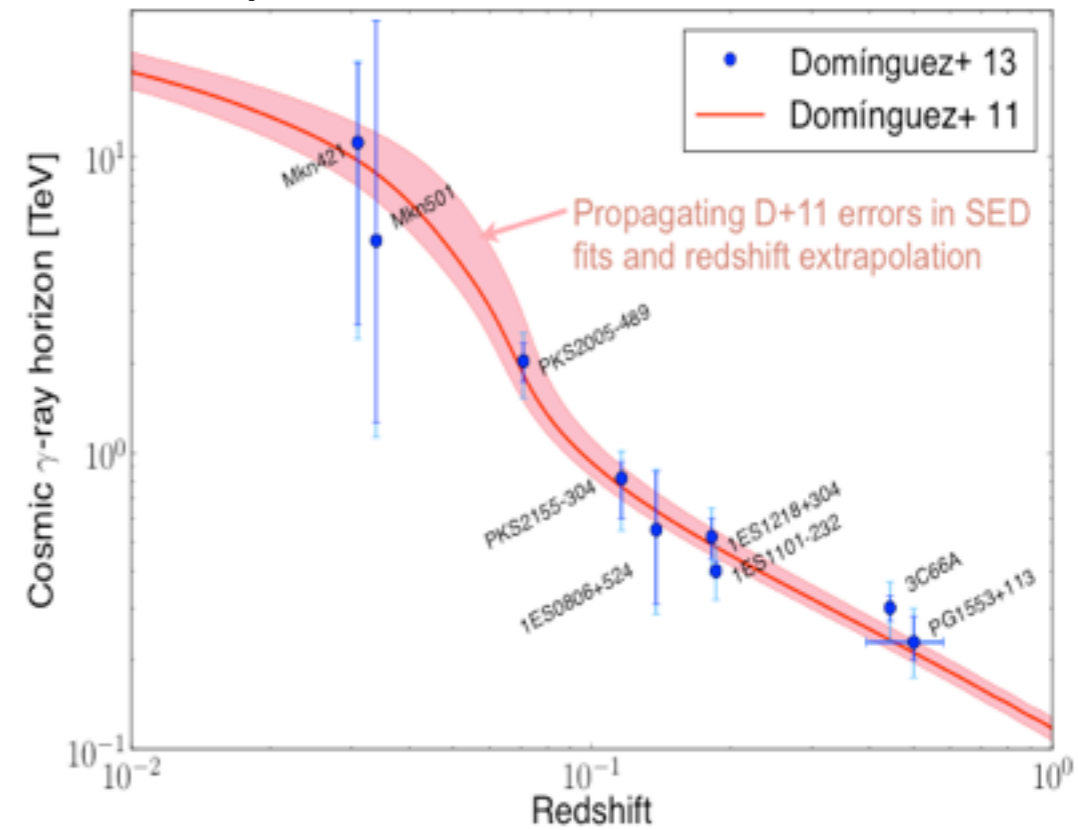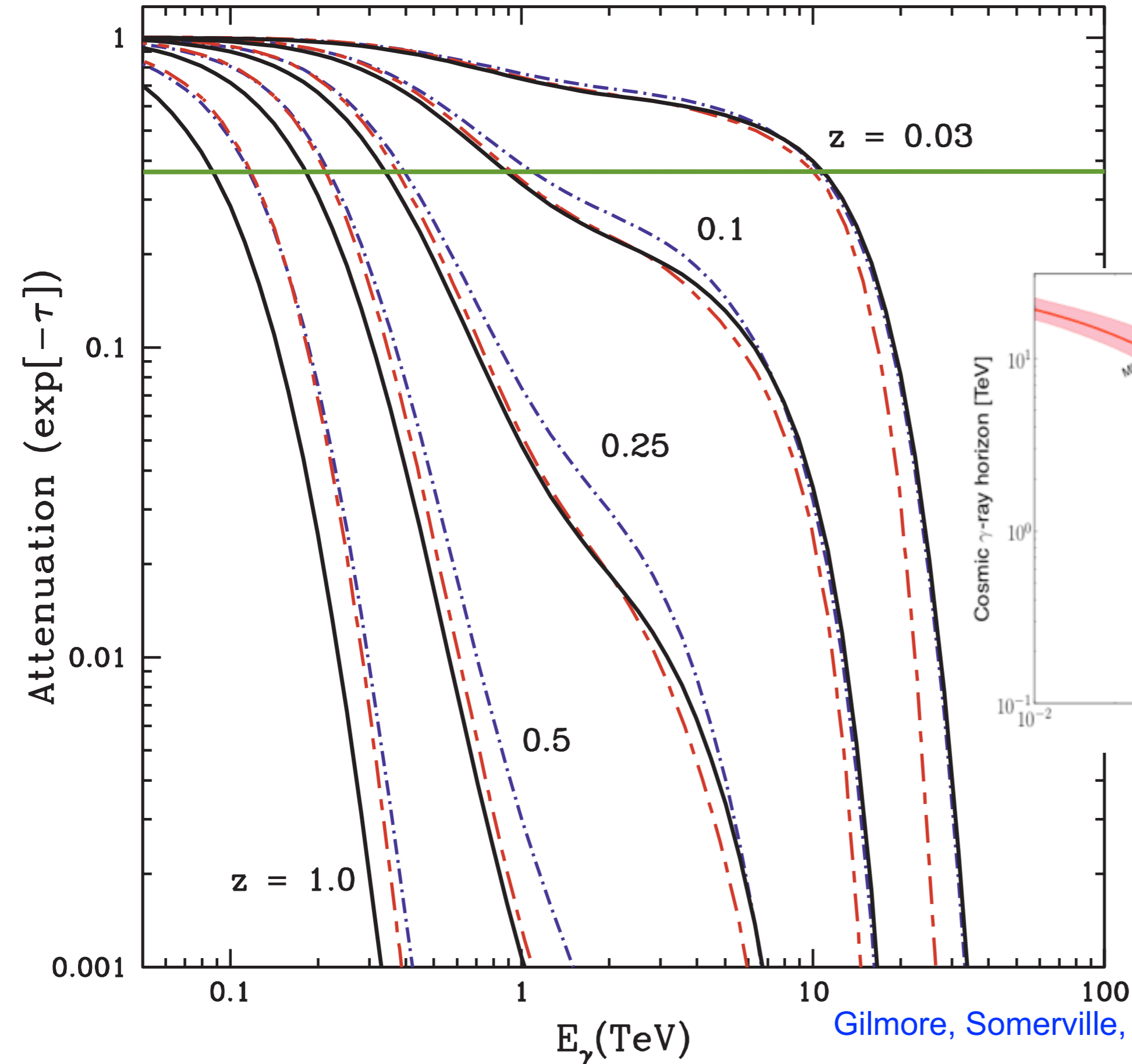
Gilmore, Somerville, Primack, & Domínguez (2012)

Cosmic Gamma-Ray Horizon

With a 50 GeV threshold, we see to z≈1.5-3 with less than 1/e attenuation!
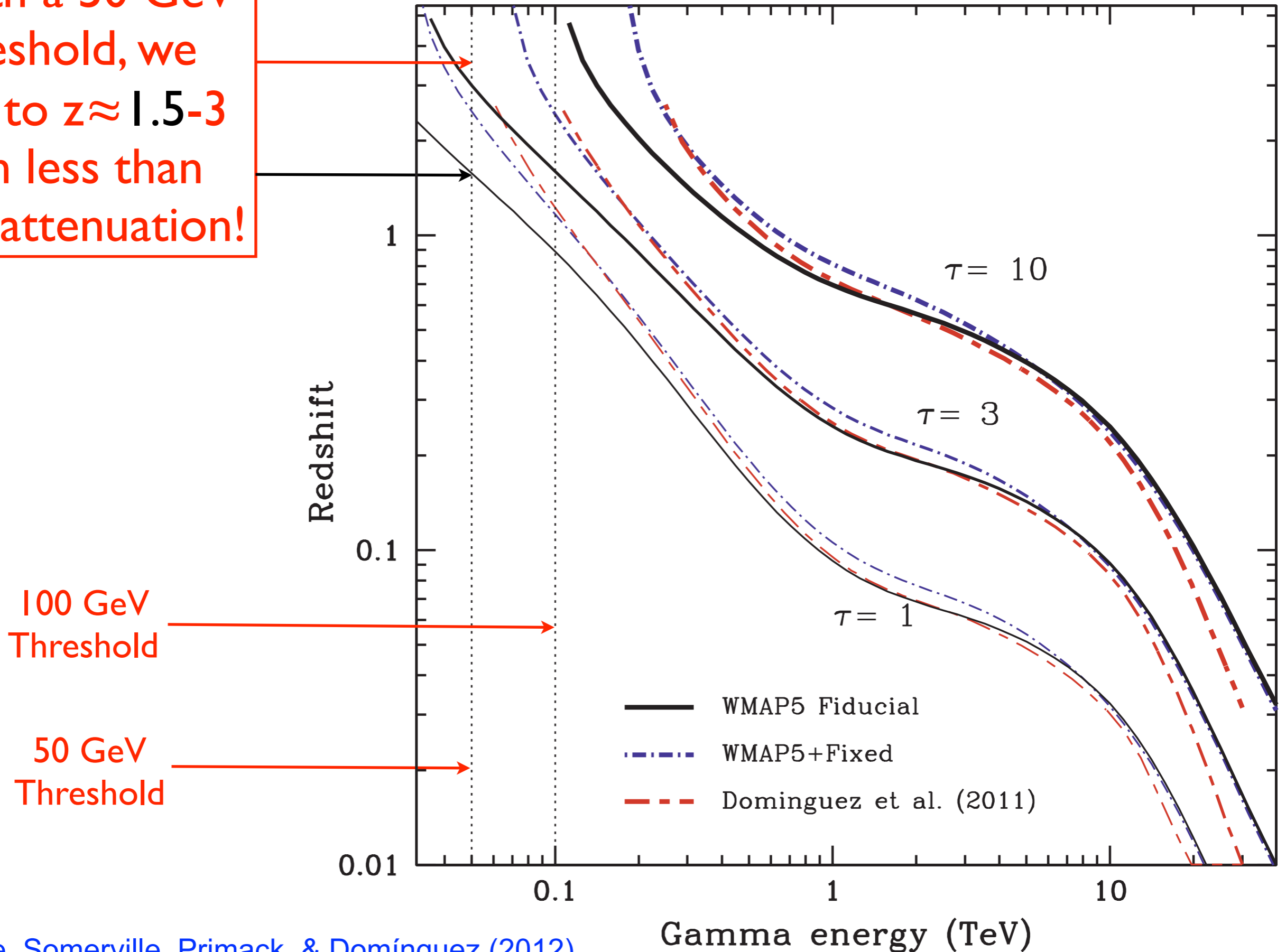
100 GeV Threshold

50 GeV Threshold

$\tau = 10$

$\tau = 3$

$\tau = 1$

Redshift

Gamma energy (TeV)

WMAP5 Fiducial

WMAP5+Fixed

Dominguez et al. (2011)

Gilmore, Somerville, Primack, & Domínguez (2012)

Thursday, March 13, 14

DETECTION OF THE COSMIC γ-RAY HORIZON FROM MULTIWAVELENGTH OBSERVATIONS OF BLAZARS

ApJ 770, 77 (2013)

A. Domínguez, J. D. Finke, F. Prada, J. R. Primack, F. S. Kitaura, B. Siana, D. Paneque

The first statistically significant detection of the cosmic γ-ray horizon (CGRH) that is independent of any extragalactic background light (EBL) model is presented. The CGRH is a fundamental quantity in cosmology. It gives an estimate of the opacity of the Universe to very-high energy (VHE) γ-ray photons due to photon-photon pair production with the EBL. The only estimations of the CGRH to date are predictions from EBL models and lower limits from γ-ray observations of cosmological blazars and γ-ray bursts. Here, we present synchrotron self-Compton models (SSC) of the spectral energy distributions of 15 blazars based on (almost) simultaneous observations from radio up to the highest energy γ-rays taken with the Fermi satellite. These SSC models predict the unattenuated VHE fluxes, which are compared with the observations by imaging atmospheric Cherenkov telescopes. This comparison provides an estimate of the optical depth of the EBL, which allows a derivation of the CGRH through a maximum likelihood analysis that is EBL-model independent. We find that the observed CGRH is compatible with the current knowledge of the EBL.

Best fit polynomial

Domínguez+11 prediction

1ES1218+304 (fast) ($z = 0.182$) $E_0 = (0.58 \pm 0.02)$ TeV

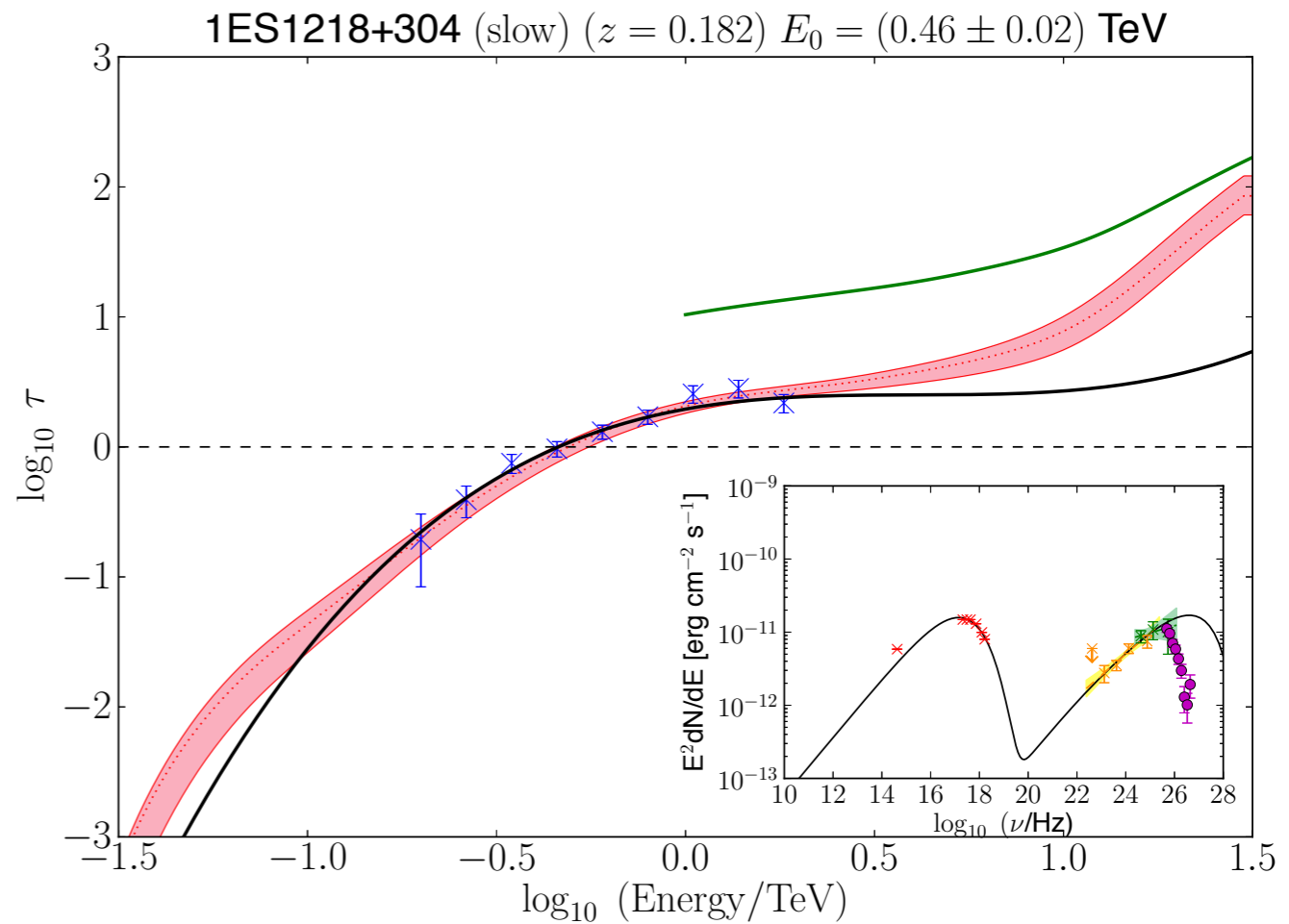1ES1218+304 (slow) ($z = 0.182$) $E_0 = (0.46 \pm 0.02)$ TeV

Thursday, March 13, 14
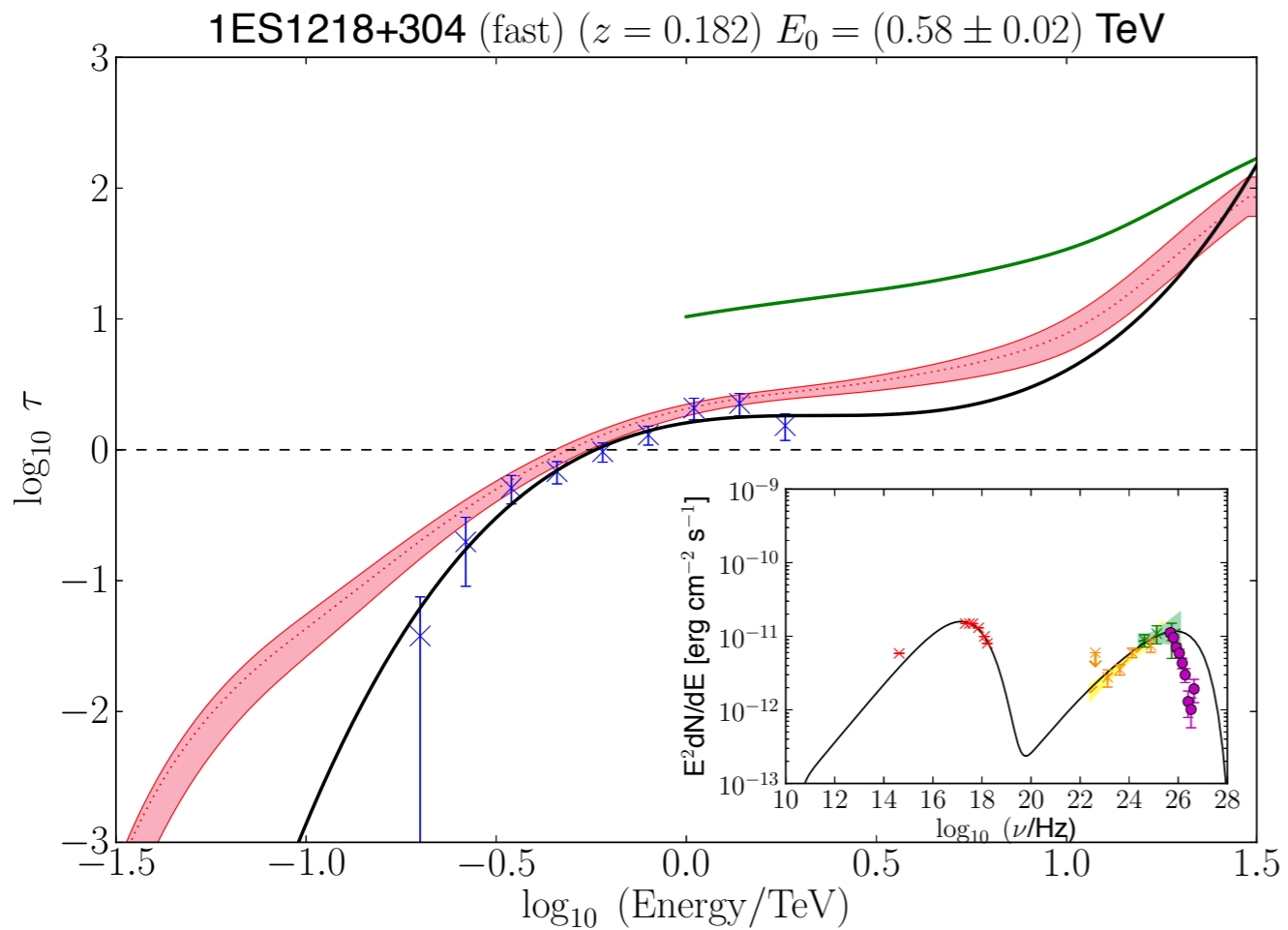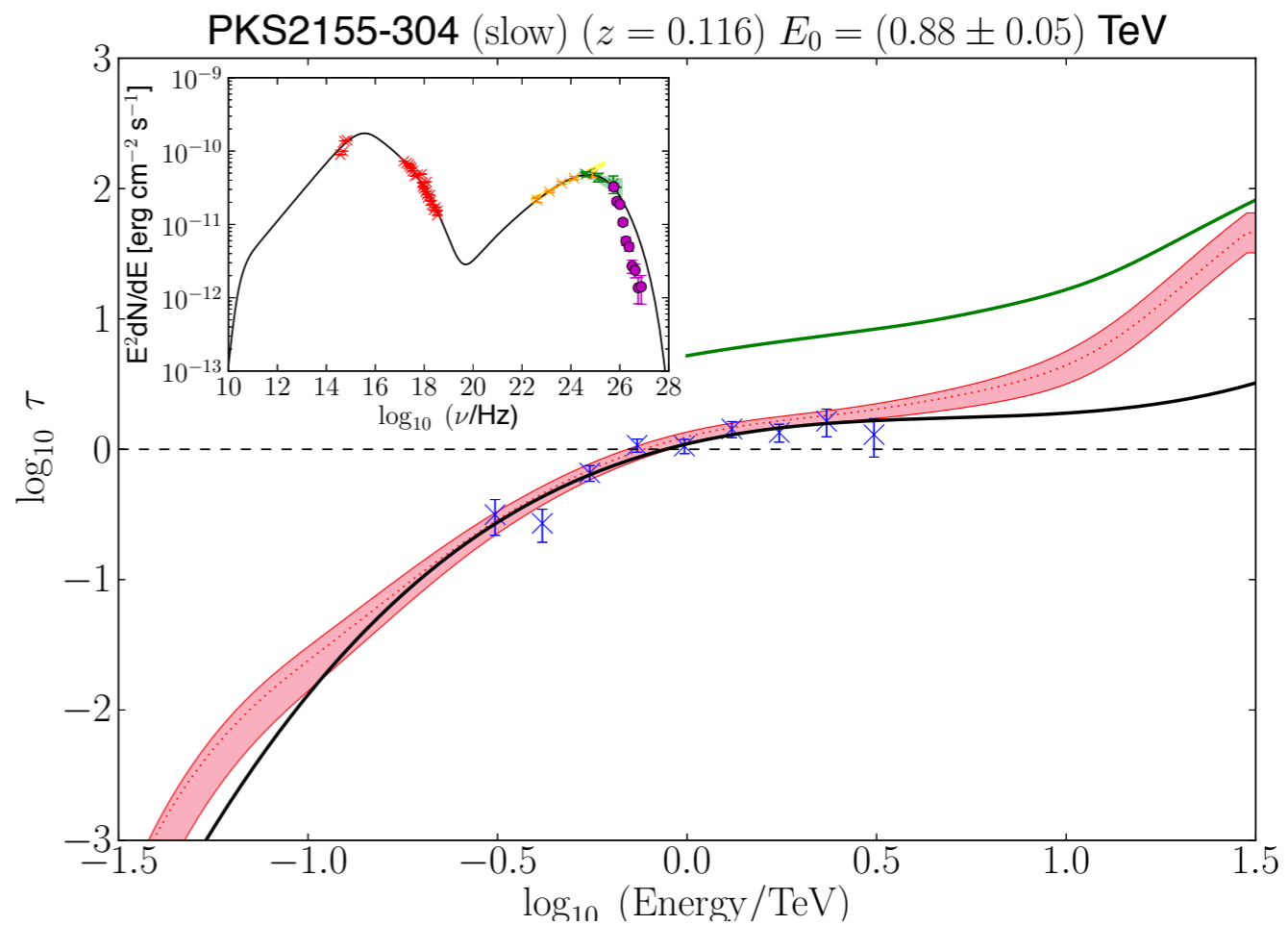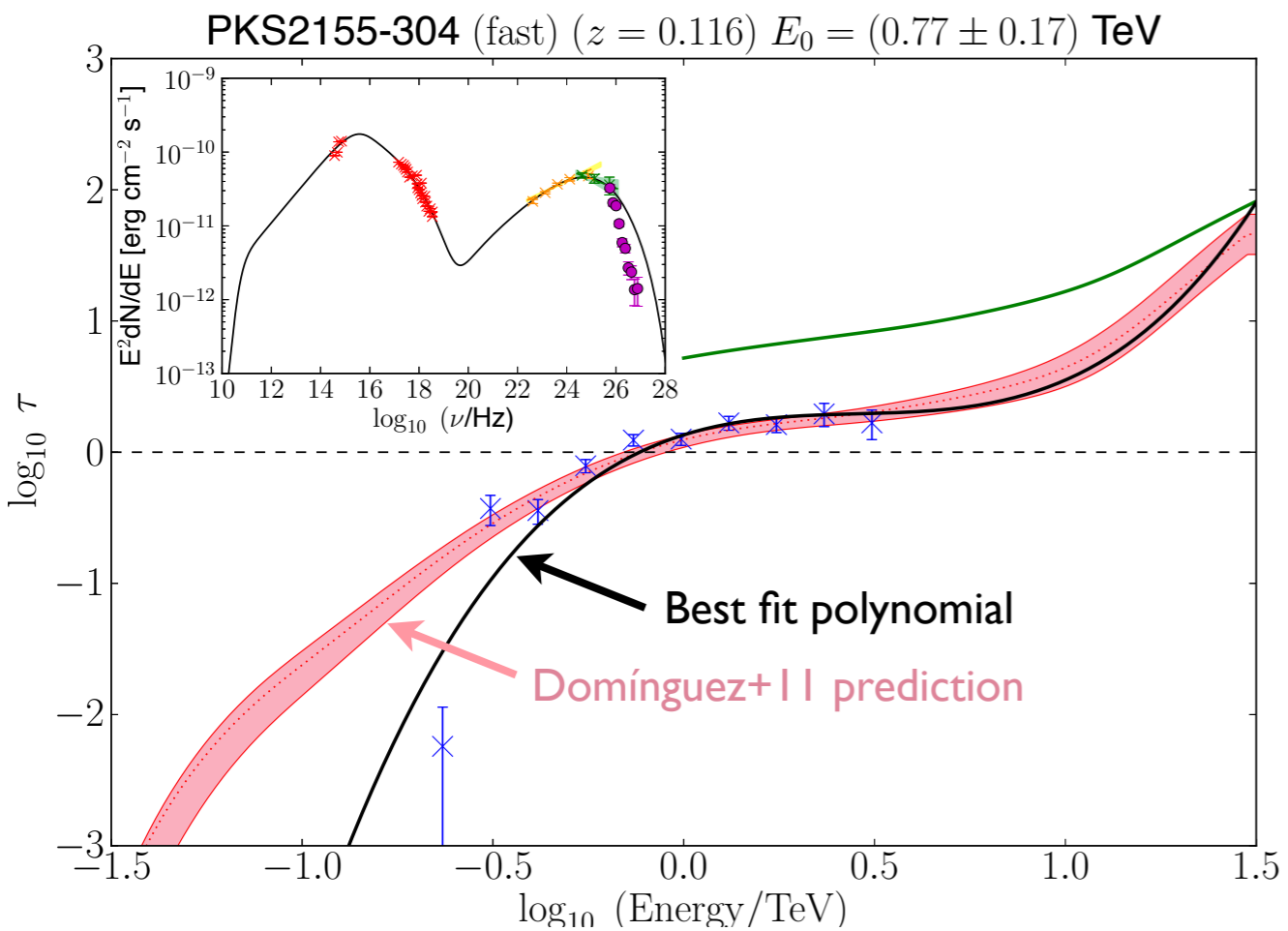
DETECTION OF THE COSMIC γ-RAY HORIZON FROM MULTIWAVELENGTH OBSERVATIONS OF BLAZARS
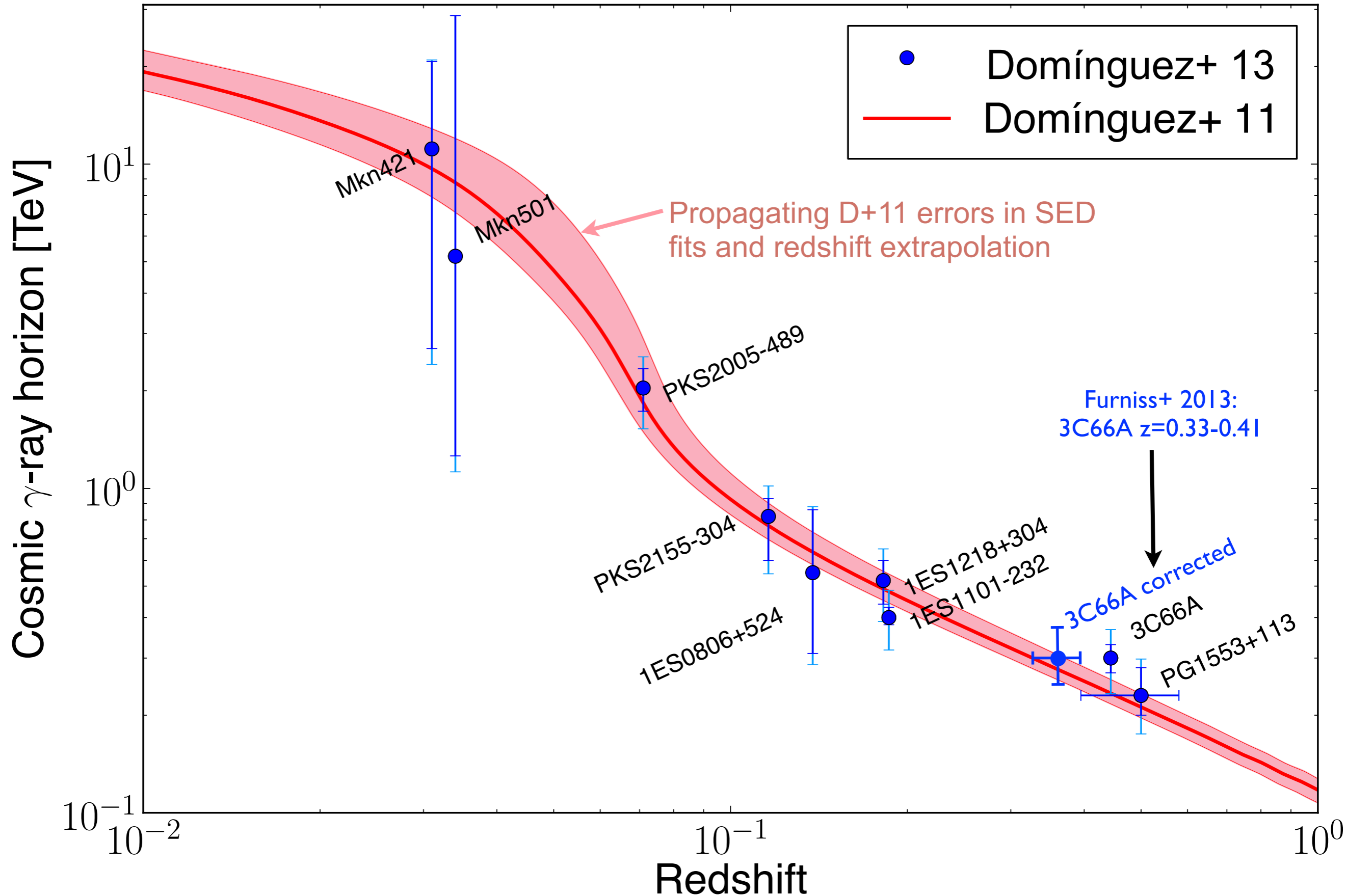
Cosmic Gamma-Ray Horizon Compared with EBL Models

Extragalactic Background Light (EBL)

blazar

$\gamma_{ev} + \gamma_{TeV}$

$= 1$ MeV in CM

$= e+ \ e-$ pair

FERMI Telescope

VERITAS

Data from (non-) attenuation of gamma rays from blazars and gamma ray bursts (GRBs) give upper limits on the EBL from the UV to the mid-IR that are only a little above the lower limits from observed galaxies. New data on attenuation of gamma rays from blazars now lead to statistically significant measurements of the cosmic gamma ray horizon (CGRH) as a function of source redshift and gamma ray energy that are independent of EBL models. These new measurements are consistent with recent EBL calculations based both on multiwavelength observations of thousands of galaxies and also on semi-analytic models of the evolving galaxy population. Such comparisons account for (almost) all the light, including that from galaxies too faint to see.

Cosmic Ray Composition
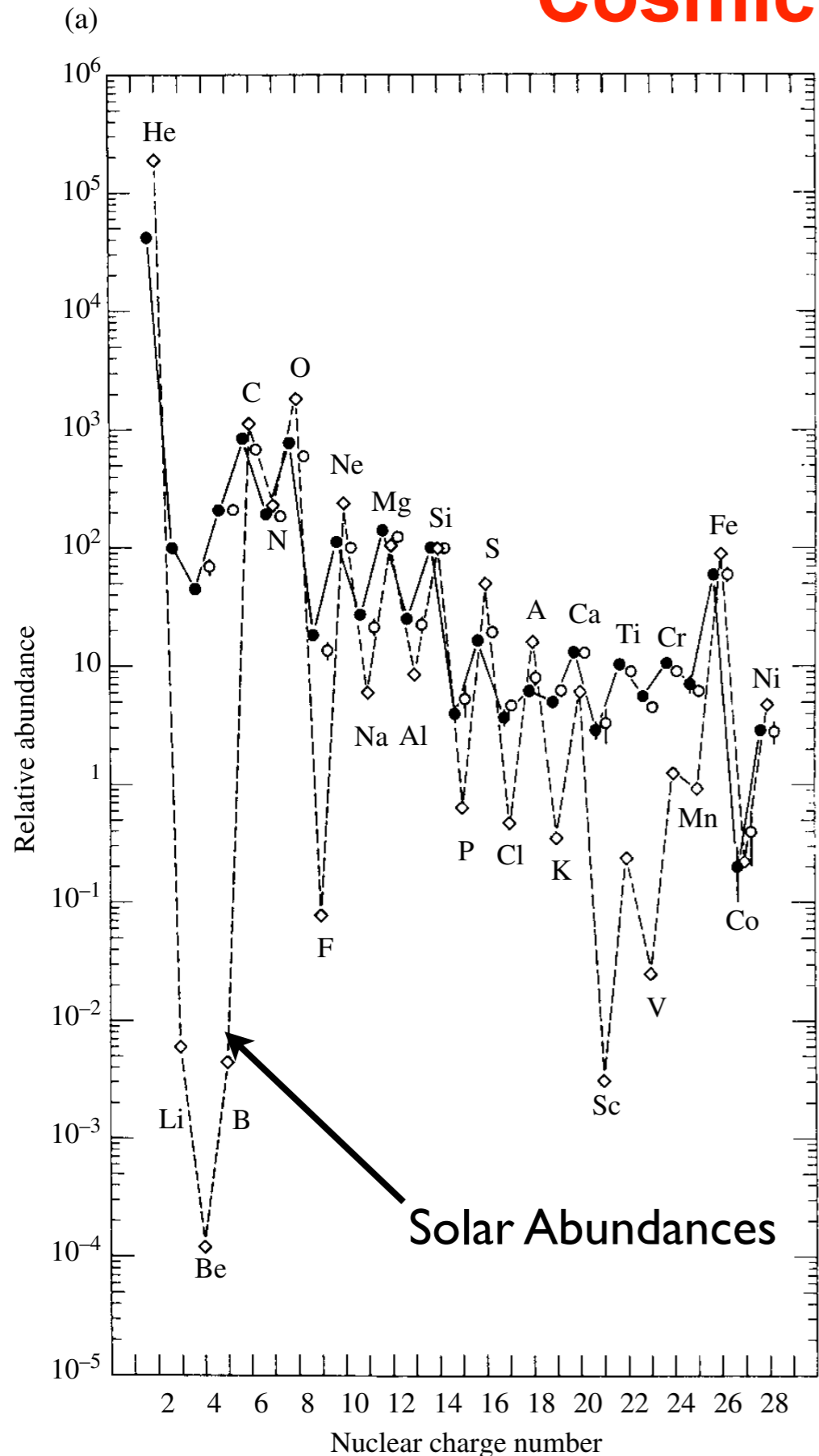
The chemical composition of the cosmic ray nuclei exhibits remarkable similarities to the solar system abundances, which are deduced from absorption lines in the solar photosphere and from meteorites, but it also shows some significant differences, as seen in the Figure at left. The cosmic and solar abundances both show the odd–even effect, associated with the fact that nuclei with Z and A even are more strongly bound than those with odd A and/or odd Z, and therefore are more frequent products in thermonuclear reactions in stars. The peaks in the normalized abundances for C, N, and O, and for Fe are also closely similar, suggesting that many of the cosmic ray nuclei must be of stellar origin.

The big differences between the cosmic and solar abundances are in those of Li, Be, and B. The abundance of such elements in stars is very small, since hardly any are produced in Big Bang nucleosynthesis -- or in stellar nucleosynthesis since they have low Coulomb barriers and are weakly bound and rapidly consumed in nuclear reactions in stellar cores. Their comparative abundance in cosmic rays is due to *spallation* of carbon and oxygen nuclei as they traverse the interstellar hydrogen.

Cosmic Rays and Magnetic Fields

For very energetic particles, with energies $E >> mc^2$, we can write the radius of the circle in which they move (the *Larmor radius*) as

$$R = E / (e\, c\, B), \quad \text{or} \quad B = E / (e\, c\, R)$$

Let's see what B field is required to keep the TeV protons at Fermilab in their R =1 km paths:

$$B = \frac{(10^{12}\ eV)(1.6 \times 10^{-19}\ J/eV)}{(1.6 \times 10^{-19}\ Coul)(3 \times 10^8\ m/s)(10^3\ m)} = 3.3\ T$$

Let's see now what R is for a 10 TeV particle in the Galactic magnetic field of ~3 μG = 3×10^{-10} T:

$$R = \frac{(10^{13}\ eV)(1.6 \times 10^{-19}\ J/eV)}{(1.6 \times 10^{-19}\ Coul)(3 \times 10^8\ m/s)(3 \times 10^{-10}\ T)} \approx 10^{14}\ m$$

1 pc = 3.1×10^{16} m. Thus in this case R $\approx 3 \times 10^{-3}$ pc, much less than the distance to the nearest star (~1.3 pc).

Energetic Cosmic Rays
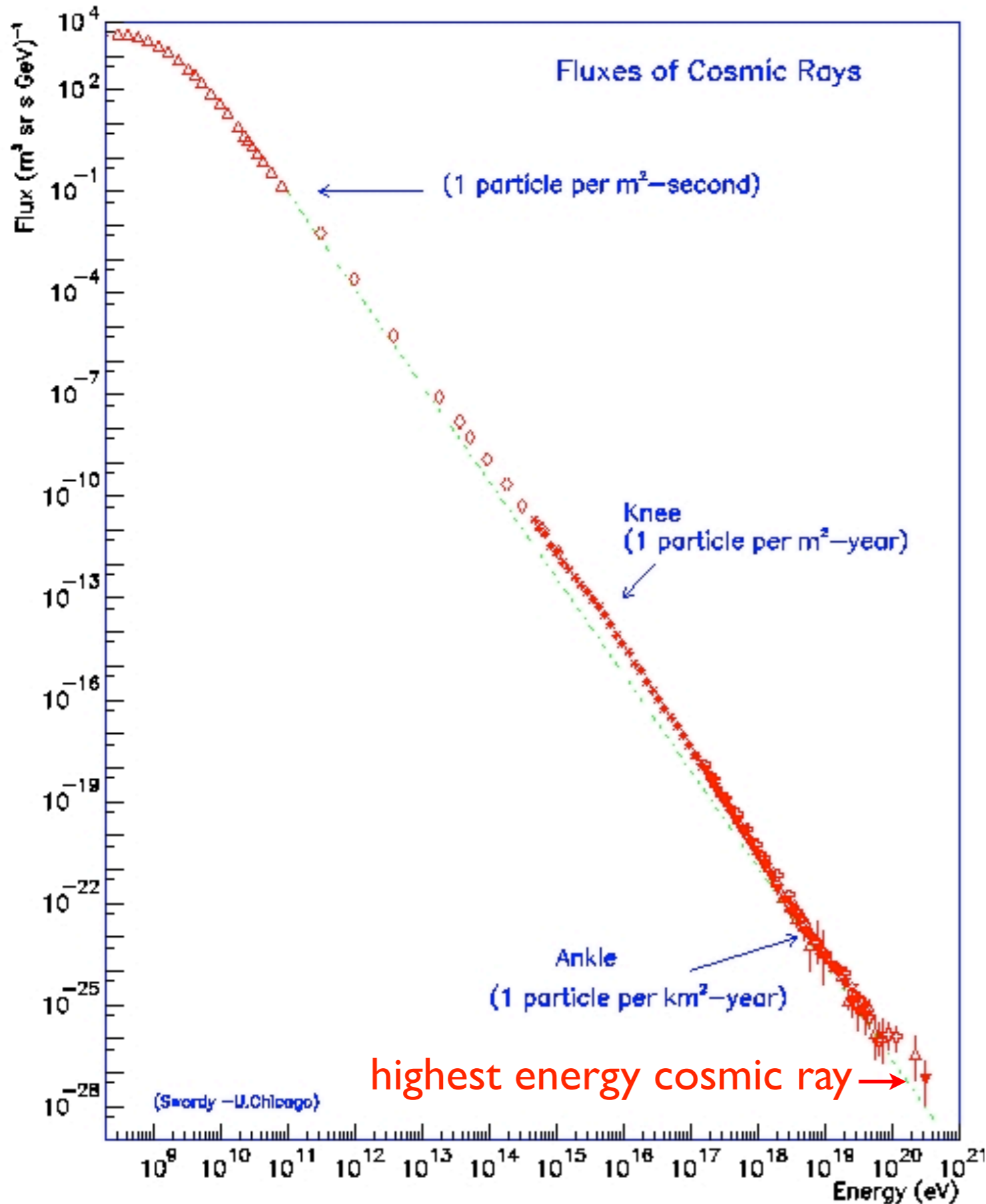
The Larmor radius R of an energetic cosmic ray with $E = 6 \times 10^{19}$ eV in the inter-galactic magnetic field of 10^{-9} G $= 10^{-13}$ T is

$$R \approx 60 \text{ Mpc}$$

Thus cosmic rays from the Virgo Cluster, 20 Mpc from us, will not point back toward their source.

Cosmic Ray Spectrum

(a)

Fluxes of cosmic rays

(1 particle per m^2–second)

$E^{-2.7}$

Knee
(1 particle per m^2–year)

Ankle
(1 particle per km^2–year)

Flux (m^2 sr s GeV)$^{-1}$

Energy (eV)

(b)

$E^{2.7}$ dN/dE (cm^{-2}sr^{-1}s^{-1}eV$^{1.7}$)

Knee

Ankle

GZK cutoff

E (eV/nucleus)

(c)

E (eV)

3×10^{18} 10^{19} 2×10^{19} 4×10^{19} 10^{20} 2×10^{20}

J/A x $E^{-2.69}$ −1

- Auger
- Hires I

GZK cutoff

lg(E/eV)
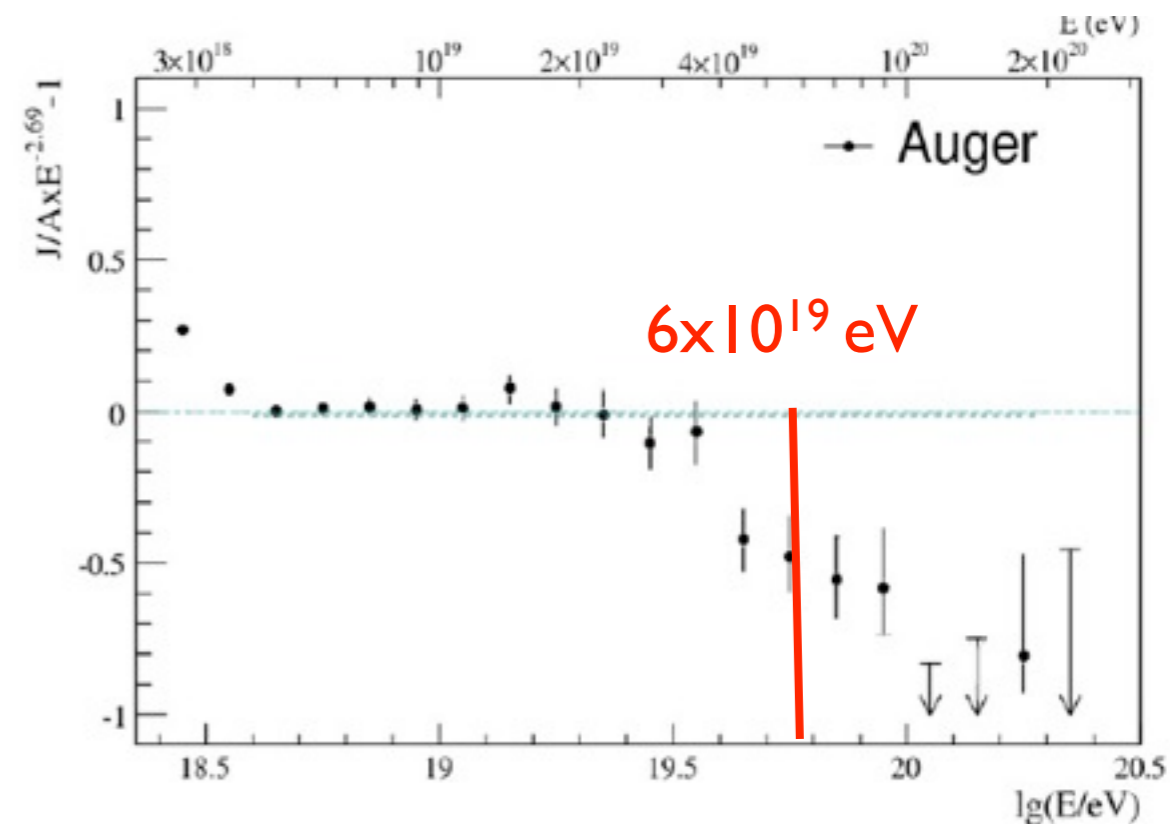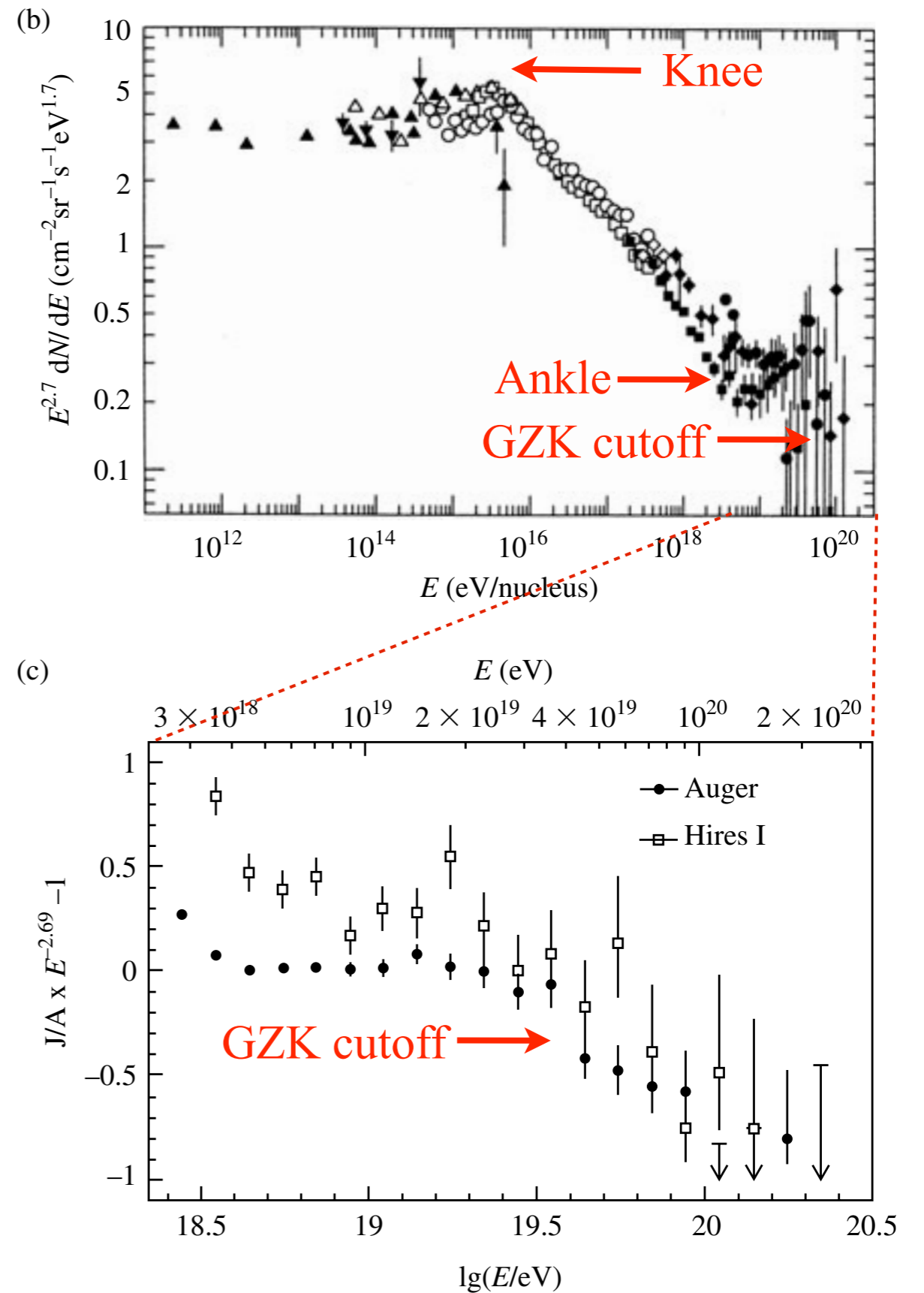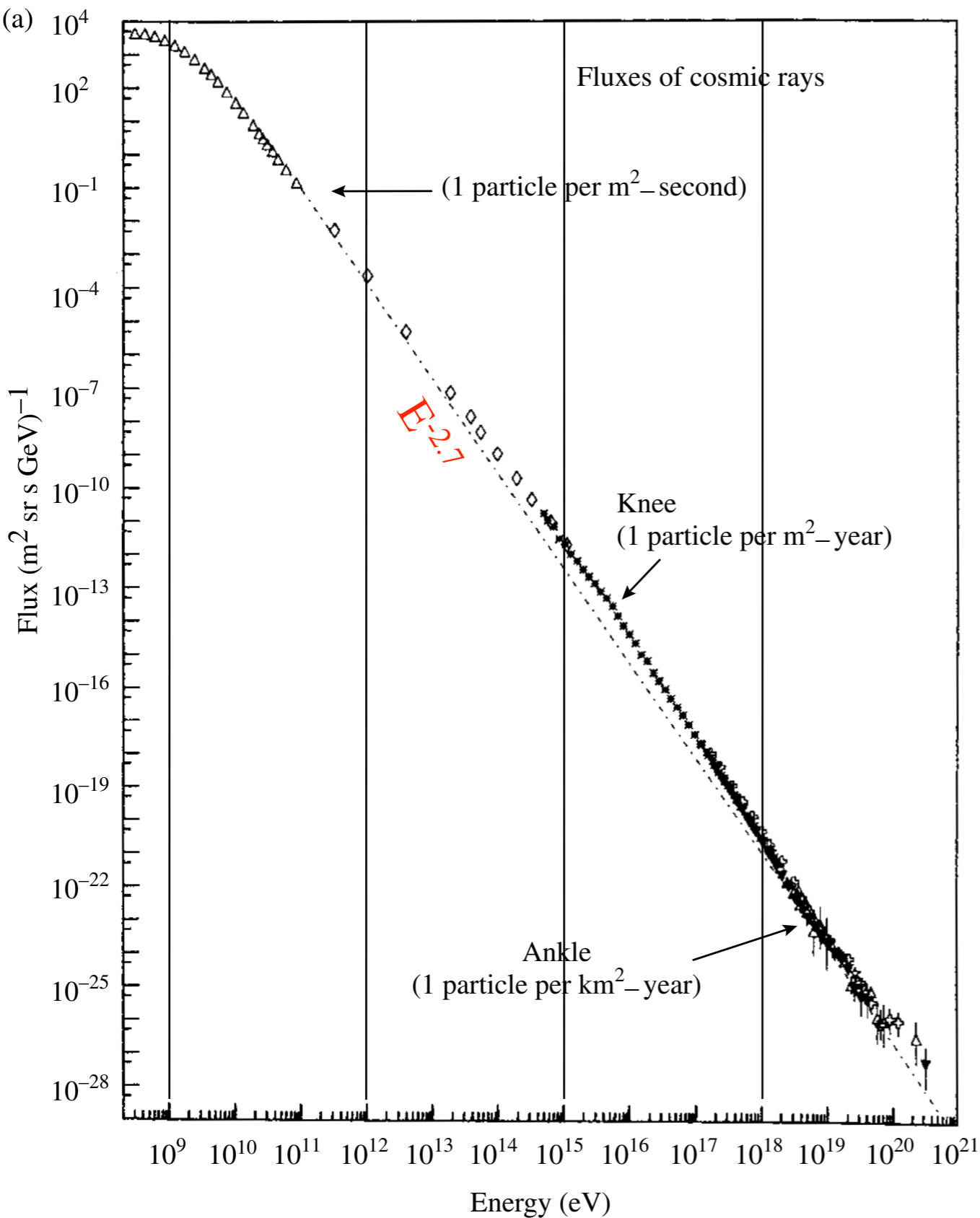
The most energetic cosmic rays have an approximately isotropic distriution.

GZK Cutoff

Many years ago, Greisen (1966), Zatsepin and Kuzmin (1966) pointed out that the universe could become opaque at such energies through photopion production excited in collisions of the primary protons with photons of the microwave background radiation, known as the GZK effect:

$$\gamma + p \rightarrow \Delta^+ \rightarrow p + \pi^0$$
$$\rightarrow n + \pi^+$$
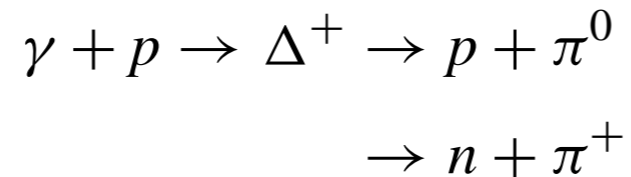
If the proton has mass M, momentum **p,** and energy E, and the microwave photon has momentum **q** and energy qc, then the square of the total centre- of-momentum energy in the collision will be

$$s = E^2_{cms} = (E + q)^2 - (\mathbf{p} + \mathbf{q})^2$$
$$= M^2 + 2q\left(E - |\mathbf{p}|\cos\theta\right)$$

in units $c = 1$. Here θ is the angle between the proton and photon directions, and E_{cms} must be at least equal to the sum of proton and pion masses. The threshold proton energy then becomes

$$E_{th} = \frac{5.96 \times 10^{20}}{[y(1 - \cos\theta)]}\,eV$$

where we take the photon energy as $q = y\,kT$ and the microwave background has $kT = 2.35 \times 10^{-4}$ eV. Typically, a proton would lose 15% of its energy in such a collision. For head-on collisions (cosθ = −1) and $y = 5$, $E = 6 \times 10^{19}$ eV. The collision mean free path $\lambda = 1/\rho\sigma = 4.1$ Mpc for all the microwave photons. For the 10% of photons with $y > 5$ the mean free path would be of order 50 Mpc.

.

Cosmic Ray Acceleration

How do cosmic rays attain their colossal energies, up to at least 10^{20} eV, and how do we account for the form of the energy spectrum? The energy density in cosmic rays, coupled with their lifetime in the galaxy, requires a power supply somewhat similar to the rate of energy generation in supernova shells. Our own galaxy has a radius $R \sim 15$ kpc and disc thickness $D \sim 0.3$ kpc. The total power requirement to accelerate the cosmic rays in the disc, for an average energy density of $\rho E = 1$ eV cm^{-3} is thus

$$W_{\text{CR}} = \frac{\rho_{\text{E}} \pi R^2 D}{\tau} = 3 \times 10^{41} \text{ Jyr}^{-1}$$

where т ~ 3 million years is the average age of a cosmic ray particle in the galaxy, before it diffuses out or is depleted and lost in interactions with the interstellar gas. A Type II supernova typically ejects a shell of material of about 10 solar masses (2×10^{31} kg), with velocity of order 10^7 m s^{-1} into the interstellar medium, at a rate based on an average over many galaxies of around 2±1 per century. (In our galaxy in fact only eight have been reported in the last 2000 years.) This gives an average power output per galaxy of $W_{\text{SN}} = 10^{43}$ J yr^{-1}, so an efficiency of a few percent to power cosmic rays would suffice.

In the 1950s, Fermi had considered the problem of cosmic ray acceleration. He first envisaged charged cosmic ray particles being reflected from 'magnetic mirrors' provided by the fields associated with massive clouds of ionized interstellar gas in random motion. It turns out, however, that such a mechanism is too slow to obtain high particle energies in the known lifetime of cosmic rays in the galaxy.
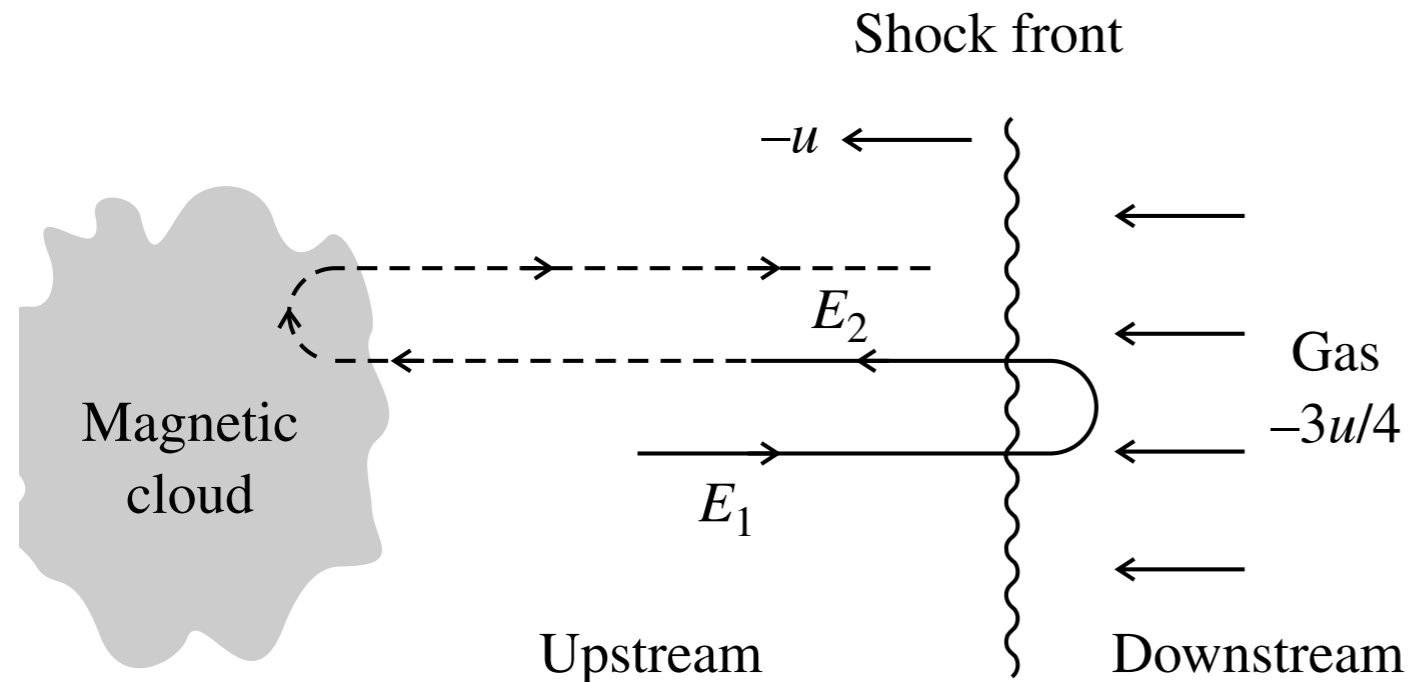
Cosmic Ray Acceleration

Shock front

Diagram depicting acceleration of a charged particle on crossing a shock front, and being scattered back across the front by the upstream gas. (Perkins, Fig. 9.6.)

Fermi also proposed that acceleration could occur due to *shock fronts*. Consider, in a simplified one-dimensional picture a relativistic particle travelling in the positive *x*-direction, which traverses a shock front moving with velocity $-u_1$ in the negative *x*-direction. Suppose that the particle is back-scattered by the field in the gas behind the front, which will have a velocity component in the direction of the shock of $u_2 = 2u_1/(C_P/C_V + 1) = 3u_1/4$, where the ratio of specific heats C_P/C_V where the ratio of specific heats $C_P/C_V = 5/3$ for an ionized gas. = 5/3 for an ionized gas. Thus the particle travels back with velocity u_2 across the shock front, to be scattered by magnetized clouds upstream of the front. If these again scatter the particle backwards (that is, in the direction of positive *x*), the particle can re-cross the front and repeat the cycle of acceleration once more. Because the front is planar (i.e. uni-directional) a straightforward application of the Lorentz transformations shows that the fractional energy gain is of the order of the shock front velocity $\Delta E/E \sim u_1/c$.

Cosmic Ray Acceleration

If in each cycle the particle gets an energy increment $\Delta E = \alpha E$, after n cycles its energy becomes $E = E_0(1 + \alpha)^n$. Let P be the probability that the particle stays for further acceleration, so that after n cycles the number of particles remaining for further acceleration will be $N = N_0 P^n$ where N_0 is the initial number of particles. Substituting for $n = \ln(E/E_0)/\ln(1 + \alpha)$, $\ln(N/N_0) = n \ln P = \ln(E/E_0) (\ln P)/\ln(1 + \alpha) = \ln (E_0/E)^s$, where $s = -(\ln P)/\ln(1 + \alpha)$. The number N is the number of particles with n or more cycles, thus with energy $\geq E$. Hence the differential energy specrum will have the power law dependence

$$\frac{\mathrm{d}N\,(E)}{\mathrm{d}E} = \text{constant} \times \left(\frac{E_0}{E}\right)^{(1+s)}$$

For shock-wave acceleration, it turns out that $s \sim 1.1$ typically, so that the differential spectrum index is −2.1, compared with the observed value of −2.7. The steeper observed spectrum could be accounted for if the escape probability $(1-P)$ was energy dependent.

The shock-wave acceleration from supernovae shells appears capable of accounting for the energies of cosmic ray nuclei of charge $Z|e|$ up to about $100z$ TeV ($10^{14}Z$ eV), but hardly beyond this. Other mechanisms must be invoked for the very-highest-energy cosmic rays, and among the processes likely to play an important part are those associated with accretion of matter from nearby stars and gas on to massive black holes at the centre of AGNs.
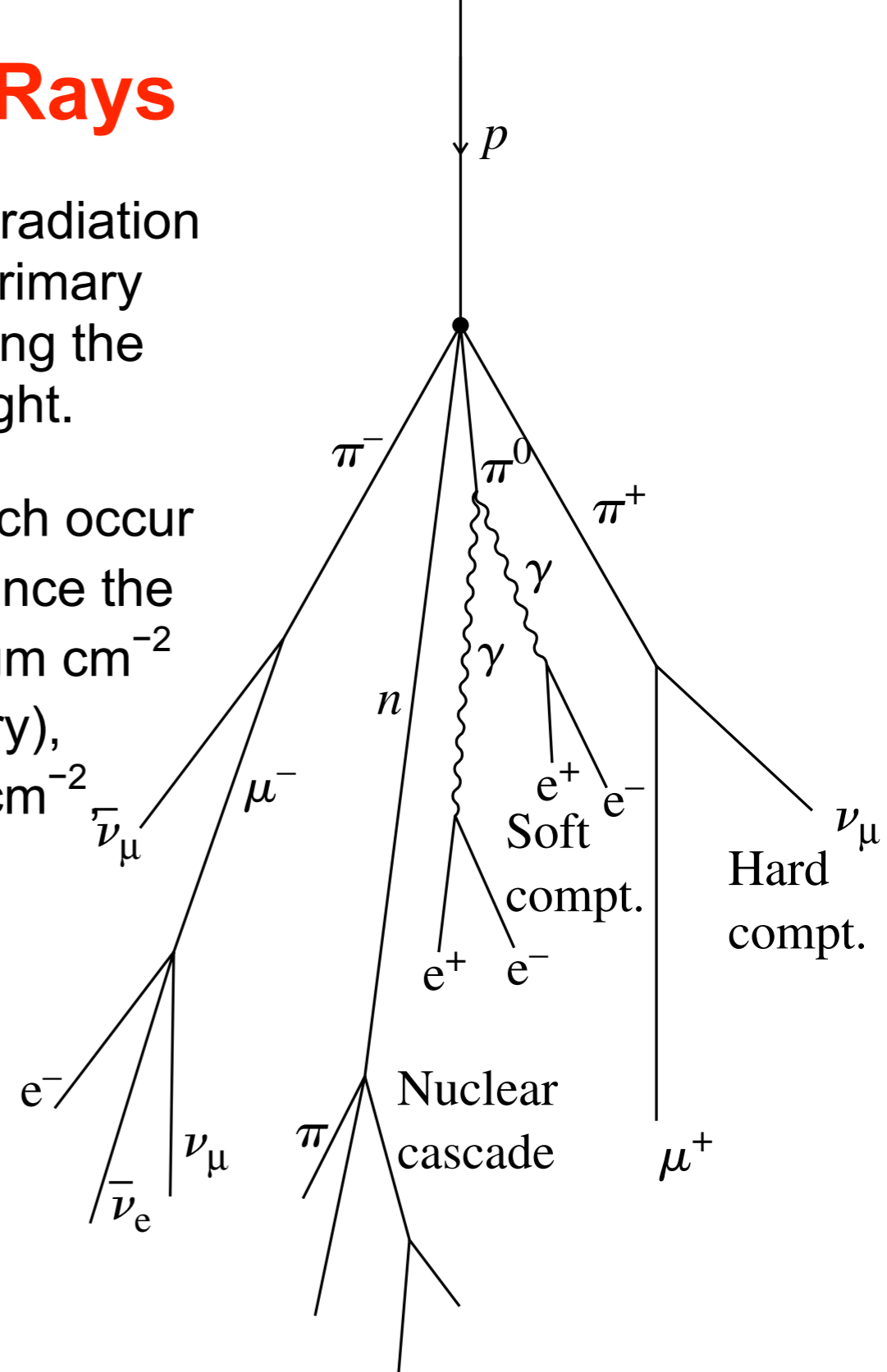
Secondary Cosmic Rays

The term 'cosmic rays' properly refers to particles and radiation incident from outside the Earth's atmosphere. These primary particles will produce secondaries (mesons) in traversing the atmosphere, as shown schematically in the figure at right.

The most commonly produced particles are pions, which occur in three charged and neutral states π^+, π^-, and π^0. Since the nuclear interaction mean free path in air is $\lambda_{int} \sim 100$ gm cm^{-2} for a proton (and much less for a heavy nuclear primary), compared with a total atmospheric depth of 1030 gm cm^{-2} the pions are created mostly in the stratosphere. The *charged pions* decay to muons and neutrinos:
$\pi^+ \rightarrow \mu^+ + \nu_\mu$ and $\pi^- \rightarrow \mu^- + \bar{\nu}_\mu$, with a proper lifetime of τ=26 ns and a mean free path before decay of $\lambda_{dec} = \gamma c\tau$ where $\gamma = E\pi/m_\pi c^2$ is the time dilation factor. With $m_\pi c^2 = 0.139$ GeV, $\lambda_{dec} = 55$ m for a 1 GeV pion. At GeV energies practically all charged pions decay in flight (rather than interact).

The daughter muons are also unstable, undergoing the decay $\mu^+ \rightarrow e^+ + \nu_e + \nu_\mu$ with a proper lifetime of $\tau = 2200$ ns. Since the muon mass is 0.105 GeV, a 1 GeV muon has a mean decay length of 6.6 km, about equal to the scale height H of the atmosphere. Muons of energy 1 GeV or less will therefore decay in flight in the atmosphere.

Secondary Cosmic Rays

A 3 GeV muon, for example, has a mean decay length of 20 km, of the same order as the typical distance from its point of production to sea-level. Moreover, with an ionization energy loss rate of 2 MeV gm^{-1} cm^2 of air traversed , muons with 3 GeV or more energy can get through the entire atmosphere without being brought to rest or decaying. Still higher-energy muons can reach deep underground, and for this reason they are said to constitute the **hard component** of the cosmic radiation.

The *neutral pions* undergo electromagnetic decay, $\pi^0 \rightarrow 2\gamma$, with an extremely short lifetime of 8×10^{-17} s. The photons from the decay develop electron–photon cascades mostly in the high atmosphere, since the absorption length of these cascades is short compared with the total atmospheric depth. The electrons and photons of these cascades constitute the easily absorbed **soft component** of the cosmic radiation.

Among the products of the nuclear interactions of primary cosmic rays in the atmosphere are radioactive isotopes, of which an important one is ^{14}C formed, for example, by neutron capture in nitrogen: $n+^{14}N\rightarrow^{14}C+^1H$.The$^{14}C$ atoms produced in this way combine to form CO_2 molecules and thus participate, like the more common, stable ^{12}C atoms, in in absorption in organic matter. Since carbon-14 has a mean lifetime of 5600 years, its abundance relative to carbon-12 in organic matter can be used to date the sample. Comparison of the age from the isotope ratio with that from ancient tree ring counts shows that the cosmic ray intensity variws in the past and was some 20% larger 5000 years ago. This variation was presumably due to long-term fluctuations in the value of the Earth's magnetic field which, associated with continental drift, is known from rock samples to have changed its sign and magnitude many times over geological time.

A Timeline of High-Energy Cosmic Ray History

1912 — Hess discovered cosmic rays

1927 — Cosmic rays seen in cloud camber

1932 — Anderson discovered antimatter. Debate over cosmic rays

1937 — Discovery of muon

1938 — Pierre Auger discovered extensive air showers

1946 — First air shower experiments

1949 — Fermi's theory of cosmic rays

1962 — First 1020 eV cosmic ray detected

1966 — Proposal of GZK cutoff energy for cosmic rays

1967 — Haverah Park cosmic ray detector begins operations

1991 — Fly's Eye detected highest-energy cosmic ray (Utah)

1994 — AGASA high-energy event (Japan)

1995 — Pierre Auger Project begun (Argentina)

1999 — Groundbreaking for Pierre Auger South

2005 — Celebration and first physics results from Auger Project

2007 — Auger discovers extragalactic origin of highest-energy cosmic rays

2008 — Inauguration of completed Pierre Auger South

Pierre Auger Observatory
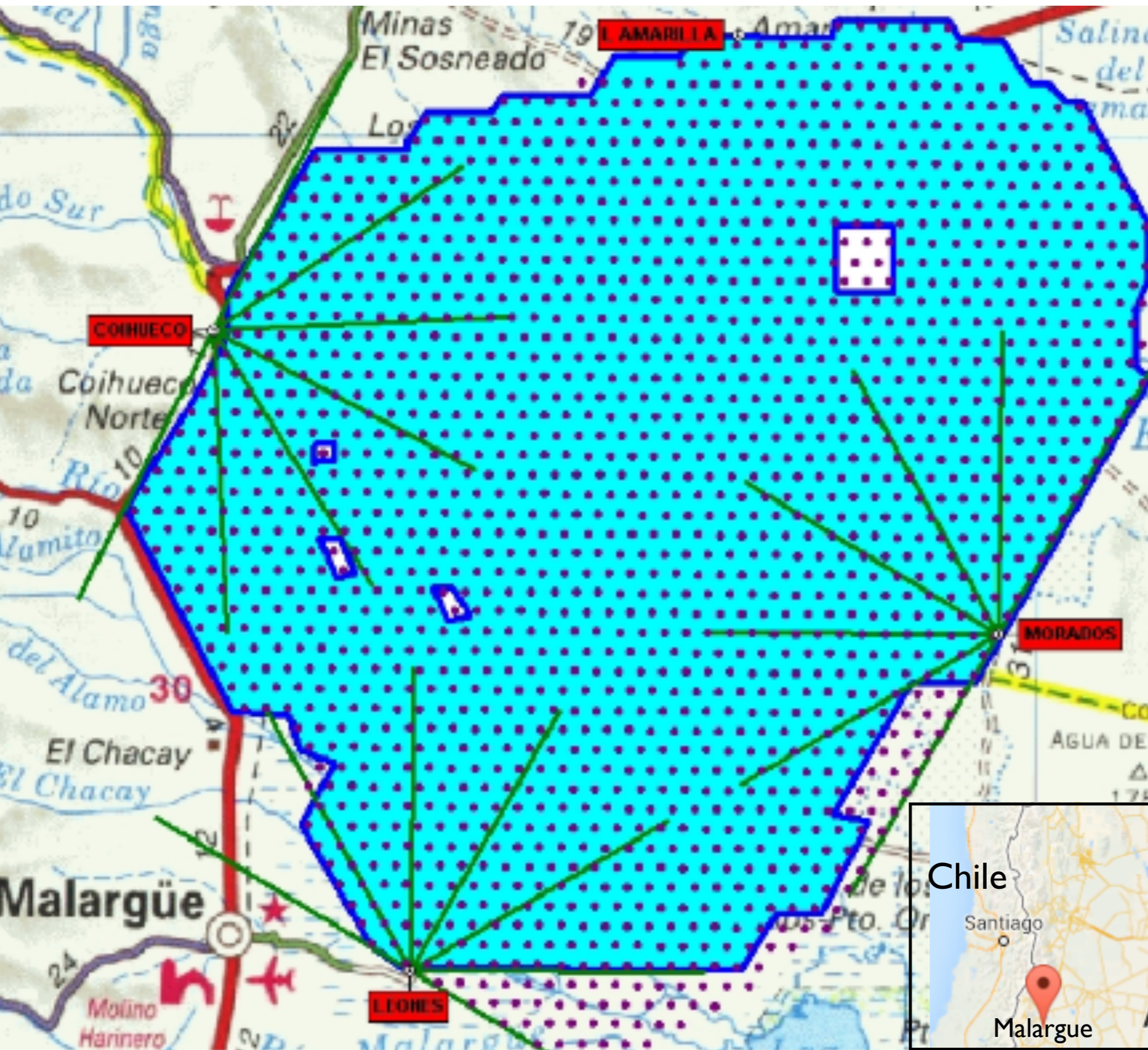
The 1600 water Cerenkov tanks forming the ground detector array are shown as dots, at 1.5 km separation. They are overlooked by four stations housing 240 mirror/photomultiplier arrays, which record the fluorescence from nitrogen molecules excited as the air shower traverses the atmosphere. The ability to combine the data from the ground array with that from air fluorescence has proved a powerful constraint on energy measurements.
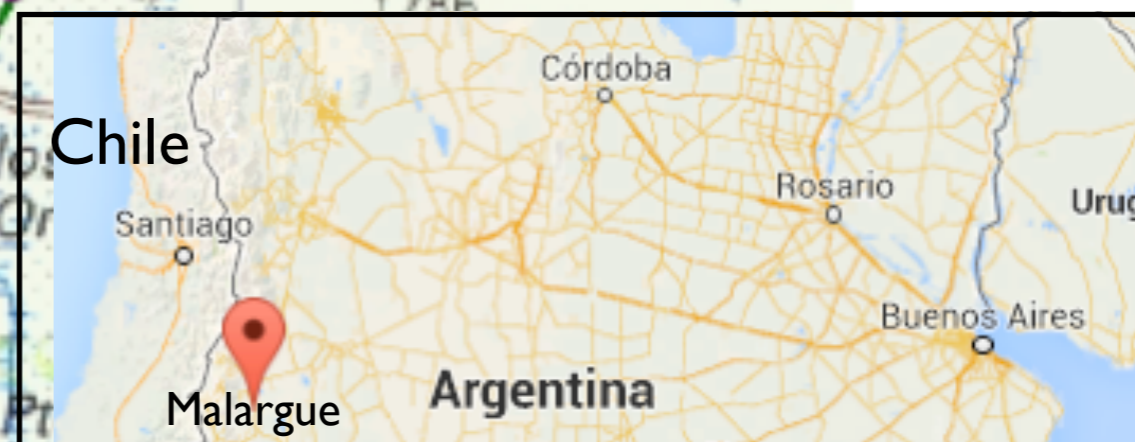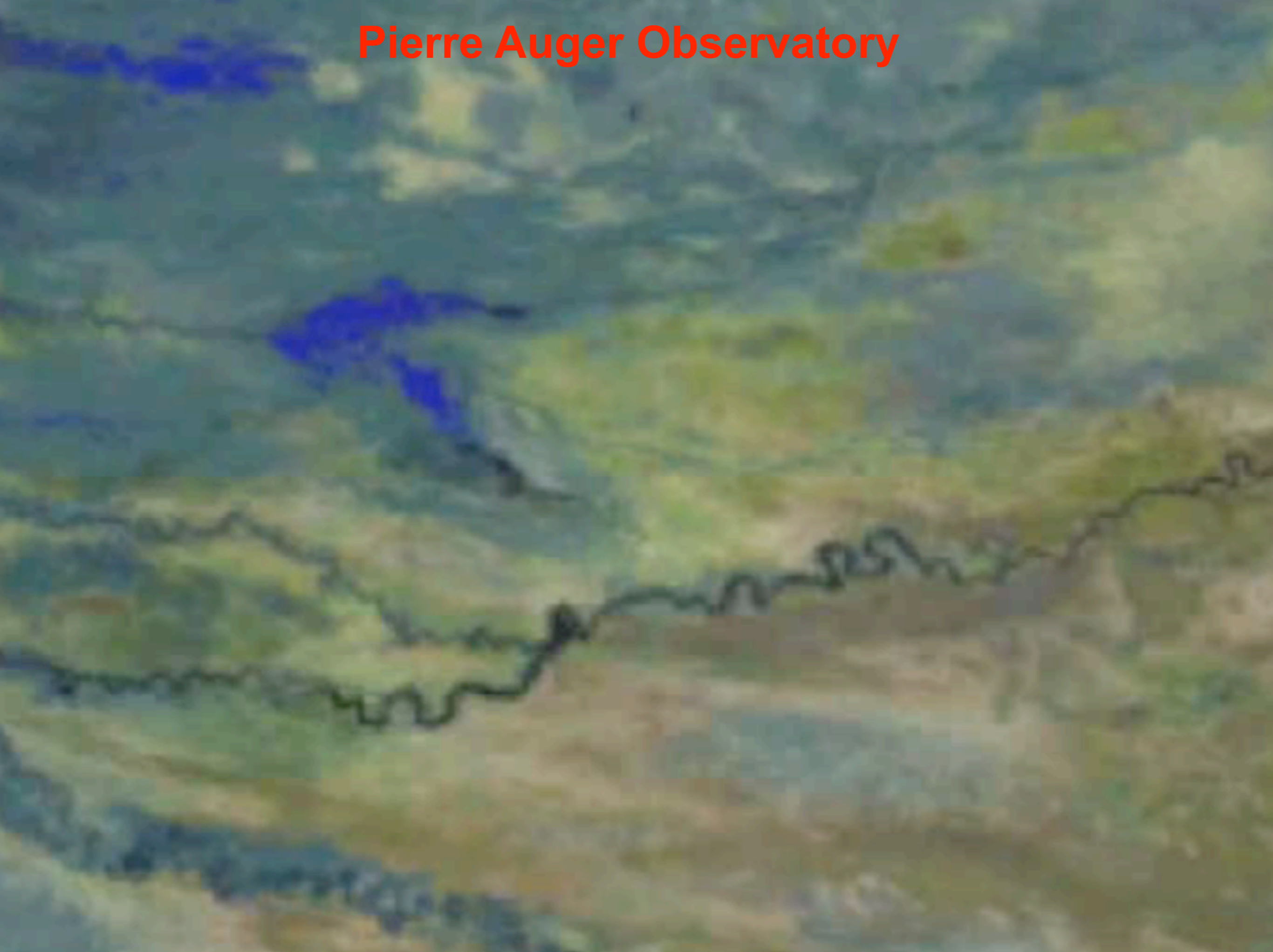
Pierre Auger Observatory

The Pierre Auger Observatory in Malargue, Argentina, is a multinational collaboration of physicists trying to detect powerful cosmic rays from outer space. The energy of the particles here is above 10^{19} eV, or over a million times more powerful than the most energetic particles in any human-made accelerator. No-one knows where these rays come from. Such cosmic rays are very rare, hitting an area the size of a football field once every 10 000 years. This means you need an enormous 'net' to catch these mysterious ultra-high-energy particles.

The Auger project has about 1600 detectors. Each detector is a tank, like the one pictured below, and is filled with 11 000 liters / 3000 gallons of pure water and sits about 1.5 km away from the next tank. This array on the Argentinian Pampas will cover an area of about 3000 km^2, which is about the size of the state of Rhode Island. A second detection system sits on hills overlooking the Pampas and on dark nights captures a faint light or fluorescence caused by the shower particles colliding with the atmosphere.
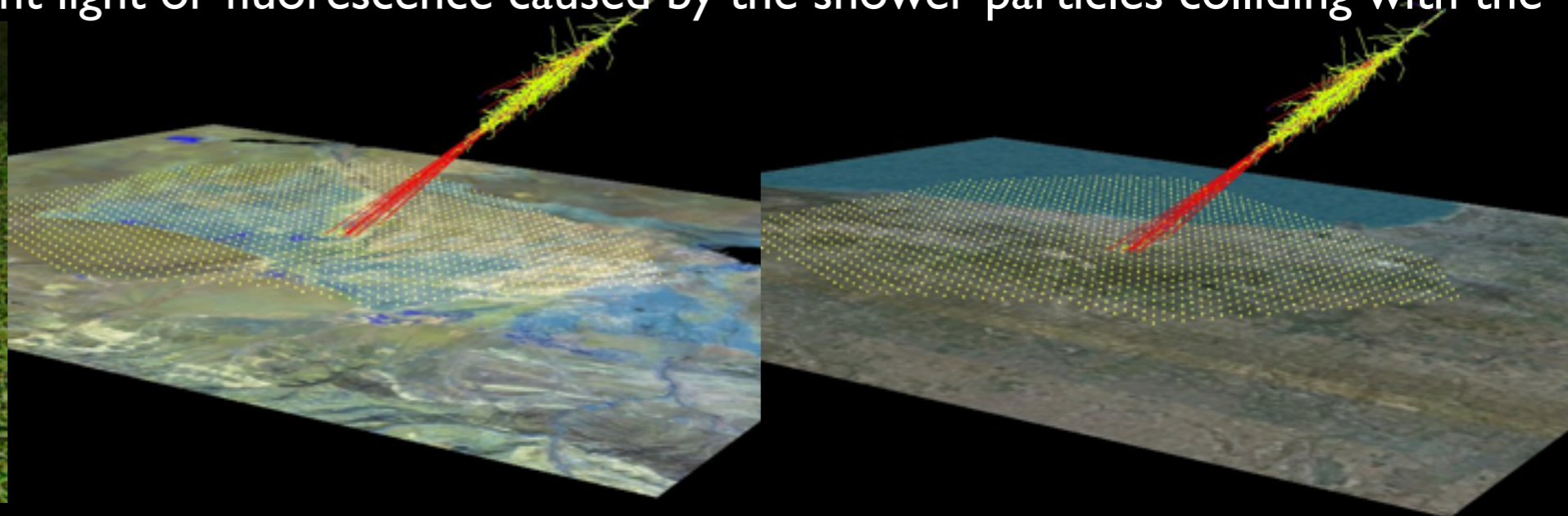

Shown above is the shower created when a proton with energy 10^{19}eV hits the atmosphere. (Color codes: muons, photons, electrons/positrons) and over the same size area (100km x 100km) around Chicago, IL & southern Lake Michigan. Also shown is the array of 1600 tanks (size greatly exaggerated) superimposed over their actual location in Malargue (left)

Pierre Auger Observatory

Thursday, March 13, 14
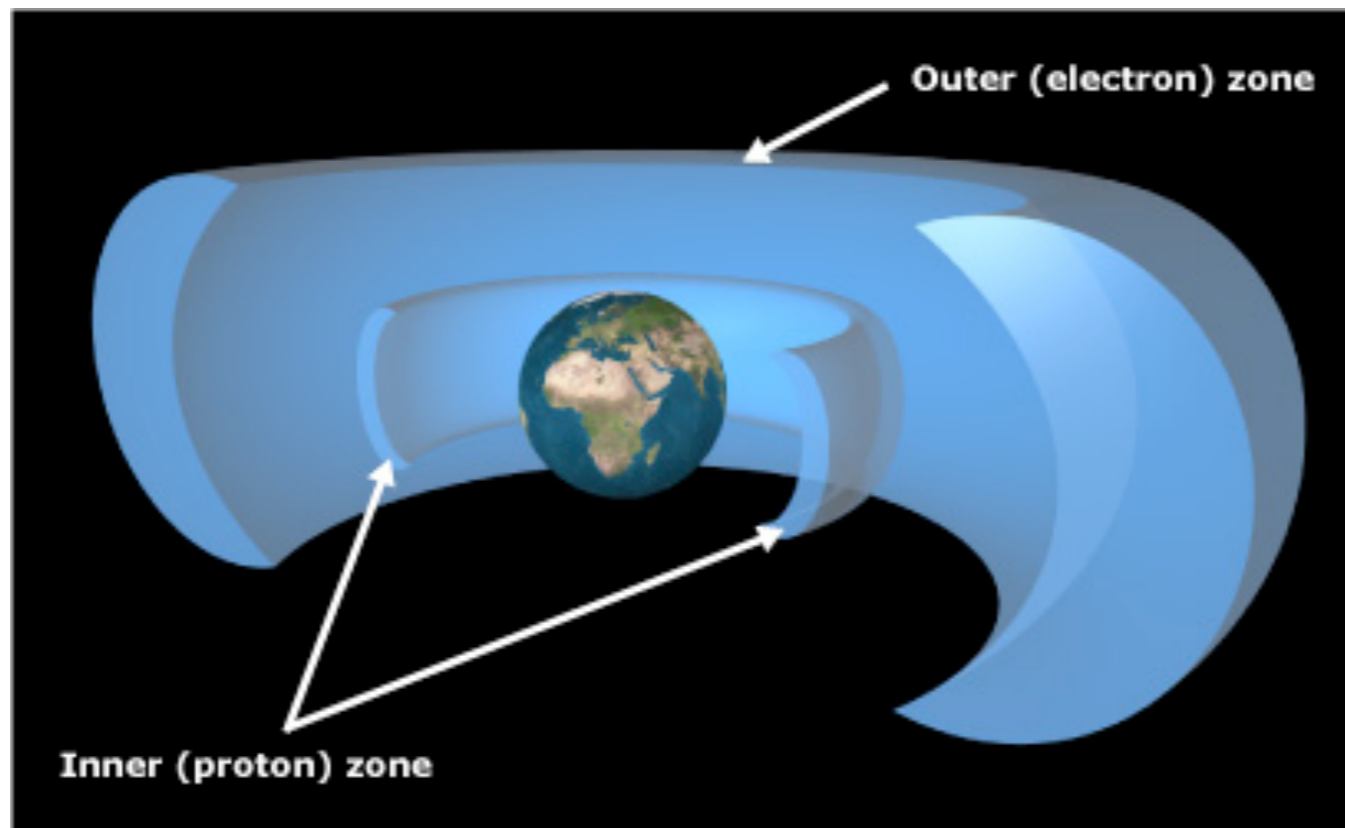
Pierre Auger Observatory
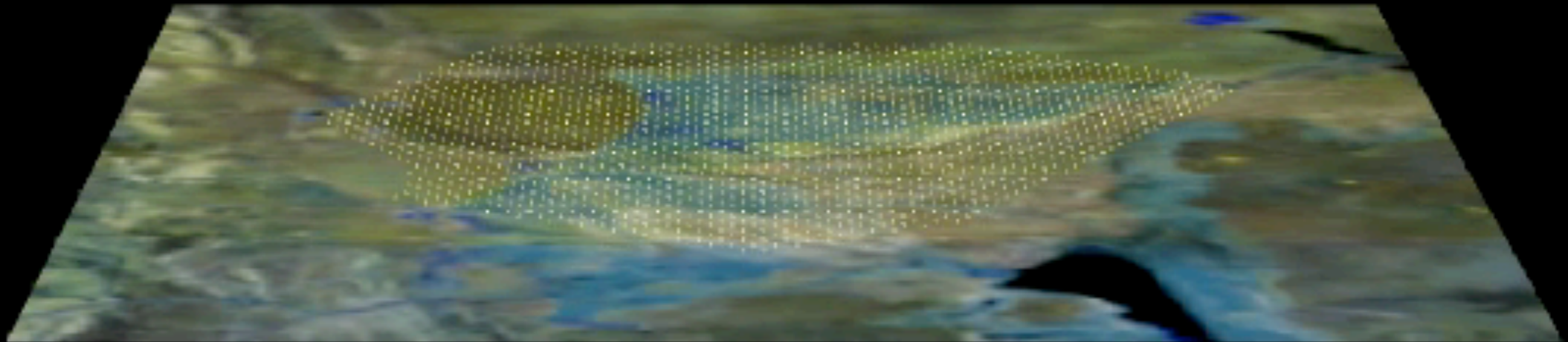
Pierre Auger Observatory
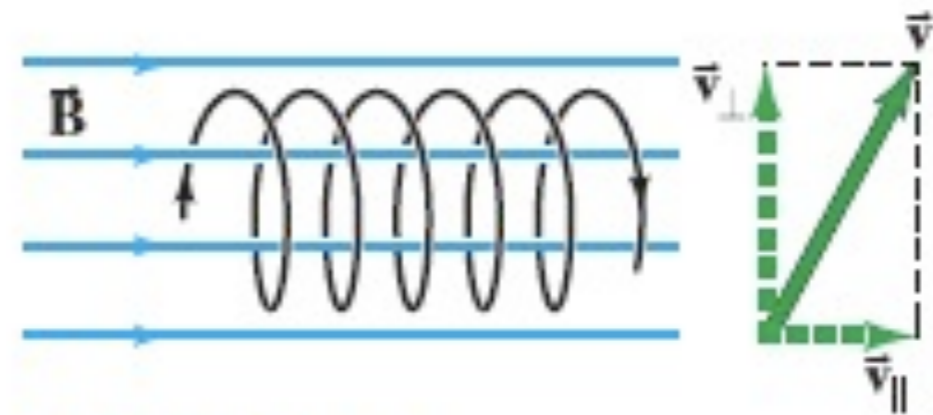
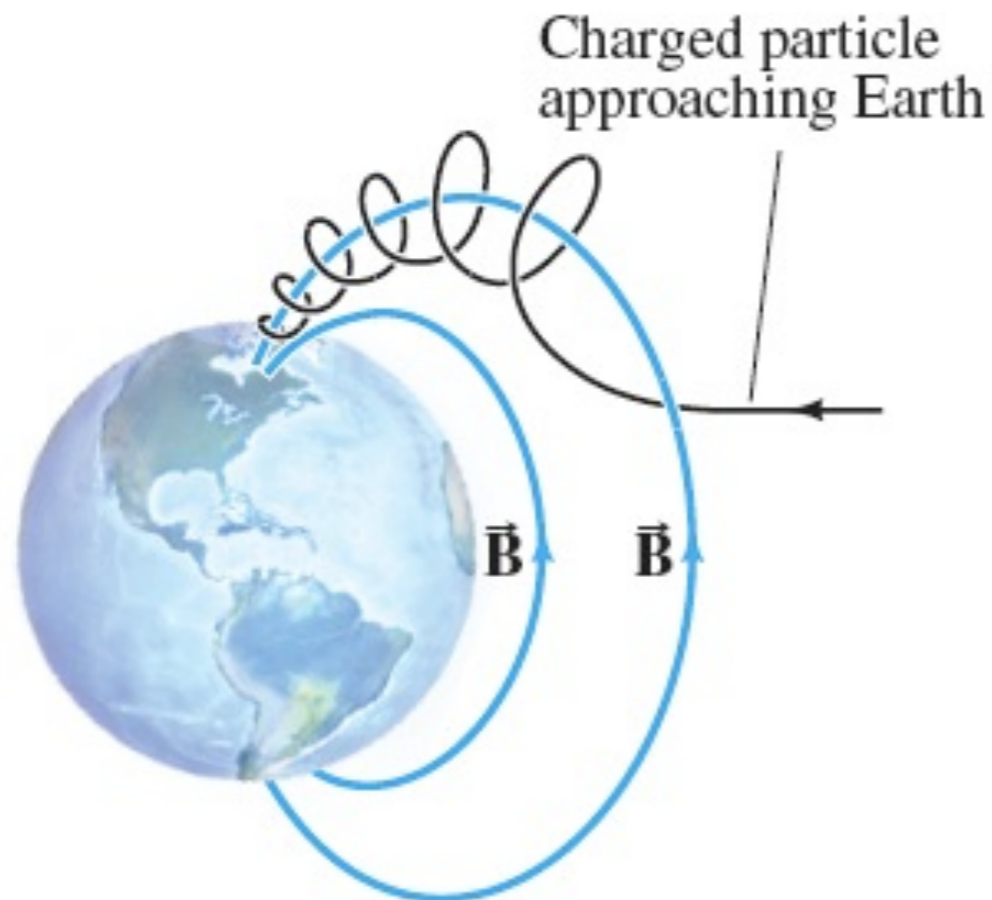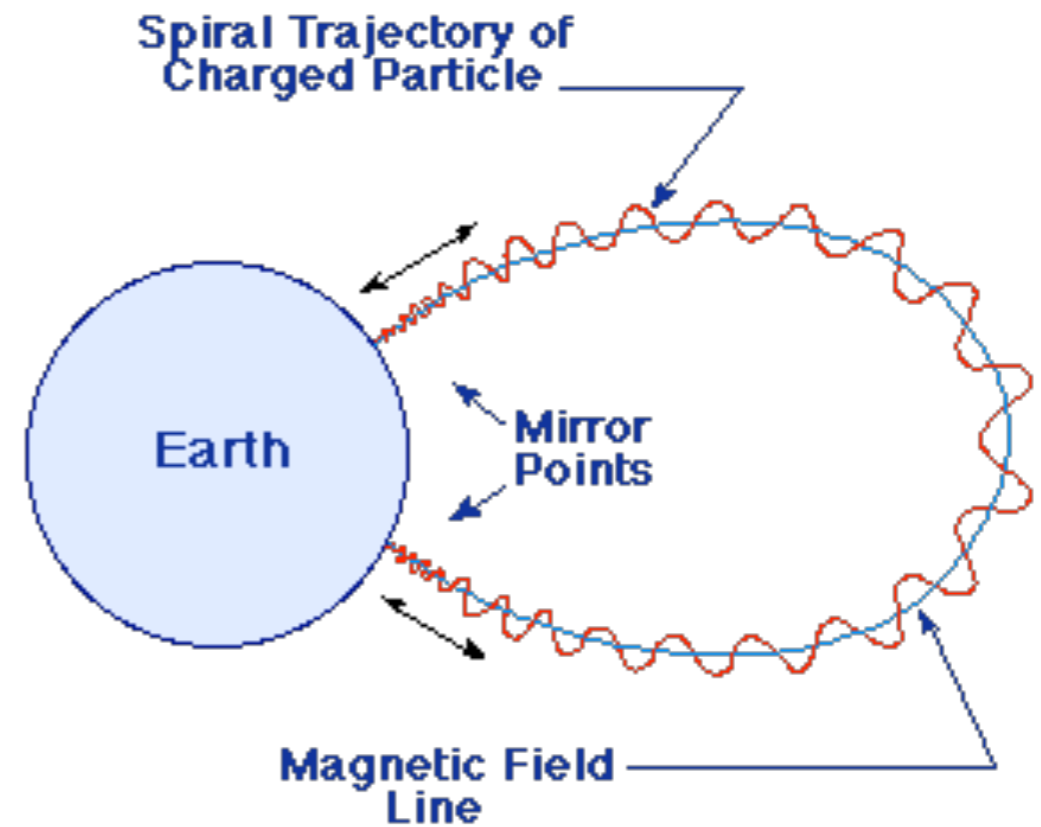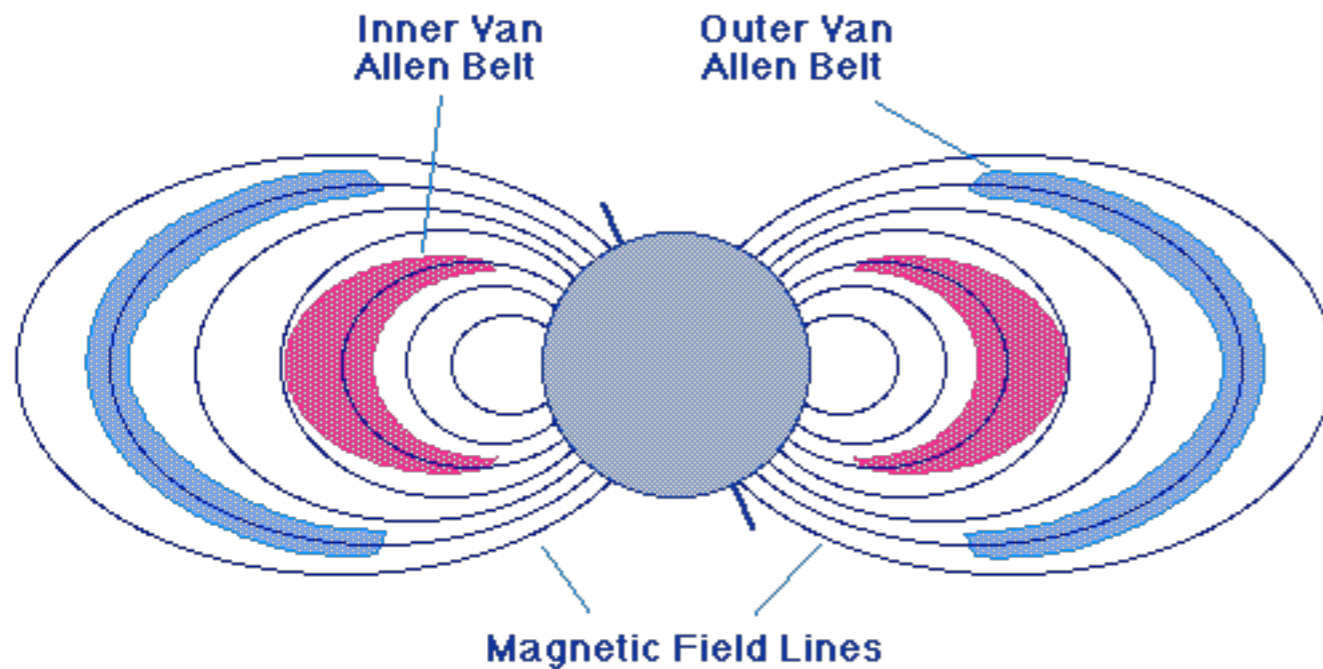10^{19} ev cosmic ray - muons, photons, electrons/positrons

The Van Allen Radiation Belts

The earth's magnetic field traps energetic electrons and protons from the sun in radiation belts around the earth.

These charged particles spiral around the earth's magnetic field lines.

Inner Van Allen Belt
Outer Van Allen Belt
Magnetic Field Lines

Spiral Trajectory of Charged Particle
Earth
Mirror Points
Magnetic Field Line

Charged particle approaching Earth
$\vec{B}$ $\vec{B}$

When a particle spirals around magnetic field lines in an increasing B field, the particle can be reflected - a "magnetic mirror." Particles that aren't reflected excite atoms in the upper atmosphere, producing auroras.

Thursday, March 13, 14

Aurora Australis: This view of the Aurora Australis, or Southern Lights, which was photographed by an astronaut aboard Space Shuttle Discovery (STS-39) in 1991, shows a spiked band of red and green aurora above the Earth's Limb. Calculated to be at altitudes ranging from 80 - 120 km (approx. 50-80 miles), the auroral light shown is due to the "excitation" of atomic oxygen in the upper atmosphere by charged particles (electrons) streaming down from the magnetosphere above.

From space, the aurora is a crown of light that circles each of Earth's poles. The <u>IMAGE</u> satellite captured this view of the aurora australis (southern lights) on September 11, 2005, four days after a record-setting solar flare sent plasma—an ionized gas of protons and electrons—flying towards the Earth. The ring of light that the solar storm generated over Antarctica glows green in the ultraviolet part of the spectrum, shown in this image. The IMAGE observations of the aurora are overlaid onto NASA's satellite-based <u>Blue Marble</u> image. From the Earth's surface, the ring would appear as a curtain of light shimmering across the night sky.
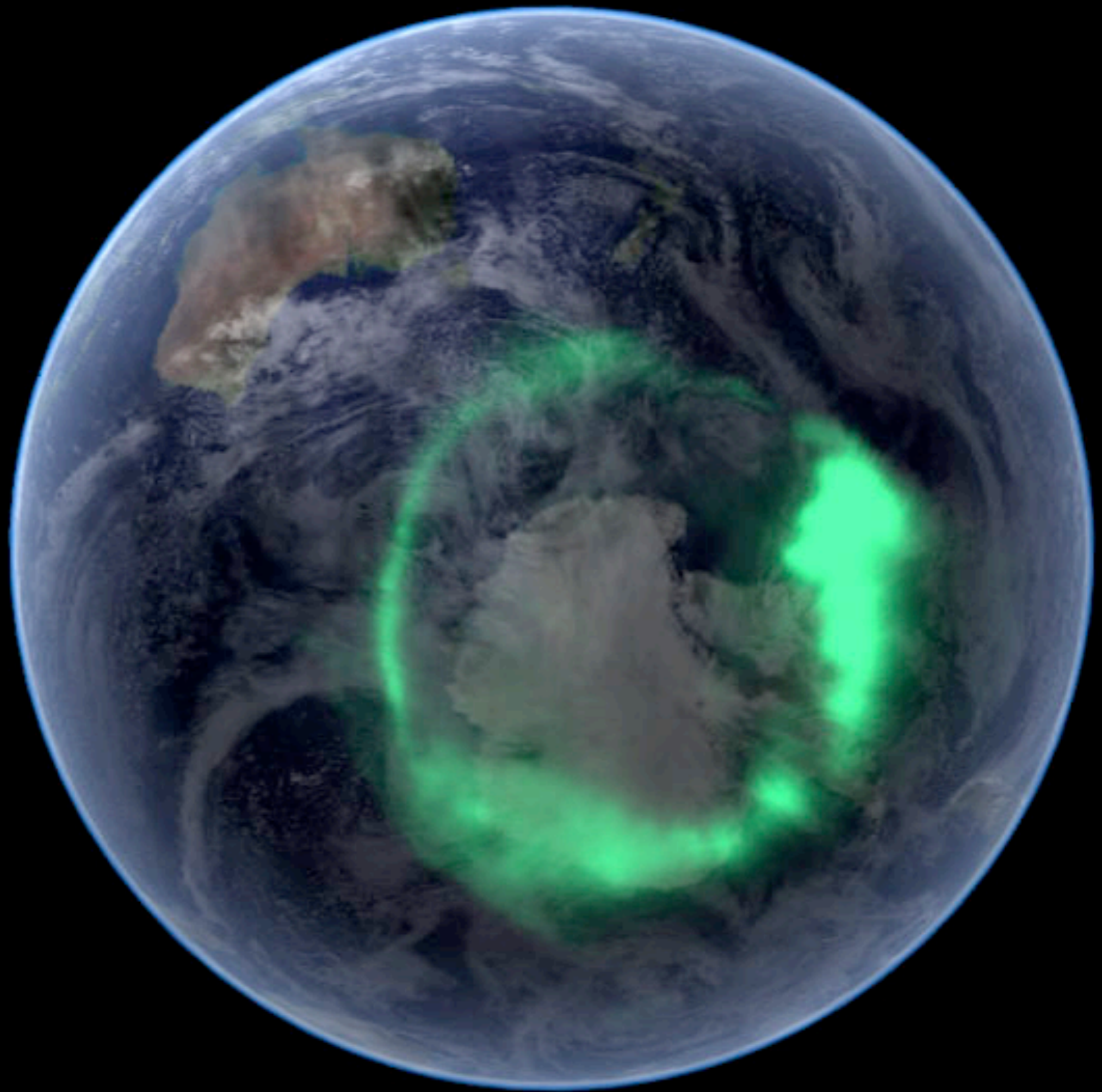
NASA's Polar spacecraft took
this series of images of the
aurora over Earth's northern
hemisphere. The images were
collected by Polar's Visible
Imaging System in February
2000, and they reveal the auroral
oval around the polar regions in
visible and ultraviolet light. The
most intense auroral activity
appears in bright red or white.
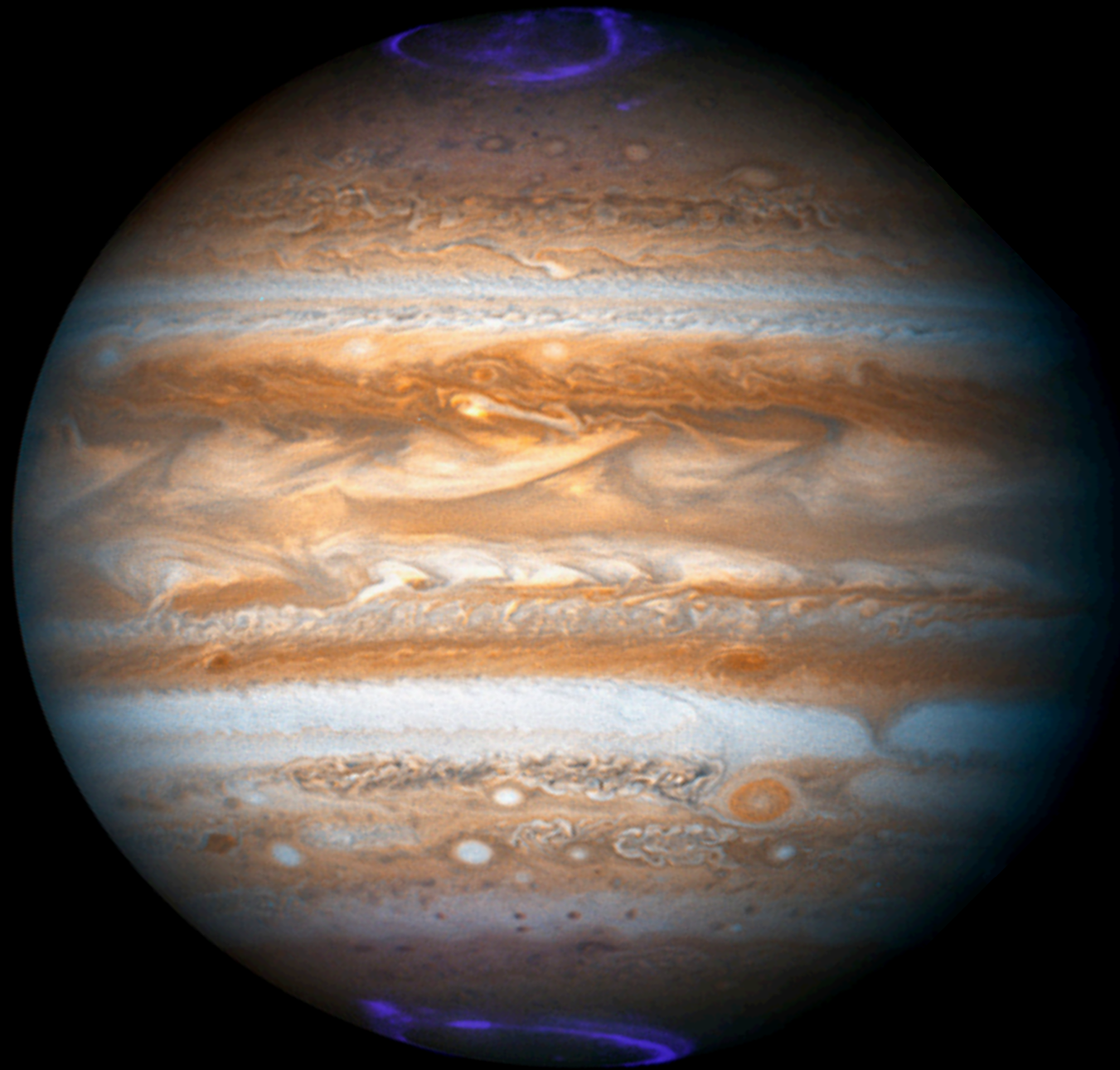
This image is a composite made from ultraviolet- and visible-light images of Jupiter taken with Hubble from February 17-21, 2007. The glowing aurorae near Jupiter's North and South Poles were imaged using Hubble's Advanced Camera for Surveys' surviving ultraviolet camera. Jupiter's ever-changing cloudtops are seen through blue and red filters with Hubble's Wide Field Planetary Camera. In this dramatic image, Jupiter shows a novel array of cloud features including the recently formed Little Red Spot, a smaller version of Jupiter's well-known and long-lived Great Red Spot. Atmospheric features as small as 100 miles (160 km) across can be discerned.